Structure Functions of Pion and Deuteron

Author:
Qin-Tao Song

Supervisor:
Professor Shunzo Kumano

Doctor of Philosophy

Department of Particle and Nuclear Physics
School of High Energy Accelerator Science
SOKENDAI (The Graduate University for Advanced Studies)

September 2019

SOKENDAI (THE GRADUATE UNIVERSITY FOR ADVANCED STUDIES)

Abstract

School of High Energy Accelerator Science
Department of Particle and Nuclear Physics

Doctor of Philosophy

Structure Functions of Pion and Deuteron

by Qin-Tao Song

Structure functions of the pion and the deuteron are studied in this thesis. The first topic is on tensor-polarized parton distributions of the deuteron and their relation to a spin asymmetry in the proton-deuteron Drell-Yan process. The second topic is on generalized distribution amplitudes in the two-photon process $\gamma^*\gamma \to \pi^0\pi^0$. The third topic is on gluon transversity of the deuteron and its relation to the prompt-photon production cross section in the proton-deuteron collision.

First, in comparison with the spin-1/2 proton, there are additional spin observables for the deuteron because of its spin-1 nature, and they are tensor-polarized structure functions. In 2005, the HERMES collaboration observed the tensor structure function b_1 in the deep inelastic scattering (DIS) process with a polarized deuteron, and this measurement is not consistent with the standard deuteron prediction. Furthermore, there was an interesting indication that a finite antiquark tensor polarization exists. These results indicate that the structure function b_1 could probe an interesting new aspect in the deuteron. In the near future, b_1 will be accurately measured at Thomas Jefferson National Accelerator Facility (JLab), and the Drell-Yan experiment is now under consideration at Fermi National Accelerator Laboratory (Fermilab) by using the unpolarized proton beam and tensor-polarized deuteron target. The tensor-polarized antiquark distributions are not easily determined from the charged-lepton DIS; however, they can be measured in a proton-deuteron Drell-Yan process with the tensor-polarized deuteron target. In this work, we provide theoretical predictions for the spin asymmetry of the Fermilab Drell-Yan experiments by using optimum tensor-polarized parton distribution functions (PDFs) to explain the HERMES measurement. We find that the asymmetry is typically a few percent, and our results were used for proposing the polarized proton-deuteron Drell-Yan measurement within the Fermilab-E1039 experiment. If it is measured, it could probe new hadron physics, and such studies could create an interesting field of high-energy spin physics.

Second, the 3-dimensional (3D) structure functions, generalized parton distributions (GPDs) and generalized distribution amplitudes (GDAs), contain information on form factors, PDFs, distribution amplitudes (DAs) and orbital-angular-momentum contributions to the hadron spin. The GPDs provide us a way to solve the proton spin puzzle. The GPDs can be measured by the deeply virtual Compton scattering (DVCS), and we could also obtain GPDs by the s-t crossing from the GDAs. As for the GDAs, they can be measured by the two-photon process $\gamma^*\gamma \to h\bar{h}$, which is possible at KEKB. For this two-photon process, the cross section can be calculated theoretically with the GDAs of the hadron h. One can obtain the GDAs by analyzing the experimental cross sections with a reasonable parameterization of the GDAs. In 2016, the Belle collaboration reported a measurement for the differential cross sections on $\gamma^*\gamma \to \pi^0\pi^0$ in e^+e^- collision. In this work, we obtained the pion GDAs by analyzing the Belle data. Moreover, we investigated matrix elements of the energy-momentum tensor and the gravitational form factors by using the obtained GDAs. The three-dimensional gravitational radii were calculated as $\sqrt{\langle r^2\rangle_{\rm mass}} = 0.32 \sim 0.39\,\text{fm}$ for mass radius and $\sqrt{\langle r^2\rangle_{\rm mech}} = 0.82 \sim 0.88\,\text{fm}$ for the mechanical radius. We found that the mass radius is smaller than the pion charge radius (0.659±0.004 fm, taken from PDG 2018 [1]) and that the mechanical radius is slightly bigger than the charge radius. At this stage, the errors of the Belle measurements are large. However, the precise measurements of $\gamma^*\gamma \to h\bar{h}$ are expected in the near future, since the Belle II collaboration just started taking data with a much higher luminosity of the Super KEKB in 2019. The GDAs are related to form factors of the energy-momentum tensor of partons. These form factors are called gravitational form factors because matrix elements of the energy-momentum tensor are source of gravity. Therefore, it is very interesting to study the gravitational form factors, which contain mass, pressure, and shear-force distributions for hadrons, by obtaining accurate GDAs.

Third, the gluon transversity does not exists in the spin-1/2 nucleons; however, one can study the gluon transversity in the spin-1 hadrons such as deuteron and ρ meson. The gluon transversity is a leading-twist distribution function which needs the helicity flip of a hadron with spin more than one, for example, the deuteron. It is a very important new quantity to probe the transverse spin structure of hadrons by using the deuteron. The deuteron is a bound state of proton and neutron. Since the nucleons themselves do not contribute directly to the gluon transversity due to their spin-1/2 nature, the gluon transversity could be very small in the deuteron. If a finite gluon transversity will be found experimentally, it reflects a new aspect inside the deuteron. At present, the only possible experimental measurement of the gluon transversity is the electron-deuteron DIS at JLab. There is no study to measure it in the proton-deuteron collision, for example, at Fermilab. In this work, we propose that one can use the prompt-photon production process to obtain the deuteron gluon transversity. However, we find that

the measurement of this process is not easy at this stage, since it is proportional to the twist-3 effect in the proton part together with helicity observation of the photon.

Contents

Chapter 1

Introduction

Internal structure of hadrons has been investigated by high-energy lepton-hadron scattering and hadron-hadron collisions. In elastic electron scattering, form factors of nucleons and nuclei can be measured to find their internal charge and magnetic distributions. To probe partonic structure of hadrons, deep inelastic scattering (DIS) of leptons has been investigated since the Stanford Linear Accelerator Center (SLAC) experiment in 1970's. We now know the existence and properties of partons inside the nucleon. In particular, the longitudinal-momentum distributions of the partons (quarks and gluons), which are called parton distribution functions (PDFs), are now well determined in a wide kinematical region.

In the polarized DIS experiment, longitudinally-polarized structure functions and PDFs are studied. It is possible to find the quark-spin content from the experiment, and it indicates the contribution to the nucleon spin from quarks. According to the simple quark model, the nucleon spin 1/2 is explained simply by the combination of three quark spins. However, the European Muon Collaboration (EMC) experiment [2, 3] indicated that a small fraction of nucleon spin is carried by quarks. Therefore, gluon spin and partonic orbital angular momenta also contribute to the nucleon spin, and their contributions are not clear. This is called the spin puzzle of the nucleon. In order to solve the spin puzzle, the generalized parton distributions (GPDs) can be used to figure out the partonic orbital angular momentum contribution to the nucleon spin, and the GPDs can be studied in the deeply virtual Compton scattering (DVCS) [4, 5]. The s-t crossing quantities of GPDs are called generalized distribution amplitudes (GDAs) which can be

measured in the two-photon process [6–8], and one could obtain the information on the GPDs by studying GDAs. Here, s and t are Mandelstam variables. Both the GPDs and the GDAs are three-dimensional structure functions of hadrons, and they reveal important physical quantities of hadrons such as PDFs, electromagnetic form factors, and gravitational form factors. The GPDs and GDAs contain information on matrix elements of the energy-momentum tensor of partons and these matrix elements are expressed by form factors. These form factors are conventionally called gravitational form factors [9, 10] because the matrix elements of the energy-momentum tensor are sources of gravity. It is difficult to probe the gravitational form factors of hadrons directly since the gravitational interaction is too weak, so that the method of using the GPDs and GDAs is a smart way to find the gravitational sources in hadrons. It became a popular topic to investigate the gravitational form factors by the GPDs and the GDAs recently.

The longitudinally-polarized structure functions and PDFs have been investigated extensively and they are relatively well determined now [11, 12]. On the other hand, the transversely-polarized structure functions are not well studied. There exist transversely-polarized PDFs called transversity distributions, which indicate the transverse-polarization of partons in the transversely-polarized hadron [13–15]. The quark transversity distributions exist in the nucleon, whereas the gluon transversity does not exist in the spin-1/2 nucleon. It means that the scale evolution of the quark transversity of the nucleon is decoupled from the gluon, and this is very different from the longitudinally-polarized PDFs. Therefore, the studies of transversity are important in understanding high-energy hadron spin physics. In the transversely-polarized nucleon, there exist the quark transversity distributions which flip the helicities of the nucleon. The quark transversity distributions are leading-twist PDFs as the longitudinally-polarized ones. Due to the chirally odd nature, the quark transversity distributions cannot be measured in the polarized DIS; however, one can study the quark transversity distributions by the Drell-Yan process. The quark transversity distributions are not well determined since there is not enough experimental data at present. As for the gluon transversity, it cannot exist in the spin 1/2 nucleon on account of the violation of angular-momentum conservation. We can only study the gluon transversity in the deuteron and $\triangle$ baryon with spin$\geqslant$1. The gluon transversity distribution could probe non-nucleonic components in the deuteron because the nucleons do not contribute to the gluon transversity . In this sense, it will be interesting to measure the deuteron gluon transversity infuture.

In addition to the gluon transversity, the tensor-polarized distributions are also interesting topics for the deuteron [16]. In general, the deuteron is considered as an S-D mixture system of proton and neutron, and the tensor-polarized distributions vanish if the deuteron is a purely S-wave state. Therefore, the tensor-polarized distributions

should be small in the deuteron since it is mainly in the S-wave. In 2005, the Hermes Collaboration observed large tensor-polarized distributions in comparison theoretical predictions by using electron-deuteron DIS [17]. This is another puzzle in high-energy spin physics. In the near future, this puzzle of the tensor-polarized structure could be solved by the experiments at JLab (DIS) and Fermilab (Drell-Yan) for the deuteron.

These topics are studied in this thesis as structure functions of pion and deuteron. In particular, GDAs of the pion, tensor structure functions and the gluon transversity of the deuteron are investigated. In this chapter, we provide basic knowledge for investigating them. The pion GDAs contain information on form factors and distribution amplitudes, so that they are introduced in Sec. 1.1. For the studies on the deuteron structure functions, we explain basics of parton model and deep inelastic scattering in Sec. 1.2. Scale dependence of parton distribution functions is described by the Dokshitzer-Gribov-Lipatov-Altarelli-Parisi (DGLAP) evolution equations, which are discussed in Sec. 1.3. The GDAs are one type of three-dimensional structure functions, and they are related to the GPDs by the s-t crossing. These three-dimensional structure functions are introduced in Sec. 1.4. Then, the formalism and results are discussed for the tensor-polarized structure functions of the deuteron, especially on a tensor-polarized spin asymmetry of the Drell-Yan process, in Chap. 2. As the second topic, we explain the GDA studies on the pion by using the two-photon process $\gamma^*\gamma \to \pi^0\pi^0$ in Chap. 3. The prompt photon production process is investigated to obtain the deuteron gluon transversity in the Chap. 4. These results are summarized in Chap. 5.

1.1 Form factors and distribution amplitudes

1.1.1 Form factor

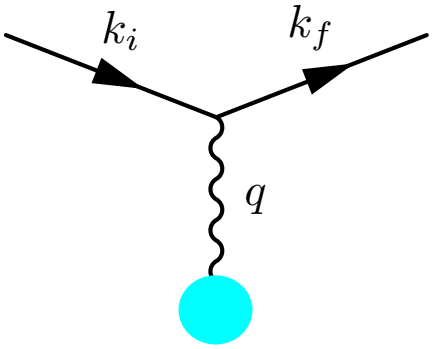

FIGURE 1.1: Elastic electron scattering from the charge distribution $e\rho(\vec{x})$.

A charge distribution of a hadron can be probed by an electron-hadron elastic scattering process. First, let us consider the simple case of a static charge distribution $e\rho(\vec{x})$, where

e is the elementary electric charge and $\vec{x}$ is the space coordinate. We consider the elastic electron scattering from this charge distribution as shown in Fig. 1.1, where k_i, k_f, and q are momenta for the initial electron, final electron, and the virtual photon, respectively. The cross section of the elastic electron scattering from this charge distribution is derived in the following way [18]. The electromagnetic field $A^\mu(\vec{x})$ of the target is expressed by the scalar potential ϕ as $A^\mu = (\phi, \vec{0})$, and ϕ is related to the charge distribution by the Gauss law as $\nabla^2\phi = -e\rho(\vec{x})$. The transition amplitude for this process is given by the electron current $j_\mu(x) = -e\bar{u}_f\gamma_\mu u_i e^{-iq\cdot x}$ and the electromagnetic field as $T_{fi} = -i\int d^4x\, j_\mu(x)A^\mu(x)$, which becomes

$$T_{fi} = ie\bar{u}_f\gamma_\mu u_i A^\mu(q), \tag{1.1}$$

where $A^\mu(q)$ is the Fourier transform of $A^\mu(x)$. Using the relation $A^\mu(q) = 2\pi\delta(E_f - E_i)$ $\int d^3x e^{i\vec{x}\cdot\vec{q}}A^\mu(\vec{x})$, we obtain

$$T_{fi} = 2i\pi\delta(E_f - E_i)(e\bar{u}_f\gamma_\mu u_i)\int d^3x e^{i\vec{x}\cdot\vec{q}}A^\mu(\vec{x}). \tag{1.2}$$

By considering the relation $\vec{\nabla}^2(e^{i\vec{x}\cdot\vec{q}}) = -\vec{q}^{\,2}e^{i\vec{x}\cdot\vec{q}}$ and integration by parts with the Gauss law, we obtain

$$T_{fi} = 2i\pi\delta(E_f - E_i)(e\bar{u}_f\gamma_0 u_i)\frac{1}{q^2}(-e)\int d^3x e^{i\vec{x}\cdot\vec{q}}\rho(\vec{x}). \tag{1.3}$$

The integral part of this equation is the Fourier transform of the charge distribution, and it is called the form factor:

$$F(q^2) = \int d^3x e^{i\vec{x}\cdot\vec{q}}\rho(\vec{x}). \tag{1.4}$$

Then, the cross section is expressed as

$$\frac{d\sigma}{d\Omega} = \left(\frac{d\sigma}{d\Omega}\right)_{\text{Mott}}|F(q^2)|^2. \tag{1.5}$$

Here, the Mott cross section is for the pointlike particle. For a scalar hadron h, the form factor is defined by the matrix element of the electromagnetic current J^μ_{em} as

$$\langle h(p_2)|J^\mu_{\text{em}}(0)|h(p_1)\rangle = (p_1 + p_2)^\mu F(q^2). \tag{1.6}$$

1.1.2 Relation between form factor and distribution amplitude

The form factor $F(q^2)$ of a hadron is factorized into a hard part calculated by perturbative quantum chromodynamics (QCD) and a soft part called a distribution amplitude

at large $Q^2 = -q^2$. Here, we try to express the pion form factor in the factorized form. It is useful to use the light-cone basis $a = (a^0, a^1, a^2, a^3)$

$$a^{\pm} = \frac{1}{\sqrt{2}}(a^0 \pm a^3), \quad a_\perp = (a^1, a^2), \tag{1.7}$$

for this description. Let us consider the process $\gamma^*\pi^+ \to \pi^+$ shown in Fig. 1.2. The amplitude of $\gamma^*\pi^+ \to \pi^+$ is defined as $\epsilon_\alpha M^\alpha$, where ϵ_α is the polarization vector of the virtual photon, and we will show how to express M^α by the distribution amplitudes (DAs) of the pion in the following [19]. In Fig. 1.2, we choose the virtual photon momentum (q) direction to be the z axis, and two timelike vectors $\nu = (1, 0, 0, 1)/\sqrt{2}$ and $\nu' = (1, 0, 0, -1)/\sqrt{2}$ are introduced. The momenta in Fig. 1.2 can be expressed with ν and ν', they are $q = \frac{Q}{\sqrt{2}}\nu - \frac{Q}{\sqrt{2}}\nu'$, $p_1 = \frac{Q}{\sqrt{2}}\nu'$, $p_2 = \frac{Q}{\sqrt{2}}\nu$, $k_1 = xp_1$, $k_3 = (1-x)p_1 = \bar{x}p_1$, $k_2 = yp_2$, $k_4 = (1-y)p_2 = \bar{y}p_2$ and $q_1 = (1-y)p_2 - (1-x)p_1$ for the gluon. The amplitude of Fig. 1.2 is

$$\begin{aligned}
M^\alpha =& (-i)\int \frac{d^4k_1}{(2\pi)^4}\int \frac{d^4k_2}{(2\pi)^4} C_F \left[(-ig\gamma^\mu)_{ce}\frac{il\!\!\!/_{ef}}{l^2}(-ie_u\gamma^\alpha)_{fa}\frac{-i(-ig\gamma_\mu)_{bd}}{q_1^2}\right. \\
&\left. +(-ie_u\gamma^\alpha)_{ce}\frac{il\!\!\!/_{1ef}}{l_1^2}(-ig\gamma^\mu)_{fa}\frac{-i(-ig\gamma_\mu)_{bd}}{q_1^2}\right] \\
&\times \int d^4z e^{-ik_2 z}\left\langle \pi^+(p_2)\left|T\bar{u}_c(z)d_d(0)\right|0\right\rangle \int d^4w e^{ik_1 w}\left\langle 0\left|T\bar{d}_b(0)u_a(w)\right|\pi^+(p_1)\right\rangle \\
=& (p_1+p_2)^\alpha \int_0^1 dx \int_0^1 dy \left[\phi(y,(1-y)Q)\frac{2\pi C_F\alpha_s(Q^2)e_u f_\pi^2}{3(1-x)(1-y)Q^2}\phi^*(x,(1-x)Q)\right],
\end{aligned} \tag{1.8}$$

where the pion decay constant $f_\pi = 130.7$ MeV [20] is defined by the matrix element

$$\left\langle \pi^+(p_2)\left|\bar{u}(0)\gamma^5\gamma^\mu d(0)\right|0\right\rangle = -if_\pi p_2^\mu. \tag{1.9}$$

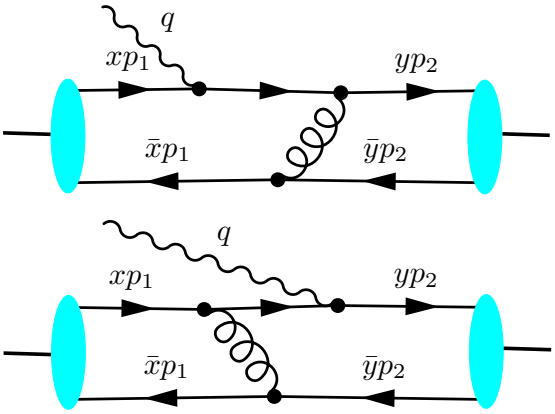

FIGURE 1.2: Electromagnetic form factor of pion in terms of distribution amplitudes.

We use the light-cone variables in Eq. (1.8) and the momentum integrals become δ functions for the variables z^+ and $\vec{z}_\perp$, and it leads to the distribution amplitude (DA) defined by

$$\phi(y) = \frac{i}{f_\pi}\int \frac{dz^-}{2\pi} e^{-i(yp_2^+)z^-} \left\langle \pi^+(p_2)\left|\bar{u}(z^-)\gamma^5\gamma^+ d(0)\right|0\right\rangle . \tag{1.10}$$

It indicates the amplitude for finding a quark and an antiquark with the momentum $k_2^+ = yp_2^+$ and $k_4^+ = (1-y)p_2^+$, respectively, in π^+. We have non-local operators $\bar{d}(z^-)\gamma^5\gamma^+ u(0)$ for π^- and $1/\sqrt{2}\left[\bar{u}(z^-)\gamma^5\gamma^+ u(0) - \bar{d}(z^-)\gamma^5\gamma^+ d(0)\right]$ for π^0 in the DA definition. Here, we consider only the case that the photon interacts with a quark, it should have the symmetry relationship ($x \to 1-x, y \to 1-y$) for the case that the photon interacts with an antiquark. By adding the antiquark term, Eq. (1.8) becomes

$$\begin{aligned} M^\alpha =& (p_1+p_2)^\alpha F(q^2) \\ =& (p_1+p_2)^\alpha \int_0^1 dx \int_0^1 dy \left[\phi(y,(1-y)Q)\frac{2\pi C_F \alpha_s(Q^2) e_u f_\pi^2}{3(1-x)(1-y)Q^2}\phi^*(x,(1-x)Q)\right. \\ &\left. + \phi(y,yQ)\frac{2\pi C_F \alpha_s(Q^2) e_{\bar{d}} f_\pi^2}{3xyQ^2}\phi^*(x,xQ)\right], \end{aligned} \tag{1.11}$$

so that the form factor $F(q^2)$ is obtained with the DAs at high Q^2. If the isospin symmetry is satisfied, the DA of π^+ is same with those of π^- and π^0. The DA of π^0 has the symmetry relation $\phi(x) = \phi(1-x)$ due to the charge-conjugation invariance, and this indicates that the probability for finding the quark with momentum fraction x is same with the probability for finding the antiquark with momentum fraction x in a pion. The pion DA is normalized as

$$\int_0^1 dx \phi(x) = 1. \tag{1.12}$$

In general, the DAs are scale dependent, and the Q dependence of $\phi(y,Q)$ follows the ERBL (Efremov-Radyushkin-Brodsky-Lepage) evolution equations [21, 22], and the general form for $\phi(x,Q)$ of the pion is given by

$$\begin{aligned} \phi(x,Q) =& 6x(1-x)\sum_{n=0,2}^{\infty} a_n C_n^{3/2}(2x-1)\left(\ln\frac{Q^2}{\Lambda_{QCD}^2}\right)^{-\gamma_n/2\beta_0}, \\ \gamma_n =& 2C_F\left(1 - \frac{2}{(n+1)(n+2)} + 4\sum_{j=2}^{n+1}\frac{1}{j}\right), \end{aligned} \tag{1.13}$$

where $C_n^{3/2}$ are the Gegenbauer polynomials and γ_n are the one-loop anomalous dimensions. Since γ_n are positive except for $\gamma_0 = 0$, and the terms with positive γ_n in Eq. (1.13)

will decrease rapidly as Q^2 increases. Therefore, only the first term in Eq.(1.13) survives at high energy Q^2, and the asymptotic form is $\phi(x) = 6x(1-x)$ which is Q^2 independent.

The DAs of mesons are important physical quantities which are often used in the high energy exclusive processes and B meson decays. In the previous part, we only discussed the DA of pion [19, 23–25] which is a pseudoscalar meson. There are also interesting papers for the DAs of other mesons. In Refs. [26–28] the DAs of scalar mesons like $f_0(980)$ are defined. The authors of Refs. [29–31] systematically studied the vector meson DAs where the higher-twist DAs are also introduced. As for the tensor meson such as $f_2(1270)$, the DAs are investigated in Refs. [32–34].

1.1.3 Form factors of nucleons

The electromagnetic form factors of nucleon are defined as

$$\langle N(p_2)|J^{\mu}_{\rm em}(0)|N(p_1)\rangle = \bar{u}(p_2)\left[\gamma^{\mu}F_1(q^2) + \frac{\kappa}{2M_N}F_2(q^2)i\sigma^{\mu\nu}q_{\nu}\right]u(p_1), \tag{1.14}$$

where κ is the anomalous magnetic moment, $\sigma^{\mu\nu}$ is defined by $\sigma^{\mu\nu} = \frac{i}{2}[\gamma^{\mu},\gamma^{\nu}]$, M_N is the nucleon mass, $F_1(q^2)$ is the Dirac form factor, and $F_2(q^2)$ is the Pauli form factor. In the limit $q^2 \to 0$, the effective charge is $F_1(0)e$ and the magnetic moment is $(F_1(0) + \kappa F_2(0))e/(2M_N)$. The elastic electron-nucleon scattering is shown in Fig. 1.3, and the differential cross section can be expressed by the electromagnetic form factors as

$$\frac{d\sigma}{d\Omega} = \frac{\alpha^2}{4E_1^2\sin^4\frac{\theta}{2}}\frac{E_2}{E_1}\left[(F_1^2 - \frac{\kappa^2q^2}{4M_N^2}F_2^2)\cos^2\frac{\theta}{2} - \frac{q^2}{2M_N^2}(F_1+\kappa F_2)^2\sin^2\frac{\theta}{2}\right], \tag{1.15}$$

where E_1 and E_2 are the initial and final electron energies, respectively. The form factors G_E and G_M are defined as linear combinations of F_1 and F_2 so that no interference terms

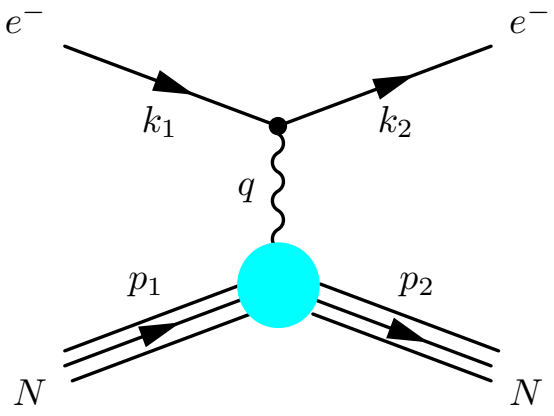

FIGURE 1.3: Electron-nucleon elastic scattering.

$G_E G_M$ appear in Eq. (1.15):

$$G_E = F_1 + \frac{\kappa q^2}{4M_N^2} F_2,$$
$$G_M = F_1 + \kappa F_2, \tag{1.16}$$

where G_E and G_M are the electric and magnetic form factors of the nucleon. Then, the differential cross section is

$$\frac{d\sigma}{d\Omega} = \frac{\alpha^2}{4E_1^2 \sin^4 \frac{\theta}{2}} \frac{E_2}{E_1} \left[\frac{G_E^2 + \tau G_M^2}{1+\tau} \cos^2 \frac{\theta}{2} + 2\tau G_M^2 \sin^2 \frac{\theta}{2} \right], \tag{1.17}$$

with $\tau = -q^2/(4M_N^2)$. In Eq. (1.17), the first term is the electromagnetic interaction and the second one is the magnetic interaction. This cross section is similar to the differential cross section of electron-muon scattering

$$\left.\frac{d\sigma}{d\Omega}\right|_{e\mu} = \frac{\alpha^2}{4E_1^2 \sin^4 \frac{\theta}{2}} \frac{E_2}{E_1} \left[\cos^2 \frac{\theta}{2} - \frac{q^2}{2M_N^2} \sin^2 \frac{\theta}{2} \right]. \tag{1.18}$$

In the limit $q^2 \to 0$, only the electric form-factor term survives in Eq. (1.17), both cross sections become the same.

In the subsection 1.1.2, the form factor of pion is expressed by the DA at high Q^2 (above a few GeV^2). In principle the nucleon from factors can be also factorized into a hard part calculated by perturbative quantum chromodynamics (QCD) and a soft part which is the nucleon DA. However, the nucleon DA is much more complicated than the one of pion meson and it is seldom studied. Here, we will not discuss the relation between nucleon form factors and DAs.

1.2 Parton model and deep inelastic scattering

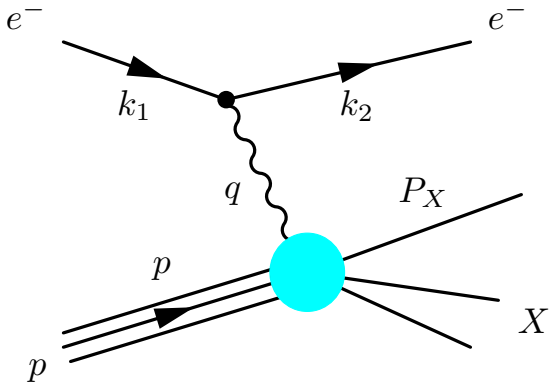

FIGURE 1.4: Electron-proton deep inelastic scattering.

In Fig. 1.3, the electron-proton elastic process can be described by the electromagnetic form factors. As the virtual-photon momentum square $Q^2 = -q^2$ increases, the proton is broken into many hadrons, and this process is called deep inelastic scattering (DIS). The electron-proton DIS is shown in Fig. 1.4, and the differential cross section is expressed as

$$d\sigma = \frac{e^4}{q^4}\frac{1}{2k_1^0}\frac{d^3k_2}{(2\pi)^3\,2k_2^0}\,2\pi\,L_{\mu\nu}W^{\mu\nu}, \tag{1.19}$$

where $L^{\mu\nu} = 2(k_1^\mu k_2^\nu + k_1^\nu k_2^\mu + \frac{q^2}{2}g^{\mu\nu})$ is the lepton tensor and $W^{\mu\nu}$ is the hadron tensor defined by

$$W^{\mu\nu} = \frac{1}{4\pi M_p}\int d^4x e^{iqx}\frac{1}{2}\sum_\sigma \langle\, p,\sigma|J^\mu_{\rm em}(x)J^\nu_{\rm em}(0)|\, p,\sigma\rangle\,. \tag{1.20}$$

Here, p is the initial proton momentum, and σ indicates its spin. Since the lepton tensor $L_{\mu\nu}$ is symmetric, the symmetric form of $W^{\mu\nu}$ is

$$W^{\mu\nu} = -W_1 g^{\mu\nu} + \frac{W_2}{M_p^2}p^\mu p^\nu + \frac{W_4}{M_p^2}q^\mu q^\nu + \frac{W_5}{M_p^2}(p^\mu q^\nu + q^\mu p^\nu). \tag{1.21}$$

In order to satisfy the current conservation $q_\mu W^{\mu\nu} = q_\nu W^{\mu\nu} = 0$, there are only two independent structure functions W_1 and W_2 left in Eq. (1.21), so it can be reexpressed as

$$W^{\mu\nu} = W_1(-g^{\mu\nu} + \frac{q^\mu q^\nu}{q^2}) + \frac{W_2}{M_p^2}(p^\mu - \frac{p\cdot q}{q^2}q^\mu)(p^\nu - \frac{pq}{q^2}q^\nu). \tag{1.22}$$

For the vertex $\gamma^* p \to X$, there are two independent Lorentz invariant variables, $Q^2 = -q^2$ and $\nu = \frac{p\cdot q}{M_p}$, whereas there is only one variable Q^2 in the elastic scattering (see Eq.(1.14)). In the rest frame of the proton, $\nu = k_1^0 - k_2^0$ is the energy loss of the incoming electron. By using the lepton tensor and the hadron tensor in Eq. (1.22), we obtain the cross section in terms of the structure functions W_1 and W_2:

$$\frac{d\sigma}{d\Omega} = \frac{\alpha^2}{4E_1^2\sin^4\frac{\theta}{2}}\frac{E_2}{E_1}\left[W_2(\nu,Q^2)\cos^2\frac{\theta}{2} + 2W_1(\nu,Q^2)\sin^2\frac{\theta}{2}\right]. \tag{1.23}$$

In the limit $Q^2 \to \infty$, the proton is considered as an assembly of free quarks, and the DIS process can be viewed as electron-quark elastic scattering. The structure functions W_1 and W_2 are expressed by the parton distribution functions (PDFs) shown in Fig. 1.5,

and the functions F_1 and F_2 are usually used instead of W_1 and W_2:

$$\begin{aligned} \nu W_1 \to F_2(x) &= \sum_i e_i^2 x \left[q_i(x) + \bar{q}_i(x) \right], \\ M_p W_2 \to F_1(x) &= \frac{1}{2x} F_2(x), \end{aligned} \tag{1.24}$$

where i indicates quark flavor and $q_i(x)$ is the probability for finding the struck quark i with the momentum fraction $x = Q^2/(2M_p\nu) = Q^2/(2p \cdot q)$ of proton momentum in the infinite momentum frame. In this Bjorken scaling limit ($Q^2 \to \infty$ and $\nu \to \infty$ limit), F_2 depends only on the Bjorken x. The second equation $2xF_1(x) = F_2(x)$ is called the Callan-Gross relation, which results from the fact that the quark is a spin-1/2 particle. Since the proton momentum is fully carried by partons, the momentum sum rule should be satisfied,

$$\int_0^1 dx\, x \left[\sum_i \{ q_i(x) + \bar{q}_i(x) \} + g(x) \right] = 1. \tag{1.25}$$

Here, $g(x)$ is the gluon distribution function. The PDFs shown in Fig. 1.5 can be expressed by the Fourier transform of a correlator as

$$q_i(x) = \frac{1}{2} \int \frac{dz^-}{2\pi} \left\langle p \left| \bar{q}_i(z^-) \gamma^+ q_i(0) \right| p \right\rangle e^{-ixp^+z^-}. \tag{1.26}$$

Here, the gauge link to satisfy the color gauge invraiance is abbreviated for simplicity.

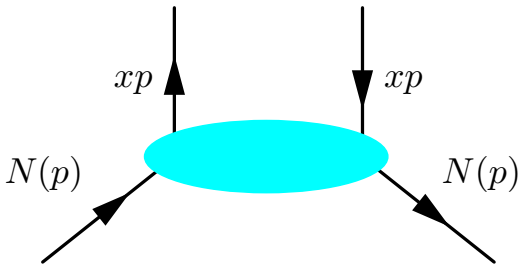

FIGURE 1.5: PDFs for quarks.

1.3 DGLAP evolution equation for PDFs

The scale dependence of the PDFs is discussed in the following. The process $\gamma^* p \to X$ is described as the quark with momentum fraction $x = -q^2/2p \cdot q$ interacts with virtual photon in the parton picture. However, the struck quark can radiate a gluon before or after it is hit by the virtual photon. Then, the quark distribution functions are modified by the process $\gamma^* q \to qg$ shown in Fig. 1.6. At the order α_s which is the running

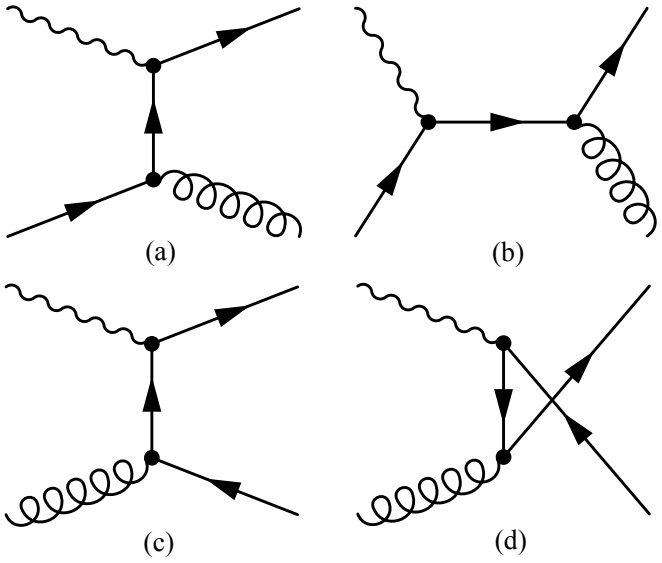

FIGURE 1.6: Quark distribution functions are modified by two types of processes. The first one is $\gamma^* q \to qg$ (see (a) and (b)), and the second one is $\gamma^* g \to q\bar{q}$ (see (c) and (d)).

coupling constant of QCD, a quark-antiquark pair can be produced by photon-gluon collision shown in Fig. 1.6. If we also consider the contribution from $\gamma^* g \to q\bar{q}$, the Q^2 dependence of the quark distribution can be described by

$$\frac{dq_i(x,Q^2)}{d\log Q^2} = \frac{\alpha_s}{2\pi}\int_x^1 \frac{dy}{y}\left[q_i(x,Q^2)P_{qq}(\frac{x}{y}) + g(x,Q^2)P_{qg}(\frac{x}{y})\right], \tag{1.27}$$

where $P_{qq}(z)$ and $P_{qg}(z)$ are splitting functions. The function $P_{qq}(z)$ is the probability that a quark has a fraction z of the initial momentum by emitting a gluon, and $P_{qg}(z)$ indicates the probability that the quark carries a fraction z of the gluon momentum in the process $g \to q\bar{q}$. They are explicitly written as

$$\begin{aligned} P_{qq}(z) =& \frac{4}{3}\frac{1+z^2}{(1-z)_+} + 2\delta(1-z), \\ P_{qg}(z) =& \frac{1}{2}\left[z^2 + (1-z)^2\right]. \end{aligned} \tag{1.28}$$

in the leading order of α_s.

Similarly, the evolution of the gluon distribution function comes from the processes of a gluon emission from quark and of three gluon vertex shown in Fig. 1.7.

$$\frac{dg(x,Q^2)}{d\log Q^2} = \frac{\alpha_s}{2\pi}\int_x^1 \frac{dy}{y}\left[\sum_i q_i(x,Q^2)P_{gq}(\frac{x}{y}) + g(x,Q^2)P_{gg}(\frac{x}{y})\right], \tag{1.29}$$

where the splitting function $P_{gq}(z)$ is given by $P_{gq}(z) = P_{qq}(1-z)$, since the final gluon with z momentum fraction means the final quark momentum fraction should be $1-z$

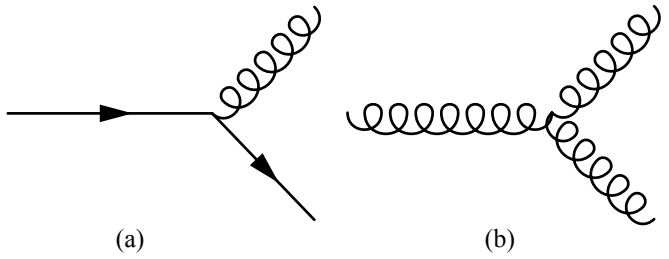

FIGURE 1.7: Splitting processes of (a) an initial quark emits a gluon and (b) a gluon splits into two gluons.

in the process $q \to qg$. The splitting functions are given by

$$\begin{aligned} P_{gq}(z) =& P_{gq}(1-z), \\ P_{gg}(z) =& 6\left[\frac{1-z}{z} + \frac{z}{(1-z)_+} + z(1-z)\right] + (\frac{11}{2} - \frac{n_f}{3})\delta(1-z). \end{aligned} \tag{1.30}$$

Equations (1.27) and (1.29) are called DGLAP (Dokshitzer-Gribov-Lipatov-Altarelli-Parisi) evolution equations.

1.4 Three-dimensional structure functions of hadrons

1.4.1 Proton spin puzzle

The quark model was proposed by M. Gell-Mann and G. Zweig in 1964 to classify numerous hadron states, and the quark model works successfully to explain major hadron properties. In this naive quark model, the proton contains three valence quarks, and the proton spin comes from the combination of spins of these valence quarks:

$$\frac{1}{2} = \frac{1}{2}(\triangle u_v + \triangle d_v), \Delta q = q^+ - q^-. \tag{1.31}$$

In the parton model, in addition to quark spins, the proton spin could also come from contributions of gluon spin and partonic orbital angular momenta. Therefore, the proton spin is written as the summation of their contributions:

$$\begin{aligned} \frac{1}{2} =& \frac{1}{2}\triangle\Sigma + L_q + (\triangle g + L_g), \\ \triangle\Sigma =& (\triangle u^+ + \triangle d^+ + \triangle s^+), \triangle q^+ = \triangle q + \triangle\bar{q}. \end{aligned} \tag{1.32}$$

In 1988, the European Muon Collaboration discovered that only a small fraction of the spin is carried by the quarks in the proton [2, 3], and this is called the proton spin puzzle illustrated in Fig. 1.8. In order to solve the spin puzzle of the proton, one needs to figure out each spin contribution in Eq. (1.32). The quark spin contribution

$\triangle\Sigma$ can be measured by longitudinally polarized DIS and Drell-Yan process, and the heavy meson production in the semi-inclusive DIS is often used to study the gluon spin contribution $\triangle g$. As for the orbital-angular momentum in the proton, the GPDs provide us a way to investigate the contribution from partonic orbital-angular momentum $\triangle L$ to the proton spin [4, 5], and the GPDs are one type of three-dimensional structure functions of hadrons.

Recently studies indicate $\triangle\Sigma \approx 0.30 \pm 0.05$, $L_q \approx 0.2 \pm 0.1$ and $\triangle g + L_g \approx 0.15 \pm 0.10$ at $Q^2 = 4$ GeV^2 [11, 12]; however, precise measurements are still needed to reduce the uncertainties.

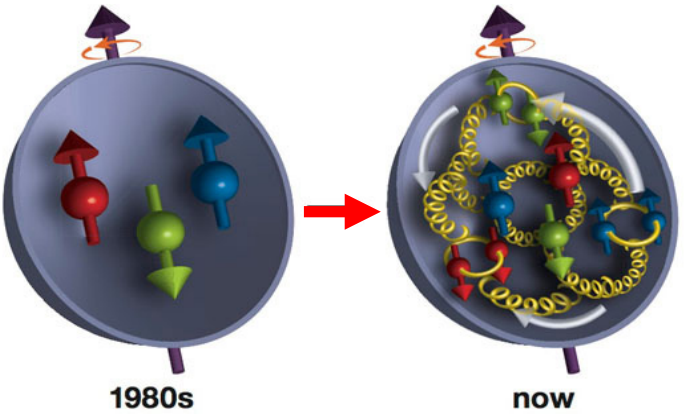

FIGURE 1.8: Proton spin puzzle, picture from BNL website.

1.4.2 Generalized parton distributions

The GPDs can be investigated in deeply virtual Compton scattering (DVCS) process [4, 5, 35–37], deeply virtual meson production (DVMP) process [38–42], timelike Compton scattering (TCS) [43], $2 \to 3$ hadronic reaction processes such as $N + N \to N + \pi + B$ (N: nucleon, B: baryon) [44], and exclusive pion-induced Drell-Yan process [45].

Here, we will use the DVCS to illustrate the properties of GPDs, and the details of GPDs can be found in the review papers [46–49]. The kinematics of DVCS is shown in Fig. 1.9, and some momentum notations are defined as follows

$$\bar{P} = \frac{p_1 + p_2}{2}, \quad \Delta = p_2 - p_1, \quad t = \Delta^2, \quad x = \frac{-q_1^2}{2p_1 \cdot q_1}, \quad \xi = \frac{\Delta^+}{p_1^+ + p_2^+}, \tag{1.33}$$

where we choose the average momentum of the nucleon $\bar{P}$ to be z axis, and $k_1^+ = (x+\xi)\bar{P}$ and $k_2^+ = (x-\xi)\bar{P}$ are the momenta of initial and final quarks, respectively. In the light-cone coordinates of Eq.(1.7), p_1 and p_2 are dominated by the $+$ components. The photon

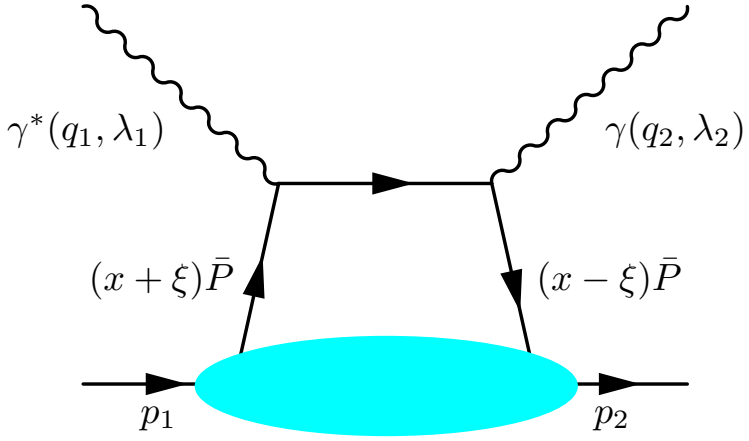

FIGURE 1.9: Deeply virtual Compton scattering of nucleon.

polarization vectors $\epsilon(\lambda_1)$ are defined as follows

$$\epsilon(0) = \frac{1}{Q}(|\vec{q}_1|, 0, 0, q_1^0), \quad \epsilon(\pm) = \frac{1}{\sqrt{2}}(0, \mp 1, -i, 0). \tag{1.34}$$

The amplitude of the DVCS can be separated into a hard part and a soft part by factorization at $Q^2 \gg \Lambda^2_{\rm QCD}$, and the soft part involves the GPDs. In the following, we show how to express the DVCS amplitude by the GPDs. The hard part is the Compton scattering $\gamma^* q \to \gamma q$. There is another Feynman diagram by exchanging two quark-photon vertices in Fig. 1.9, so that the amplitude is expressed as [50]

$$\begin{aligned} T = &- i\sum_q (-e^2 e_q^2)\epsilon(\lambda_1)_\mu \epsilon(\lambda_2)^*_\nu \int \frac{d^4k_2}{(2\pi)^4}\left[\frac{\gamma^\mu i(\not{k}_1 + \not{q}_1)\gamma^\nu}{(k_1+q_1)^2+i\epsilon} + \frac{\gamma^\nu i(\not{k}_1 - \not{q}_2)\gamma^\mu}{(k_1-q_2)^2+i\epsilon}\right]_{ba} \\ &\times \int d^4y e^{-ik_2 y} \left\langle h(p_2)\left|T\bar{q}_b(y)q_a(0)\right|h(p_1)\right\rangle, \end{aligned} \tag{1.35}$$

where a and b are the spinor indices, and the physical meaning of the second line is to remove an incoming quark with momentum k_1 in the nucleon h and to absorb a outgoing quark with momentum k_2. We use the Fierz identity

$$\bar{q}_b(y)q_a(0) = \frac{1}{4}\gamma^\lambda_{ab}\bar{q}\gamma_\lambda q + \frac{1}{4}(\gamma^5\gamma^\lambda)_{ab}\bar{q}\gamma_\lambda\gamma^5 q + \frac{1}{4}I^\lambda_{ab}\bar{q}q + \frac{1}{4}(\gamma^5)_{ab}\bar{q}\gamma^5 q + \frac{1}{4}\sigma^{\alpha\beta}_{ab}\bar{q}\sigma_{\alpha\beta}q, \tag{1.36}$$

in Eq. (1.35). Here, since the trace of an odd number of γ^μ is zero, only the first two terms remain, and they are the leading-twist contributions. Then, Eq. (1.35) becomes

$$\begin{aligned}
T =& -\sum_q (e^2 e_q^2)\epsilon(\lambda_1)_\mu \epsilon(\lambda_2)^*_\nu \int \frac{d^4k_2}{(2\pi)^4}\frac{1}{4}\left\{ Tr\left[\frac{\gamma^\mu(\not{k}_1+\not{q}_1)\gamma^\nu\gamma^-}{(k_1+q_1)^2+i\epsilon}+\frac{\gamma^\nu(\not{k}_1-\not{q}_2)\gamma^\mu\gamma^-}{(k_1-q_2)^2+i\epsilon}\right]\right. \\
&\times \int d^4y e^{-ik_2 y}\left\langle h(p_2)\left|T\bar{q}(y)\gamma^+ q(0)\right|h(p_1)\right\rangle \\
&+ Tr\left[\frac{\gamma^\mu(\not{k}_1+\not{q}_1)\gamma^\nu\gamma^5\gamma^-}{(k_1+q_1)^2+i\epsilon}+\frac{\gamma^\nu(\not{k}_1-\not{q}_2)\gamma^\mu\gamma^5\gamma^-}{(k_1-q_2)^2+i\epsilon}\right] \\
&\left.\times \int d^4y e^{-ik_2 y}\left\langle h(p_2)\left|T\bar{q}(y)\gamma^+\gamma^5 q(0)\right|h(p_1)\right\rangle\right\}. \qquad (1.37)
\end{aligned}$$

The traces of the γ matrices are calculated, and then the amplitude becomes

$$\begin{aligned}
T =& -\sum_q (e^2 e_q^2)\epsilon(\lambda_1)_\mu \epsilon(\lambda_2)^*_\nu \left\{ g_T^{\mu\nu}\left[\frac{1}{x-\xi+i\epsilon}+\frac{1}{x+\xi+i\epsilon}\right]\right. \\
&\times \frac{1}{2}\int \frac{dy^-}{2\pi}e^{-ix\bar{P}y^-}\left\langle h(p_2)\left|T\bar{q}(y^-)\gamma^+ q(0)\right|h(p_1)\right\rangle + i\epsilon^{\mu\nu+-}\left[-\frac{1}{x-\xi+i\epsilon}+\frac{1}{x+\xi+i\epsilon}\right] \\
&\left.\times\frac{1}{2}\int \frac{dy^-}{2\pi}e^{-ix\bar{P}y^-}\left\langle h(p_2)\left|T\bar{q}(y^-)\gamma^+\gamma^5 q(0)\right|h(p_1)\right\rangle\right\}, \qquad (1.38)
\end{aligned}$$

where $g_T^{\mu\nu}$ is defined as

$$g_T^{\mu\nu} = \begin{pmatrix} 0 & 0 & 0 & 0 \\ 0 & -1 & 0 & 0 \\ 0 & 0 & -1 & 0 \\ 0 & 0 & 0 & 0 \end{pmatrix}. \qquad (1.39)$$

The terms $g_T^{\mu\nu}$ and $\epsilon^{\mu\nu+-}$ in Eq. (1.38) indicate that the incoming and outgoing photons have same transverse helicities according to Eq. (1.34).

The DVCS amplitude (1.38) contains two kinds of GPDs. One is defined by the matrix element of $\bar{q}(y^-)\gamma^+ q(0)$, and the other is by the one of $\bar{q}(y^-)\gamma^+\gamma^5 q(0)$. In this way, the quark GPDs, $H^q(x,\xi,t)$, $E^q(x,\xi,t)$, $\tilde{H}^q(x,\xi,t)$, and $\tilde{E}^q(x,\xi,t)$, are defined by the relations

$$\begin{aligned}
&\frac{1}{2}\int \frac{dy^-}{2\pi}e^{-ix\bar{P}y^-}\left\langle h(p_2)\left|\bar{q}(y^-)\gamma^+ q(0)\right|h(p_1)\right\rangle \\
=&\frac{1}{2P^+}\left[H^q(x,\xi,t)\bar{u}(p_2)\gamma^+ u(p_1)+E^q(x,\xi,t)\bar{u}(p_2)\frac{i\sigma^{+\alpha}\Delta_\alpha}{2m}u(p_1)\right], \qquad (1.40) \\
&\frac{1}{2}\int \frac{dy^-}{2\pi}e^{-ix\bar{P}y^-}\left\langle h(p_2)\left|\bar{q}(y^-)\gamma^+\gamma^5 q(0)\right|h(p_1)\right\rangle \\
=&\frac{1}{2P^+}\left[\tilde{H}^q(x,\xi,t)\bar{u}(p_2)\gamma^+\gamma^5 u(p_1)+\tilde{E}^q(x,\xi,t)\bar{u}(p_2)\frac{\gamma^5\Delta^+}{2m}u(p_1)\right]. \qquad (1.41)
\end{aligned}$$

The functions $H^q(x,\xi,t)$ and $\tilde{H}^q(x,\xi,t)$ are nucleon helicity-conserving ones, while $E^q(x,\xi,t)$ and $\tilde{E}^q(x,\xi,t)$ are nucleon helicity-flipping ones. The helicity-flipping term $E^q(x,\xi,t)$ indicate a contribution from quark angular momenta, which can be use to solve the proton spin puzzle [48, 51, 52]. In the forward limit ($p_1 = p_2$), the GPDs are related to the PDFs of Eq. (1.26),

$$\begin{aligned} H^q(x,0,0) =& q(x)\theta(x) - \bar{q}(-x)\theta(-x), \\ \tilde{H}^q(x,0,0) =& \Delta q(x)\theta(x) + \Delta\bar{q}(x)\theta(-x), \end{aligned} \tag{1.42}$$

where $\Delta q(x)$ is the polarized PDF. If we integrate Eq. (1.40) over x, it becomes the electromagnetic form factors in Eq.(1.14):

$$\begin{aligned} \int_{-1}^{1} dx H^q(x,\xi,t) =& F_1(t), \\ \int_{-1}^{1} dx E^q(x,\xi,t) =& \kappa F_2(t), \end{aligned} \tag{1.43}$$

where the ξ dependence disappears after the integral. As for Eq. (1.41), it is related to the axial and pseudoscalar form factors,

$$\begin{aligned} \int_{-1}^{1} \tilde{H}^q(x,\xi,t) =& g_A^q(t), \\ \int_{-1}^{1} \tilde{E}^q(x,\xi,t) =& g_P^q(t), \end{aligned} \tag{1.44}$$

where these form factors are defined by

$$\left\langle h(p_2) \left| \bar{q}(0)\gamma^\mu\gamma^5 q(0) \right| h(p_1) \right\rangle = \bar{u}(p_2) \left[\gamma^\mu\gamma^5 g_A^q(t) + \frac{\gamma^5\Delta^\mu}{2m} g_P^q(t) \right] u(p_1). \tag{1.45}$$

It is possible to find the orbital-angular-momentum contribution L_q to the proton spin by using the GPDs in combination with Δq:

$$\begin{aligned} J_q =& \frac{1}{2}\int_{-1}^{1} dx x \left[H^q(x,\xi,t=0) + E^q(x,\xi,t=0) \right] \\ =& \frac{1}{2}\Delta q + L_q. \end{aligned} \tag{1.46}$$

Therefore, important physical quantities, the PDFs, the form factors, and the orbital-angular-momentum contributions, can be studied by the GPDs.

In the above discussion, the nucleon GPDs are defined through the operators $\bar{q}\gamma^\mu q$ and $\bar{q}\gamma^\mu\gamma^5 q$ in Eq. (1.40) and Eq. (1.41), and the parton helicities are conserved because of the vector current operator and the axial vector current operator. In Ref. [53], the nucleon

GPDs which flip the parton helicities are shown for both quarks and gluon, and they are called transversity GPDs ($H_T,\ E_T,\ \tilde{H}_T,\ \tilde{E}_T$).

So far, we considered the nucleon case; however, there are also GPDs of the scalar and vector hadrons. For example, the GPDs of pion [54, 55] are also defined in the same way as the nucleon ones,

$$H^q_\pi(x,\xi,t) = \frac{1}{2}\int \frac{dy^-}{2\pi} e^{-ix\bar{P}y^-} \left\langle \pi^+(p_2) \left| \bar{q}(y^-)\gamma^+ q(0) \right| \pi^+(p_1) \right\rangle . \tag{1.47}$$

There is no axial-vector matrix element of Eq. (1.41) due to the spinless pion. There are more GPDs for the vector hadrons such as deuteron and ρ meson than nucleon GPDs due to the spin-1 nature. The parton-helicity conserved GPDs of deuteron are first studied in Ref. [56, 57], and parton-helicity flipped GPDs are investigated in Ref. [58].

In addition to the quark GPDs, there also exist gluon GPDs for mesons and nucleons shown in Fig. 1.10 , and it is defined for the pion as

$$H^g_\pi(x,\xi,t) = \frac{1}{\bar{P}^+}\int \frac{dy^-}{2\pi} e^{-ix\bar{P}^+y^-} \left\langle \pi^+(p_2) \left| G^{+\mu}(y^-) G^+_\mu(0) \right| \pi^+(p_1) \right\rangle . \tag{1.48}$$

However, the details of gluon GPDs will not be discussed in this thesis since they are involved in higher-order calculations.

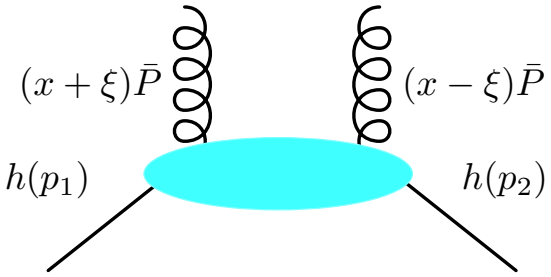

FIGURE 1.10: Gluon GPDs of hadrons

The leading-twist (twist-2) GPDs are introduced in the above section, and there are also studies for twist-3 GPDs of nucleon, one can check the details in Refs. [59–61].

1.4.3 Generalized distribution amplitudes

In the previous section, we studied the GPDs by the DVCS. If we consider the s-t crossed channel of the DVCS, it is $\gamma^*\gamma \to h\bar{h}$ in Fig. 1.11. In this two-photon process, we have a new physical quantity called the generalized distribution amplitude (GDA) in the soft part by factorization [6–8, 62], and the GDAs are the s-t crossing quantity of the GPDs. The GDAs describe the production of $h\bar{h}$ from a quark-antiquark or gluon pair, and it

is similar to the DA of Eq. (1.10) except for the difference in the final state: there is one hadron in the DA and a hadron pair in the GDA. The $\gamma^*\gamma \to h\bar{h}$ process is shown in Fig. 1.11, and the kinematical variables are given as

$$P = q_1 + q_2, \quad Q^2 = -q_1^2, \quad q_2^2 = 0, \quad \frac{k_1^+}{P^+} = z, \quad \frac{p_1^+}{P^+} = \zeta, \quad s = W^2 = (p_1 + p_2)^2, \quad (1.49)$$

where k_1 and k_2 are the momenta of quark and antiquark, and p_1 and p_2 are the momenta of final-state hadron and anti-hadron. The direction of q_1 is along the z axis, and q_2 is along the negative z axis. In the light-cone coordinate, k_1, k_2, p_1 and p_2 are dominated by the $+$ components. We need to have $Q^2 \gg \Lambda^2_{\rm QCD}, W^2$ to satisfy the factorization condition for describing the process by the GDAs and a hard part. Here, we take the pion as an example to study the GDA properties. The GDAs are defined by

$$\Phi_q^{\pi\pi}(z, \zeta, W^2) = \int \frac{dy^-}{2\pi} e^{-iy^-(zP^+)} \langle \pi(p_1)\pi(p_2)| \, \bar{q}(y^-)\gamma^+ q(0) \, |0\rangle \, . \quad (1.50)$$

The variables of the GDAs can be related to those of the GPDs $H_\pi^q(x, \xi, t)$ in Eq. (1.47) by the s-t crossing, and one can get the expression of GPDs from GDAs by the following replacements

$$\begin{aligned} &1 - 2\zeta = \frac{1}{\xi}, \quad 1 - 2z = \frac{x}{\xi}, \quad W^2 = t, \\ &\Phi_q^{\pi\pi}(z, \xi, W^2) \leftrightarrow H_q^\pi \left(\frac{1-2z}{1-2\xi}, \frac{1}{1-2\xi}, W^2 \right) . \end{aligned} \quad (1.51)$$

Therefore, the GDA can be considered as another way to study the GPD. However, we should note that the GDAs may not necessarily correspond to the physical region of the GPDs under the replacement, and it could lead to the unphysical region.

For the $\pi\pi$ state with a fixed C party, we have the following relation

$$\Phi_q^{\pi\pi}(1 - z, \zeta, W^2) = -C\Phi_q^{\pi\pi}(z, \zeta, W^2) = -\Phi_q^{\pi\pi}(z, 1 - \zeta, W^2), \quad (1.52)$$

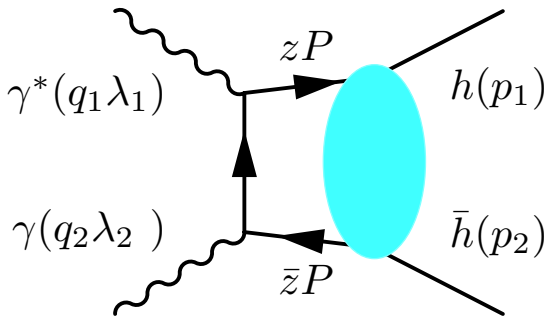

FIGURE 1.11: Generalized distribution amplitudes can be studied in two-photon process.

under the charge conjugation. Therefore, the GDAs for $\pi^+\pi^-$ with the fixed C party can be expressed as

$$\Phi_q^{\pm}(z,\zeta,W^2) = \frac{1}{2}\left[\Phi_q^{\pi^+\pi^-}(z,\zeta,W^2) \pm \Phi_q^{\pi^+\pi^-}(z,1-\zeta,W^2)\right], \tag{1.53}$$

where $\pm$ indicates the C party of $\pi^+\pi^-$. Then, we have

$$\Phi_q^{\pi^+\pi^-}(z,\zeta,W^2) = \Phi_q^{+}(z,\zeta,W^2) + \Phi_q^{-}(z,\zeta,W^2). \tag{1.54}$$

Therefore, $\Phi^{\pi^+\pi^-}$ contains both C-even and C-odd GDAs. Since the C parity of the $\gamma\gamma^*$ is even, only $\Phi_q^+(z,\zeta,W^2)$ is involved in the two-photon process. As for the case of $\pi^0\pi^0$, the C party is even, so it contains only the $\Phi_q^+(z,\zeta,W^2)$ part. If $s = W^2$ is large enough, namely, $Q^2 \gg s \gg \Lambda^2_{\rm QCD}$, the GDA $\Phi_q^{\pi^+\pi^-}(z,\zeta,W^2)$ can be expressed by the pion DA [63].

Now, we consider the isospin (I) of the $\pi\pi$ state. The $I = 0$, 1, and 2 $\pi\pi$ states are

$$\begin{aligned}
|0,0\rangle =& \frac{1}{\sqrt{3}}(\pi^+\pi^- - \pi^0\pi^0 + \pi^-\pi^+),\\
|1,0\rangle =& \frac{1}{\sqrt{2}}(\pi^+\pi^- - \pi^-\pi^+),\\
|2,0\rangle =& \frac{1}{\sqrt{6}}(\pi^+\pi^- + 2\pi^0\pi^0 + \pi^-\pi^+).
\end{aligned} \tag{1.55}$$

The $\pi^0\pi^0$ contains the $I = 0$ and $I = 2$ components, and the $\pi^+\pi^-$ contains the $I = 0$, 1 and 2 components. According to the definition of the GDAs, the isospin of $\bar{q}q$ can be 0 or 1, so that the possible choices for the final $\pi\pi$ state are $I = 0$ ($\pi^0\pi^0, \pi^+\pi^-$) and $I = 1$ ($\pi^+\pi^-$). For the $I = 1$ case, the angular momentum L should be even to keep the positive C party. At the same time, the Pauli-exclusion-principle relation

$$(-1)^L \times (-1)^I \times (-1)^S = +1, \tag{1.56}$$

should be satisfied, so that the $I = 1$ GDAs do not exist in the two-photon process. Therefore, the $\pi\pi$ states should be $I = 0$ and $L = 0, 2$. As a consequence of the isospin invariance, we have

$$\begin{aligned}
\Phi_q^{\pi^0\pi^0}(z,\zeta,W^2) &= \Phi_q^{+}(z,\zeta,W^2),\\
\Phi_u^{+}(z,\zeta,W^2) &= \Phi_d^{+}(z,\zeta,W^2).
\end{aligned} \tag{1.57}$$

In this case, the amplitude is same for both $\pi^0\pi^0$ and $\pi^+\pi^-$ in the two-photon process. There is a momentum sum rule for $\Phi_u^+(z,\zeta,W^2)$ [6–8],

$$\int_0^1 dz(2z-1)\Phi_q^+(z,\zeta,W^2) = \frac{2}{(P^+)^2}\left\langle \pi^+(p_1)\pi^-(p_2)\left|T_q^{++}(0)\right|0\right\rangle, \tag{1.58}$$

where $T_q^{\mu\nu}$ is the energy-momentum tensor for quarks. Here, we have $W^2 > 0$, so that $\langle\pi^+(p_1)\pi^-(p_2)|T_q^{++}(0)|0\rangle$ is a timelike energy-momentum tensor for quarks in the pion. In the spacelike region ($W^2 < 0$), it is $\langle\pi^+(p_1)|T_q^{++}(0)|\pi^+(p_2)\rangle$. By the analytical continuation from the timelike region to the spacelike one, we have the sum rule at $W^2 = 0$ [6–8],

$$\int_0^1 dz(2z-1)\Phi_q^+(z,\zeta,W^2=0) = -2R_\pi\zeta(1-\zeta), \tag{1.59}$$

where R^π is the momentum fraction carried by quarks in the pion.

Now, let us briefly discuss the C-odd (I=1) GDAs of $\pi^+\pi^-$ in order to show the relation to the DAs and the electromagnetic form factor, although they do not appear in the current two-photon process. If Eq.(1.50) is integrated over z, we obtain [8]

$$\int_0^1 dz\Phi_q^-(z,\zeta,W^2) = (2\zeta-1)F(W^2), \tag{1.60}$$

where $F(W^2)$ is the timelike electromagnetic form factor, which is different from the spacelike electromagnetic form factor of Eq. (1.6). $\Phi_q^-(z,\zeta,W^2)$ can be related to the pion DA if the momentum of one of the pions goes to zero ($\zeta = 0$ or 1) [8] as

$$\Phi_q^-(z,\zeta=1,W^2=0) = -\Phi_q^-(z,\zeta=0,W^2=0) = \phi(z), \tag{1.61}$$

where $W^2 = 0$ is taken by neglecting the pion mass, and $\phi(z)$ is defined in Eq. (1.10). As for the gluon GDA, it is defined by

$$\begin{aligned}\Phi_g(z,\zeta,W^2) =& \frac{1}{P^+}\int\frac{dy^-}{2\pi}e^{-izP^+y^-}\left\langle\pi(p_1)\pi(p_2)\left|G^{+\mu}(y^-)G_\mu^+(0)\right|0\right\rangle \\ =& z(1-z)P^+\int\frac{dy^-}{2\pi}e^{-izP^+y^-}\left\langle\pi(p_1)\pi(p_2)\left|A^\mu(y^-)A_\mu(0)\right|0\right\rangle.\end{aligned} \tag{1.62}$$

The symmetry relation of the gluon GDA reads

$$\Phi_g(z,\zeta,W^2) = \Phi_g(1-z,\zeta,W^2) = \Phi_g(1-z,1-\zeta,W^2), \tag{1.63}$$

which is obtained by the exchanges of gluons and also final-state pions.

In Sec. 1.1, we discussed the Q^2 evolution of the DAs for the pion. It is slightly different for the GDAs, since the C-even GDAs Φ_q^+ ($I = 0$) can be mixed with the gluon GDA

due to the evolution. The general expressions of the Q^2-evolved Φ_q^+ and Φ_g are

$$\sum_{q=1}^{nf}\Phi_q^+(z,\zeta,W^2,Q^2) = z(1-z)\sum_{odd\,n} 6n_f \sum_{even\,l}^{n+1} B_{nl}(W^2,Q^2)P_l(2\zeta-1)C_n^{3/2}(2z-1),$$
$$\Phi_g(z,\zeta,W^2,Q^2) = z^2(1-z)^2\sum_{odd\,n}\sum_{even\,l}^{n+1} B'_{nl}(W^2,Q^2)P_l(2\zeta-1)C_{n-1}^{5/2}(2z-1), \quad (1.64)$$

where P_l is the Legendre polynomial, and it indicates that the final $\pi\pi$ state is in the angular-momentum state $L=l, L_z=0$, and B_{nl} and B'_{nl} are expansion coefficients. The Q^2 dependence for $B_{nl}(W^2,Q^2)$ is written as

$$B_{nl}(W^2,Q^2) = B_{nl}^+(W^2)\left(\frac{\alpha_s(Q^2)}{\alpha_s(Q_0^2)}\right)^{K_n^+} + B_{nl}^-(W^2)\left(\frac{\alpha_s(Q^2)}{\alpha_s(Q_0^2)}\right)^{K_n^-}, \quad (1.65)$$

where Q_0^2 is the initial scale. This Q^2 dependence is the same for $B'_{nl}(W^2,Q^2)$ in the gluon GDA. The detailed expressions of $K_n^\pm$ are found in Ref. [7]. Since $K_n^\pm$ is positive except for $K_1^- = 0$, only the term with K_1^- survives in Eq. (1.65) at very large Q^2. Therefore, we have the asymptotic form for GDAs as

$$\sum_{q=1}^{nf}\Phi_q^+(z,\zeta,W^2) = 18n_f z(1-z)\left[B_{10}^-(W^2) + B_{12}^-(W^2)P_2(2\zeta-1)\right],$$
$$\Phi_g(z,\zeta,W^2) = 48z^2(1-z)^2\left[B_{10}'^-(W^2) + B_{12}'^-(W^2)P_2(2\zeta-1)\right]. \quad (1.66)$$

By using Eq. (1.59) and Eq. (1.64), we have [6–8]

$$B_{12}^-(0) = -B_{10}^-(0) = \frac{10R_\pi}{9n_f}, \quad (1.67)$$

where n_f is the number of flavors.

As for the $\Phi_q^-(z,\zeta,W^2)$, it is very similar to the pion DA, since it does not mix with the gluon GDA:

$$\Phi_q^-(z,\zeta,W^2,Q^2) = 6z(1-z)\sum_{even\,n}\sum_{odd\,l}^{n+1} B_{nl}(W^2,Q^2)C_l^{1/2}(2\zeta-1)C_n^{3/2}(2x-1). \quad (1.68)$$

The Q^2 dependence of $B_{nl}(W^2,Q^2)$ is same as that of the pion DA in Eq. (1.13). According to Eq. (1.60), $B_{01}(W^2)$ is the timelike electromagnetic form factor of π^+. With isospin invariance, we have the relation $\Phi_u^- = -\Phi_d^-$.

In the above case, the leading-twist GDAs are discussed for pion, and the twist-3 GDAs of pion are investigated in Ref. [64]. There are also studies of GDAs for other types of hadrons such as baryons and vector hadrons. For example, the GDAs of baryon [65] are

involved in the process $\gamma^*\gamma \to B\bar{B}$ (B for baryon), and the proton GDAs are just the s-t crossing quantities of the proton GPDs which reveal the orbital-angular momentum contribution in the proton. As for the GDAs of vector hadrons, the authors of Ref. [66] studied the ρ GDA in the process of $\gamma^*\gamma \to \rho^0\rho^0$. To generalize the process $\gamma^*\gamma \to \pi\pi$, the 3π GDAs are proposed for $\gamma^*\gamma \to \pi\pi\pi$ [67].

Chapter 2

Spin Asymmetry for Drell-Yan Process at Fermilab with Tensor-Polarized Deuteron

2.1 Puzzle of tensor-polarized structure function in the deuteron

Tensor-polarized structure functions of the deuteron are different spin observables from the polarized proton structure functions [16, 68], and they are not well understood. It is an interesting topic and the field of tensor structure functions could become a hot topic in a few years, because the JLab experiment will start soon, as the proton spin puzzle created the field of high-energy spin physics. The deuteron could be considered as a nucleus which contains proton and neutron in S wave. In this case, the magnetic moment of deuteron is equal to the sum of magnetic moments of proton and neutron, and the experimental measurement of the magnetic moment supported this S-wave idea. However, the existence of the electric quadrupole moment indicated that the deuteron should also contains a small fraction of the D wave in addition to the S wave. This D-wave admixture is now widely accepted. The D-wave contribution implies finite tensor-polarized structure functions in the deuteron, because there is no tensor polarization for a purely S-wave deuteron. One of the tensor-polarized structure functions is b_1, and it was measured by the HERMES collaboration in 2005 [17]. Although their errors are large,

the data showed that b_1 is much larger than the theoretical prediction in the S-D mixture picture [16, 69]. Therefore, the standard S-D mixture cannot explain the experimental data. In order to solve this puzzle, there are several possible explanations such as six quarks configuration of the deuteron [70], shadowing effects of the nucleus [71–73], and pion effects in the deuteron [70]. Recently, the original calculation of Refs.[16, 69] on the S-D mixture was corrected [74]; however, the theoretical results still indicate large discrepancies from the HERMES data. In this work, we study tensor structure of the tensor-polarized PDFs through the spin asymmetries in the proton-deuteron Drell-Yan process [75], and we hope that future measurements will provide crucial information to find a mechanism for solving the issue.

2.2 Tensor-polarized structure function b_1

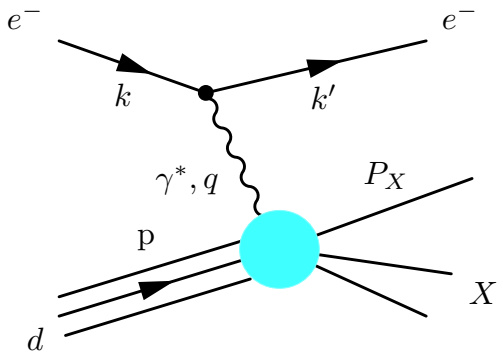

FIGURE 2.1: Deep inelastic scattering of unpolarized electron from polarized deuteron.

The tensor structure function b_1 of deuteron can be studied by DIS, where the beam is unpolarized lepton and the target is the polarized deuteron in Fig. 2.1. For the spin-1 deuteron, there are 8 structure functions in the hadron tensor $W_{\mu\nu}^{\lambda_f\lambda_i}$ [16, 76]:

$$\begin{aligned} W_{\mu\nu}^{\lambda_f\lambda_i} =& \frac{1}{4\pi M}\int d^4x e^{iqx}\,\langle p\,\lambda_f|J_\mu(x)J_\nu(0)|p\,\lambda_i\rangle \\ =& -F_1\hat{g}_{\mu\nu} + \frac{F_2}{M_d\nu}\hat{p}_\mu\hat{p}_\nu + \frac{ig_1}{\nu}\epsilon_{\mu\nu\lambda\sigma}q^\lambda s^\sigma + \frac{ig_2}{M_d\nu^2}\epsilon_{\mu\nu\lambda\sigma}q^\lambda(p\cdot q s^\sigma - s\cdot q p^\sigma) \\ & - b_1 r_{\mu\nu} + \frac{1}{6}b_2(s_{\mu\nu}+t_{\mu\nu}+u_{\mu\nu}) + \frac{1}{2}b_3(s_{\mu\nu}-u_{\mu\nu}) + \frac{1}{2}b_4(s_{\mu\nu}-t_{\mu\nu}). \end{aligned} \tag{2.1}$$

where M_d, p, and q are deuteron mass, deuteron momentum, and momentum transfer. $\hat{g}_{\mu\nu}$ and $\hat{p}_\mu$ are defined by $\hat{g}_{\mu\nu} \equiv g_{\mu\nu} - q_\mu q_\nu/q^2$ and $\hat{p}_\mu \equiv p_\mu - (p\cdot q/q^2)\,q_\mu$. We have $\nu = p\cdot q/M_d$, and the antisymmetric tensor is defined by $\epsilon_{0123} = +1$. The initial and final spin states of the deuteron are denoted as λ_i and λ_f, respectively. The spin vector of the deuteron is s^μ which is expressed by the polarization vectors of the deuteron

$E^\mu(\lambda)$ as

$$
\begin{aligned}
&(s_{\lambda_f\lambda_i})^\mu = -\frac{i}{M_d}\epsilon^{\mu\nu\alpha\beta}E^*_\nu(\lambda_f)E_\alpha(\lambda_i)p_\beta,\\
&E^\mu(\lambda=\pm1) = \frac{1}{\sqrt{2}}(0,\mp1,-i,0), \quad E^\mu(\lambda=0)=(0,0,0,1).
\end{aligned}
\tag{2.2}
$$

The tensors $r_{\mu\nu}$, $s_{\mu\nu}$, $t_{\mu\nu}$, and $u_{\mu\nu}$ are defined as

$$
\begin{aligned}
r_{\mu\nu} =& \frac{1}{\nu^2}\left[q\cdot E^*(\lambda_f)q\cdot E(\lambda_i) - \frac{1}{3}\nu^2\kappa\right]\hat{g}_{\mu\nu},\\
s_{\mu\nu} =& \frac{2}{\nu^2}\left[q\cdot E^*(\lambda_f)q\cdot E(\lambda_i) - \frac{1}{3}\nu^2\kappa\right]\frac{\hat{p}_\mu\hat{p}_\nu}{M_d\nu},\\
u_{\mu\nu} =& \frac{M_d}{\nu}\left[\hat{E}^*_\mu(\lambda_f)\hat{E}_\nu(\lambda_i) + \hat{E}^*_\nu(\lambda_f)\hat{E}_\mu(\lambda_i) + \frac{2}{3}\hat{g}_{\mu\nu} - \frac{2}{3M_d^2}\hat{p}_\mu\hat{p}_\nu\right],\\
t_{\mu\nu} =& \frac{1}{2\nu^2}\left\{q\cdot E^*(\lambda_f)\left[\hat{p}_\mu\hat{E}_\nu(\lambda_i) + \hat{p}_\nu\hat{E}_\mu(\lambda_i)\right]\right.\\
&\left. + \left[\hat{p}_\mu\hat{E}^*_\nu(\lambda_f) + \hat{p}_\nu\hat{E}^*_\mu(\lambda_f)\right]q\cdot E(\lambda_i) - \frac{4\nu}{3M_d}\hat{p}_\mu\hat{p}_\nu\right\}.
\end{aligned}
\tag{2.3}
$$

The structure functions b_1, b_2, b_3 and b_4 are the new quantities for the spin-1 deuteron, whereas F_1, F_2, g_1 and g_2 also exist in the spin-1/2 proton.

In the parton picture, F_1 can be expressed by the PDFs, $F_1 = \frac{1}{2}\sum_i e_i^2\left[q_i(x,Q^2) + \bar{q}_i(x,Q^2)\right]$. Similarly, b_1 is expressed by tensor-polarized PDFs as

$$
\begin{aligned}
b_1 &= \frac{1}{2}\sum_i e_i^2\left[\delta_T q_i(x,Q^2) + \delta_T\bar{q}_i(x,Q^2)\right],\\
\delta_T q_i(x,Q^2) &= q_i^0(x,Q^2) - \frac{q_i^{+1}(x,Q^2) + q_i^{-1}(x,Q^2)}{2},
\end{aligned}
\tag{2.4}
$$

where $\delta_T q_i(x,Q^2)$ is the tensor-polarized PDF, and q_i^λ indicates an unpolarized quark distribution of flavor i in the deuteron spin state λ. The Callan-Gross relation is known as $2xF_1 = F_2$ in the Bjorken scaling limit, and b_1 and b_2 are also related to each other by the similar relation $2xb_1 = b_2$. There exits a sum rule based on the parton model [77]. From the expression (2.4), we obtain the relation

$$
\int dx\, b_1(x) = -\lim_{t\to0}\frac{5}{24}\,t\,F_Q(t) + \frac{1}{9}\int dx\left[4\delta_T\bar{u}(x) + 4\delta_T\bar{d}(x) + \delta_T\bar{s}(x)\right],
\tag{2.5}
$$

where $F_Q(t)$ is the electric quadrupole form factor. If the tensor-polarized antiquark distributions does not exist, it leas to an interesting sum rule for b_1:

$$
\int dx\, b_1(x) = 0.
\tag{2.6}
$$

However, finite antiquark distributions exist, the sum becomes $\int dx\, b_1(x) = \int dx[4\delta_T\bar{u}(x) + 4\delta_T\bar{d}(x) + \delta_T\bar{s}(x)]/9$. Therefore, a finite sum indicates that there exist tensor-polarized

antiquark distributions in the deuteron.

The HERMES collaboration conducted the first measurement of the deuteron structure function b_1 in 2005; however, the experimental measurements indicated that b_1 is not as small as the prediction by the standard convolution model based on the S-D admixture [17]. In this case, it is necessary to study the tensor structure puzzle of the deuteron by considering other mechanisms on the tensor structure in terms of quark and gluon degrees of freedom. The HERMES collaboration also reported the integrals of b_1 as

$$\begin{aligned}\int_{0.002}^{0.85} dx\, b_1(x) &= [1.05 \pm 0.34(stat) \pm 0.35(sys)] \times 10^{-2}, \\ \int_{0.02}^{0.85} dx\, b_1(x) &= [0.35 \pm 0.10(stat) \pm 0.18(sys)] \times 10^{-2},\end{aligned} \tag{2.7}$$

where the first value is obtained in the measured energy range, and the second one is in the range of $Q^2 > 1$ GeV^2. The nonzero integral of b_1 indicates the existence of tensor-polarized distributions for antiquarks $\delta_T\bar{q}(x)$ in the deuteron. In the near future, the structure function b_1 can be measured at JLab, and this could help us to solve the puzzle of tensor structure in the deuteron.

2.3 Tensor-polarized spin asymmetry in proton-deuteron Drell-Yan process

The tensor structure of the deuteron can also be studied by the proton-deuteron Drell-Yan process, and it has the merit in probing $\delta_T\bar{q}(x)$ directly. The Drell-Yan process $p + d \to \mu^+\mu^- + X$ is shown in Fig. 2.2. In the Fermilab-E1309 experiment, the unpolarized proton beam (120 GeV) is provided by the Main Injector, and the polarized deuteron is the target. The center-of-mass energy is $s = (p_1 + p_2)^2$, and the dimuon-mass squared

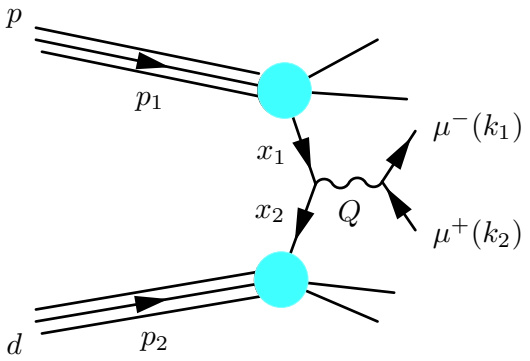

FIGURE 2.2: Drell-Yan process for unpolarized proton and tensor-polarized deuteron.

is given by $M_{\mu\mu}^2 = Q^2 = x_1 x_2 s$. In this process, the hadron tensor is defined as

$$W_{\mu\nu}^{DY} = \frac{1}{4\pi M_d} \int d^4\xi \, e^{-i(k_1+k_2)\cdot\xi} \langle \, p \, d \, | \, J_\mu^{em}(\xi) J_\nu^{em}(0) \, | \, p \, d \, \rangle. \tag{2.8}$$

There exists many structure functions and polarization asymmetries in the Drell-Yan process with unpolarized proton and polarized deuteron. Among them, the tensor-polarized spin asymmetry A_Q [78, 79] can reveal the tensor-polarized PDFs of deuteron. It is defined by

$$A_Q = \frac{1}{\langle \sigma \rangle} \left[\sigma(\bullet, 0) - \frac{\sigma(\bullet, +1) + \sigma(\bullet, -1)}{2} \right], \tag{2.9}$$

where $\pm$ and 0 indicate the deuteron spin states and $\bullet$ is the unpolarized proton. In the parton model, the asymmetry A_Q is expressed by the PDFs and the tensor-polarized PDFs of the deuteron as

$$A_Q = \frac{\sum_i e_i^2 \left[q_i(x_1) \delta_T \bar{q}_i(x_2) + \bar{q}_i(x_1) \delta_T q_i(x_2) \right]}{\sum_i e_i^2 \left[q_i(x_1) \bar{q}_i(x_2) + \bar{q}_i(x_1) q_i(x_2) \right]}. \tag{2.10}$$

In this case, the tensor-polarized distributions $\delta_T q(x)$ and $\delta_T \bar{q}(x)$ of the deuteron can be studied by the spin asymmetry A_Q. Since the antiquark PDFs are extremely small in the large x_1 region, we have the relations $q_i(x_1)\delta_T \bar{q}_i(x_2) \gg \bar{q}_i(x_1)\delta_T q_i(x_2)$ and $q_i(x_1)\bar{q}_i(x_2) \gg \bar{q}_i(x_1) q_i(x_2)$, so that the spin asymmetry of A_Q at large $x_F = x_1 - x_2$ can be simplified as

$$A_Q \simeq \frac{\sum_i e_i^2 \left[q_i(x_1) \delta_T \bar{q}_i(x_2) \right]}{\sum_i e_i^2 \left[q_i(x_1) \bar{q}_i(x_2) \right]} \quad \text{at large } x_F. \tag{2.11}$$

Therefore, the tensor-polarized antiquark distributions $\delta_T \bar{q}_i(x)$ can be directly probed by the measurements of the spin asymmetry A_Q at large x_F. It is necessary to measure the tensor-polarized antiquark distributions by the Drell-Yan process, since they were already indicated by the HERMES data in Eq. (2.7). This Drell-Yan process with the unpolarized proton and polarized deuteron is now under consideration within the Fermilab-E1309 experiment as a future project.

2.4 Results

In calculating $A_Q(x_1, x_2)$ for the Fermilab-E1309 experiment, the unpolarized distributions of proton and deuteron are taken from the MSTW (Martin, Stirling, Thorne, and Watt) PDFs in the leading order of α_s [80]. We adopt the functional form of parameterizations for the tensor-polarized distributions of deuteron based on the HERMES

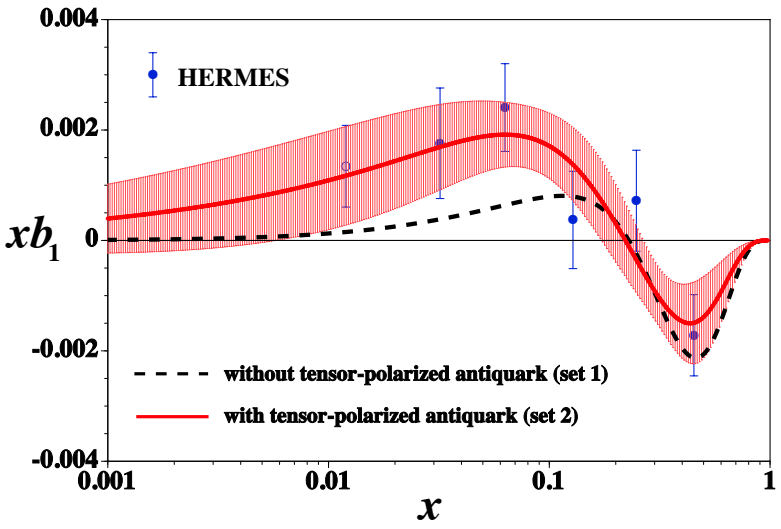

FIGURE 2.3: The structure functions xb_1 are shown for both set 1 and set 2. The orange bands is the uncertainties for the set-2 curve [81].

data at the average scale $Q^2 = 2.5$ GeV^2 in Ref. [81]. In the parameterization, there are two analysis types in order to check the impact of tensor-polarized antiquark distributions. In set 1, only the tensor-polarized valence-quark distributions are considered at $Q^2 = 2.5$ GeV^2, while finite tensor-polarized antiquark distributions ($\delta_T\bar{u}$=$\delta_T\bar{d}$=$\delta_T\bar{s}$) are also assumed to be available at the initial scale for the set-2 analysis. With the tensor-polarized PDFs for both set 1 and set 2, the values and error bands of xb_1 are shown in Fig. 2.3 in comparison with experimental data. The error bands of a physical quantity $f(x)$ are expressed by the Hessian matrix H_{ij},

$$[\delta f(x)]^2 = \Delta\chi^2 \sum_{i,j} \left[\frac{\partial f(x)}{\partial \xi_i}\right]_{\hat{\xi}} H_{ij}^{-1} \left[\frac{\partial f(x)}{\partial \xi_j}\right]_{\hat{\xi}}, \tag{2.12}$$

where ξ_i is a parameter, and $\hat{\xi}$ is the minimum parameter set. The Hessian matrix is obtained by expanding χ^2 around the minimum parameter set as $\hat{\xi}$

$$\chi^2(\hat{\xi} + \delta\hat{\xi}) - \chi^2(\hat{\xi}) = \sum_{i,j} H_{ij}\delta\xi_i\delta\xi_j. \tag{2.13}$$

Here, we take $\Delta\chi^2 = 1$ for the error bands in our results. The set-2 tensor-polarized PDFs provides a better description of the HERMES data in comparison with those of the set 1. Moreover, the experimental measurements of the b_1 integral in Eq. (2.7) indicate that the tensor-polarized antiquark distributions are necessary at the initial scale.

In Fig. 2.4, we show the tensor-polarized distributions at $Q^2 = 2.5$ GeV^2. The tensor-polarized antiquark distributions are dominant in the small-x region ($x < 0.02$) in the set 2. There is a node at $x = 0.229$ for set 1 and $x = 0.221$ for set 2 to satisfy the

sum rule $\int dx(b_1)_{valence} = 0$, and this node is also predicted by standard S-D mixture calculations for the deuteron [16, 69, 74]. The tensor-polarized gluon distribution is set to be 0 at $Q^2 = 2.5$ GeV^2.

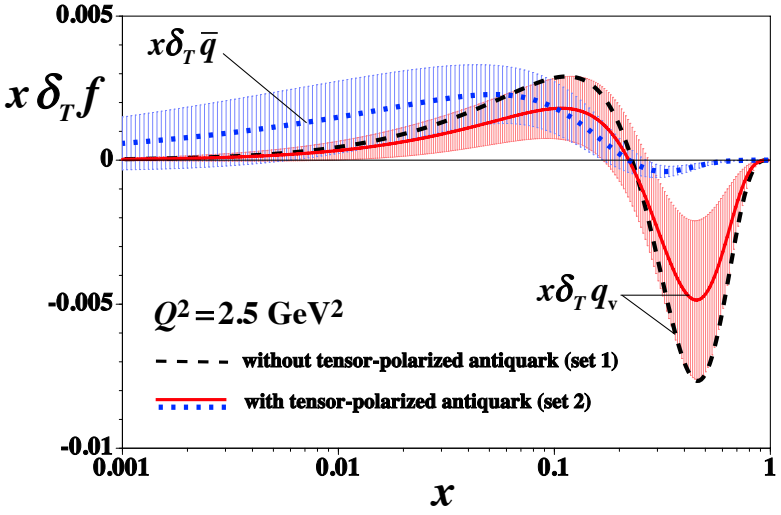

FIGURE 2.4: Tensor-polarized PDFs at the initial energy scale ($Q^2 = 2.5$GeV^2). The dashed curve is the valence-quark distributions $x\delta_T q_v$ in set-1 analysis, where there is no antiquark distribution $x\delta_T \bar{q}$. The solid and dotted curves are the valence-quark distributions $x\delta_T q_v$ and the antiquark distribution $x\delta_T \bar{q}$ in set 2, respectively. [75].

The tensor-polarized distributions at other Q^2 scales ($Q^2 = x_1 x_2 s$) can be obtained by using the DGLAP evolution equations [16]. In Fig. 2.5, we present the tensor-polarized PDFs of the set 1 at the typical Q^2 scale $Q^2 = 30$ GeV^2 for the Fermilab-E1309 Drell-Yan process. We notice that there also exists the finite tensor-polarized distribution for gluon, even though it is set to be zero at the initial scale $Q^2 = 2.5$ GeV^2. Because there are

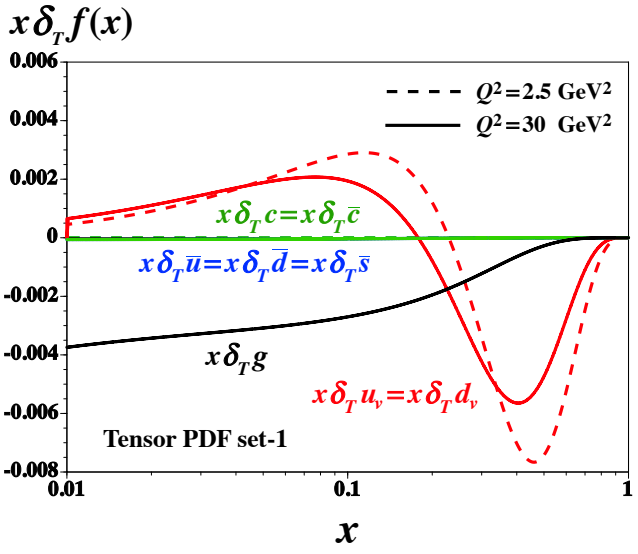

FIGURE 2.5: Tensor-polarized PDFs at $Q^2 = 30$ GeV^2 (solid curves) are compared with the tensor-polarized PDFs at the initial scale (dashed curves) in the set-1 analysis [75].

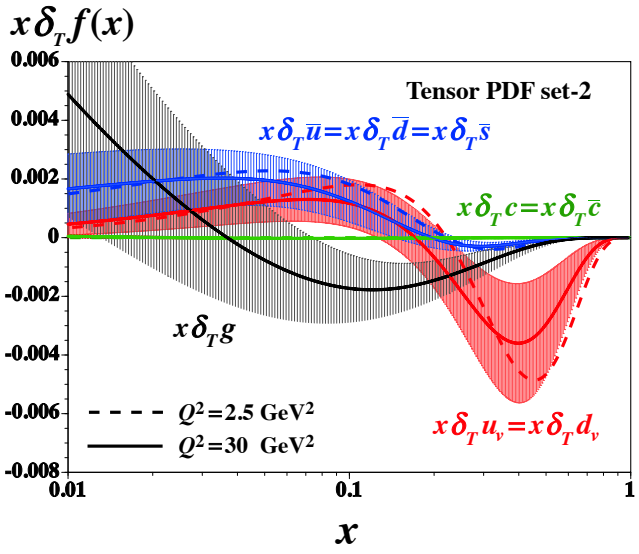

FIGURE 2.6: Tensor-polarized PDFs (solid curves) at $Q^2 = 30$ GeV^2 in comparison with the tensor-polarized PDFs (dashed curves) at the initial energy scale for set-2 analysis [75].

no antiquark tensor-polarized distributions at $Q^2 = 2.5$ GeV^2, the symmetric antiquark distributions ($\delta_T\bar{u} = \delta_T\bar{d} = \delta_T\bar{s} = \delta_T\bar{c} = 0$) hold for any Q^2 scale in the leading order of α_s. The set-2 tensor-polarized distributions at $Q^2 = 2.5$ GeV^2 and $Q^2 = 30$ GeV^2 are shown in Fig. 2.6, and their magnitude is the 10^{-3} order for both tensor-polarized quark and antiquark PDFs. The equality for the antiquarks ($\delta_T\bar{u} = \delta_T\bar{d} = \delta_T\bar{s} \neq 0$) also holds as we change the Q^2 scale.

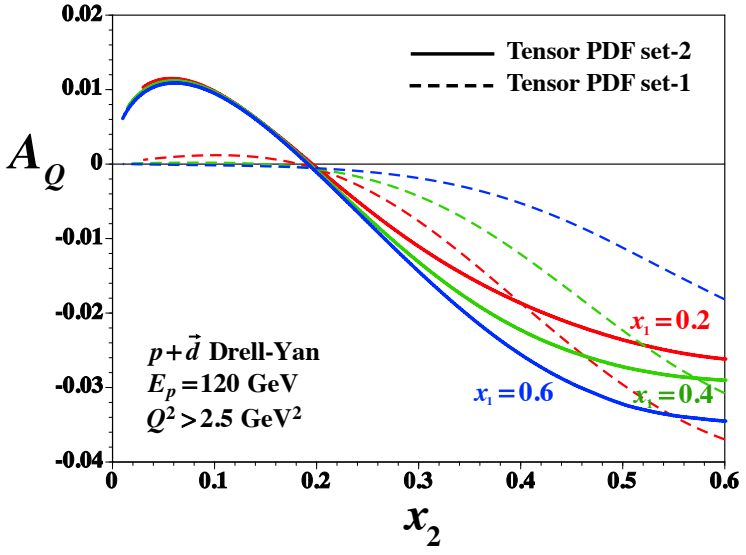

FIGURE 2.7: The spin asymmetries A_Q estimated at typical values $x_1 = 0.2, 0.4$ and 0.6. The solid and dashed curves indicate the spin asymmetries of set 2 and set 1, respectively [75].

The spin asymmetries $A_Q(x_1, x_2)$ of set 1 and set 2 are shown in Fig. 2.7 at the typical values of $x_1 = 0.2$, $x_1 = 0.4$ and $x_1 = 0.6$ [75]. The set-1 results are very different

from those of set 2 at small x_2, and this is because that the antiquark tensor-polarized distributions play an important role when x_2 is small according to Eq. (2.11). The spin asymmetries $A_Q(x_1, x_2)$ are of the oder 10^{-2} for both set 1 and set 2. In Fig. 2.8, we show the spin asymmetries $A_Q(x_1, x_2)$ and its error bands at $Q^2 = 30$ GeV^2, which is typical energy scale for the Fermilab-E1309 Drell-Yan process. We believe that the set-2 results should be more reliable than those of set 1, because the tensor-polarized antiquark PDFs are indicated by the HERMES data with Eq. (2.7). The measurements of the spin asymmetries are now under consideration by the Fermilab-E1309 Collaboration by using our results, and we hope that our studies should be useful for the upcoming experiment.

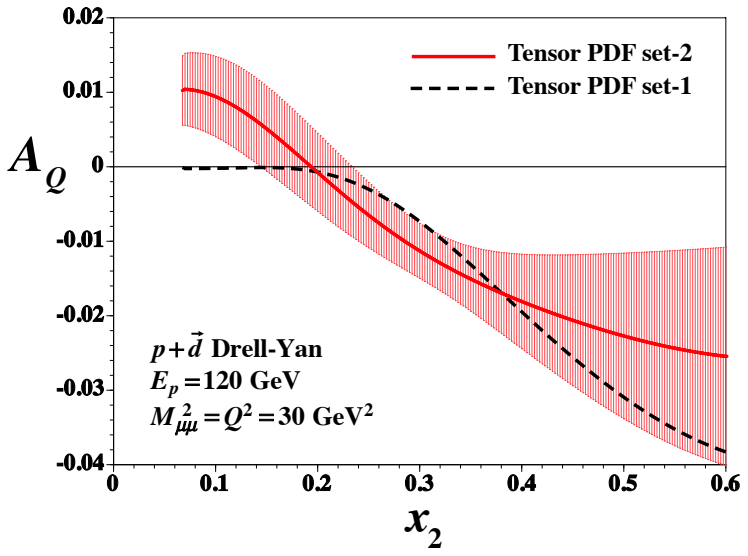

FIGURE 2.8: Spin asymmetries A_Q estimated at $Q^2 = 30$ GeV^2. The dashed curve is set-1 results, and the solid curve indicates spin asymmetries A_Q of the set 2 with the error bands [75].

2.5 Summary

There are new structure functions for the deuteron associated with its tensor structure in comparison with those of proton. In 2005, the tensor-polarized distributions were first measured by HERMES collaboration; however, there is a discrepancy between the experimental data and the theoretical prediction. In order to understand this puzzle, one can use DIS and Drell-Yan process to measure the details of the tensor-polarized distributions. In the Drell-Yan process, the spin asymmetry A_Q is expressed by the tensor-polarized distributions, and it has the advantage to study the tensor-polarized antiquark distributions. In this work, we estimated of the spin asymmetry A_Q for Drell-Yan process at Fermilab, and we found that it is of the order of a few percent. In future,

the tensor-polarized distributions will be measured by JLab (b_1) and Fermilab (A_Q), which may reveal the puzzle of deuteron.

Chapter 3

Generalized Distribution Amplitudes for Pion in Two-Photon Process

3.1 Motivation

The proton spin puzzle indicates that only a small fraction of the spin is carried by the quarks in the proton, and this issue could be solved by investigating the GPDs in the DVCS. As shown in Eq. (1.46), we can obtain the orbital-angular-momentum contribution to the proton spin from the GPDs. In the kinematics where the factorization works, the soft part of the DVCS is expressed by the GPDs. In addition, the GPDs could be measured in the deeply virtual meson production [42], the exclusive hadoronic $2 \to 3$ process [44], and the exclusive pion-induced Drell-Yan process [45]. If we consider the s-t cross channel of DVCS, we get the exclusive process $\gamma^*\gamma \to h\bar{h}$. Similarly, the soft part is described by the amplitude of $q\bar{q} \to h\bar{h}$, which is the GDA. These three-dimensional structure functions will provide us valuable information on internal structure of hadrons such as form factors, PDFs, DAs, and angular-momentum contribution of partons to the nucleon spin.

The GPDs are mainly investigated by $ep \to e\gamma p$ process, for example, at JLab, and the exclusive pion-induced Drell-Yan process $\pi^- + p \to \mu^+\mu^- + n$ could be conducted at Japan Proton Accelerator Research Complex (J-PARC) in future. As for the GDAs,

the Belle Collaboration recently released the measurement of differential cross section for $\gamma^*\gamma \to \pi^0\pi^0$ [82]. In this work, we try to obtain the pion GDAs by analyzing the Belle data. In 2019, the Belle II colloration started to collect data with the updated super KEKB, and the GDAs of other hadrons can be investigated with more precise measurements of $\gamma\gamma^* \to h\bar{h}$ in the near future.

3.2 Pion GDA in process $\gamma^*\gamma \to \pi^0\pi^0$

There are two subprocesses for the reaction $e\gamma \to e\pi\pi$ in Fig. 3.1. The $\pi\pi$ pair must have $C = +$ for the charge conjugation in the $\gamma^*\gamma$ scattering process, so that both $\pi^+\pi^-$ and $\pi^0\pi^0$ can be produced, and the cross section is determined by GDAs $\Phi_q^{\pi\pi}(z, \xi, W^2)$. The amplitudes of $\pi^+\pi^-$ and $\pi^0\pi^0$ are same due to Eqs. (1.54) and (1.57). As for the bremsstrahlung process, the $\pi\pi$ pair must have $C = -1$ for the charge conjugation on account of the single virtual photon and only $\pi^+\pi^-$ is available, and this subprocess is determined by the electromagnetic form factor or distribution amplitudes of $\pi^\pm$ (see Fig. 2.1 in Sec. 1.1).

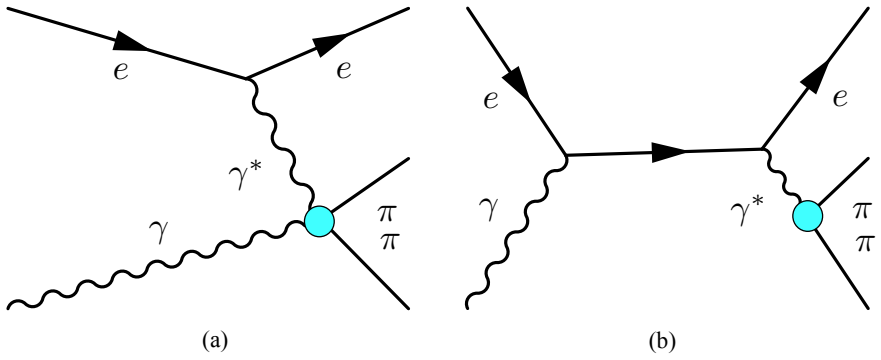

FIGURE 3.1: Subprocess (a) $\pi\pi$ production through $\gamma^*\gamma$ scattering and subprocess (b) $\pi\pi$ production through bremsstrahlung.

In 2016, the Belle Collaboration reported a measurement of the differential cross section for $\gamma^*\gamma \to \pi^0\pi^0$ in the e^+e^- collision, where the electron (or positron) is detected with $\pi^0\pi^0$ while the positron (or electron) is scattered in the forward direction and undetected [82]. In the e^+e^- collision, the $\pi^0\pi^0$ can also come from the collision of two virtual photons, namely, $\gamma^*\gamma^* \to \pi^0\pi^0$. However, the contribution of $\gamma^*\gamma^* \to \pi^0\pi^0$ is very small in comparison with the one of $\gamma^*\gamma \to \pi^0\pi^0$[83]. The Q^2 and W regions of the Belle data are 3.46 GeV$^2 \leqslant Q^2 \leqslant$ 24.25 GeV^2 and 0.5 GeV $< \sqrt{s} = W <$ 2.1 GeV. Due to the charge conjugation, only the subprocess $\gamma^*\gamma$ scattering in the Fig. 3.1 contributes to the Belle data, and the GDAs for π^0 can be obtained without the interference from bremsstrahlung progress. Therefore, only the GDAs $\Phi_q^{\pi^0\pi^0}(z, \xi, W^2)$ are needed to explain the Belle data.

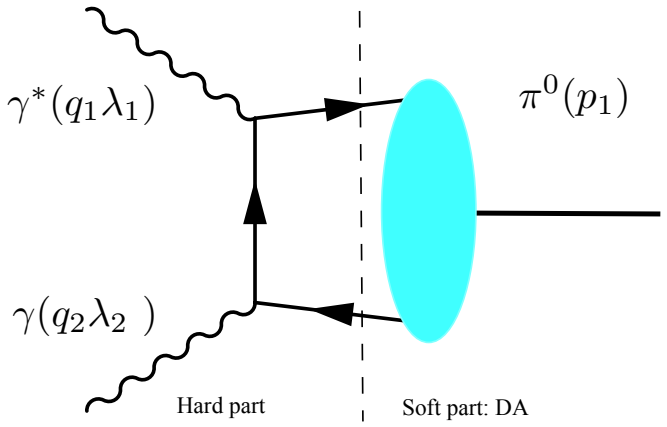

FIGURE 3.2: The transition form factor $F_{\gamma^*\gamma\to\pi^0}$.

The process of $\gamma^*\gamma \to \pi^0\pi^0$ is very similar to $\gamma^*\gamma \to \pi^0$ shown in Fig. 3.2, and the latter one is determined by the transition form factor $F_{\gamma^*\gamma\to\pi^0}$ or the pion DAs [19]. In the factorized processes, they have the same hard part $\gamma^*\gamma \to q\bar{q}$. However, the soft part of the GDAs corresponds to the vector current $\bar{q}\gamma^\mu q$, since the $\pi\pi$ state has the same quantum numbers as the scalar meson f_0 and the tensor meson f_2. The pion DAs are for the axial current $\bar{q}\gamma^\mu\gamma^5 q$ due to the pseudoscalar properties of π. In the process of $\gamma^*\gamma \to \pi^0$, the two photons have the same helicities since π^0 spin is 0. The hadron tensor of $\gamma^*\gamma \to \pi^0$ is expressed by the DA of pion [7, 19, 84–86],

$$\begin{aligned} T^{\mu\nu} &= i\int d^4x e^{-iq_1x}\left\langle \pi^0(P)|TJ^\mu(x)J^\nu(0)|0\right\rangle \\ &= \epsilon_T^{\mu\nu}\sum_q \frac{e_q^2}{2}\int_0^1 dz \frac{\phi_q(z)}{z(1-z)}, \end{aligned} \tag{3.1}$$

where $\phi_q(z)$ is the DA of pion, and antisymmetric tensor $\epsilon_T^{\mu\nu}$ only has nonvanishing transverse components ($\epsilon_T^{12} = 1$). In $\gamma^*\gamma \to \pi^0\pi^0$, the photon helicities are also same and transverse in the leading twist and leading order, and the angular momentum of $\pi^0\pi^0$ should be $L = 0, 2$ and $L_z = 0$.

In the following, we show the relation between the GDAs and the cross section of $\gamma^*\gamma \to \pi^0\pi^0$ in Fig. 3.3. In the center mass frame of γ^* and γ, the momentum of the virtual photon is along z axis, and the polarization vectors $\epsilon(\lambda_1)$ of the virtual photon can be found in Eq. (1.34). The polarization vectors $\epsilon(\lambda_2)$ of the real photon are

$$\epsilon(\pm) = \frac{1}{\sqrt{2}}(0, \mp 1, i, 0). \tag{3.2}$$

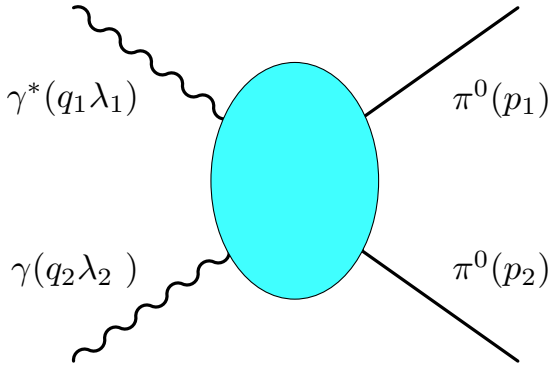

FIGURE 3.3: $\gamma^*\gamma \to \pi^0\pi^0$ process.

The cross section of two-photon process is expressed as

$$d\sigma = \frac{1}{4}\frac{1}{4\sqrt{(q_1\cdot q_2)^2 - q_1^2 q_2^2}} \sum_{\lambda_1,\lambda_2} |(-iT_{\mu\nu}\epsilon^\mu(\lambda_1)\epsilon^\nu(\lambda_2))|^2 d\Phi_2, \tag{3.3}$$

where $d\Phi_2$ is the two-body phase space, and the factor $1/4$ is from the spin average, and $4\sqrt{(q_1\cdot q_2)^2 - q_1^2 q_2^2}$ is the flux factor according to the conventions of Refs. [82, 87]. The hadron tensor $T_{\mu\nu}$ is defined as

$$T_{\mu\nu} = i\int d^4x e^{-iq_1x}\,\langle\pi(p_1)\pi(p_2)|TJ_\mu(x)J_\nu(0)|0\rangle\,, \tag{3.4}$$

and the two-body phase space is given by

$$\begin{aligned}\int d\Phi_2 &= \int \frac{d^3p_1}{(2\pi)^3 2E_1}\frac{d^3p_2}{(2\pi)^3 2E_2}(2\pi)^4\delta^4(P-p_1-p_2)\\ &= \frac{1}{32\pi^2}\sqrt{1-4m_\pi^2/s}\int sin\theta d\theta d\phi,\end{aligned} \tag{3.5}$$

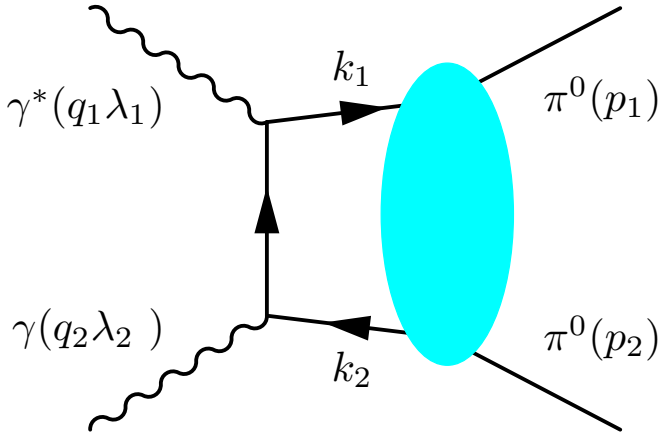

FIGURE 3.4: In the process $\gamma\gamma^* \to \pi^0\pi^0$, the amplitude contains the hard part $\gamma\gamma^* \to q\bar{q}$ and the soft part of the GDAs by factorization. Here, only the leading-twist and leading-order contributions are considered.

where m_π is the pion mass. Here, θ and ϕ are polar and azimuthal angles of the pion in the center-of-mass frame.

In Fig. 3.4, we have $q_1^2 = -Q^2$, $q_2^2 = 0$, and $s = W^2 = (q_1 + q_2)^2 = P^2$ for the center-of-mass energy squared. In the Breit frame, q_1 is defined along the z axis, and we introduce two timelike vectors $\nu = (1,0,0,1)/\sqrt{2}$ and $\nu' = (1,0,0,-1)/\sqrt{2}$. The vectors can be expressed by ν and ν', and they are $q_1 = \frac{Q}{\sqrt{2}}\nu - \frac{Q}{\sqrt{2}}\nu'$, $q_2 = \frac{Q^2+W^2}{\sqrt{2}Q}\nu'$, $k_1 = z\frac{Q}{\sqrt{2}}\nu$ and $k_2 = (1-z)\frac{Q}{\sqrt{2}}\nu$. By the factorization at $Q^2 \gg W^2, \Lambda^2$, the hadron tensor can be expressed by the GDAs in the following way. First, $T_{\mu\nu}$ is expressed by considering the process of Fig. 3.4 as

$$\begin{aligned} T_{\mu\nu} &= i\int d^4x e^{-iq_1x}\,\langle \pi(p_1)\pi(p_2)|TJ_\mu(x)J_\nu(0)|0\rangle \\ &= \sum_q(-e^2e_q^2)\int\frac{d^4k_1}{(2\pi)^4}\left[\frac{\gamma^\mu(\not{k}_1-\not{q}_1)\gamma^\nu}{(k_1-q_1)^2+i\epsilon}+\frac{\gamma^\nu(\not{q}_1-\not{k}_2)\gamma^\mu}{(q_1-k_2)^2+i\epsilon}\right]_{ba} \\ &\quad\times\int d^4y e^{-ik_1y}\,\langle\pi(p_1)\pi(p_2)|T\bar{q}_b(y)q_a(0)|0\rangle\,. \end{aligned} \tag{3.6}$$

For $\bar{q}_b(y)q_a$ in this equation, we use the Fierz identity of Eq. (1.36), where the first two terms $[\gamma^\lambda_{ab}\bar{q}\gamma_\lambda q/4,\ (\gamma^\lambda\gamma_5)_{ab}\bar{q}\gamma_\lambda\gamma_5 q/4]$ and the last one $[\sigma^{\alpha\beta}_{ab}\bar{q}\sigma_{\alpha\beta}q/4]$ are the leading twist terms, while the third and fourth ones $[I^\lambda_{ab}\bar{q}q/4,\ (\gamma_5)_{ab}\bar{q}\gamma_5 q/4]$ are twist-3 terms. Since the trace of an odd number of γ^λ is zero, only the first two terms survive. The second term is the axial-vector current, which cannot exist for $\pi^0\pi^0$ state due to the parity invariance. Then, we obtain

$$\begin{aligned} T_{\mu\nu} &= \sum_q(-e^2e_q^2)\frac{1}{4}\int\frac{dk_1^+}{(2\pi)}Tr\left(\frac{\gamma^\mu(\not{k}_1-\not{q}_1)\gamma^\nu\not{\psi}}{(k_1-q_1)^2+i\epsilon}+\frac{\gamma^\nu(\not{q}_1-\not{k}_2)\gamma^\mu\not{\psi}}{(q_1-k_2)^2+i\epsilon}\right) \\ &\quad\times\int dy^- e^{-iy^-(zP^+)}\left\langle\pi(p_1)\pi(p_2)|T\bar{q}(y^-)\gamma^+q(0)|0\right\rangle. \end{aligned} \tag{3.7}$$

Calculating the hard parts of this equation, we finally obtain the expression in terms of the GDAs as

$$\begin{aligned} T_{\mu\nu} &= -g_T^{\mu\nu}\sum_q\left(\frac{e^2e_q^2}{2}\right)\int_0^1 dz\frac{2z-1}{z(1-z)}\int\frac{dy^-}{2\pi}e^{-iy^-(zP^+)}\left\langle\pi(p_1)\pi(p_2)|T\bar{q}(y^-)\gamma^+q(0)|0\right\rangle \\ &= -g_T^{\mu\nu}\sum_q\left(\frac{e^2e_q^2}{2}\right)\int_0^1 dz\frac{2z-1}{z(1-z)}\Phi_q^{\pi\pi}(z,\xi,W), \end{aligned} \tag{3.8}$$

where the matrix $g_T^{\mu\nu}$ is found in Eq. (1.39). Next, $T_{\mu\nu}$ is multiplied by the photon polarization vectors of Eqs. (1.34) and (3.2) to obtain the cross section of Eq. (3.3), we have the differential cross section

$$d\sigma = \frac{1}{4}\alpha^2\pi\frac{\sqrt{1-\frac{4m^2}{s}}}{Q^2+s}|A_{++}|^2\sin\theta d\theta. \tag{3.9}$$

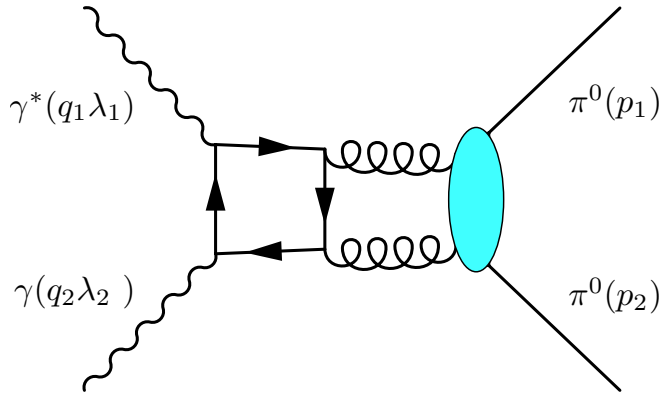

FIGURE 3.5: $\gamma^*\gamma \to \pi^0\pi^0$.

Here, the helicity amplitude is defined as $A_{\lambda_1\lambda_2} = \frac{1}{e^2}\epsilon^\mu(\lambda_1)\epsilon^\nu(\lambda_2))T_{\mu\nu}$, and only the leading-twist and leading-order contributions A_{--} and A_{++} are considered. The leading-twist amplitude A_{++} is expressed by the GDA $\Phi_q^{\pi^0\pi^0}(z,\xi,W^2)$ as

$$A_{++} = \sum_q \frac{e_q^2}{2}\int_0^1 dz \frac{2z-1}{z(1-z)}\Phi_q^{\pi^0\pi^0}(z,\xi,W^2). \tag{3.10}$$

We have $A_{--} = A_{++}$ due to the parity invariance.

For the $\gamma^*\gamma \to \pi^0\pi^0$ process, there are only three independent helicity amplitudes A_{++}, A_{+-} and A_{0+} by the parity invariance. The amplitude A_{++} is the leading-twist, so it is dominant at large Q^2. In this case, the helicities of two photons are same and transverse. The A_{+-} indicates that the angular momentum projection is $L_z = 2$ for the two photons, while the collinear quark-antiquark pair can not have $L_z = 2$. Therefore, A_{+-} contributes to the cross ssction with the gluon GDA at the next-to-leading order [88], and it is suppressed by $\alpha_s(Q^2)$ (see Fig. 3.5). The higher-twist contribution A_{0+} with a longitudinal polarization requires a helicity flip along the fermion line, and it decreases as $1/Q$ [7, 64, 88]. Therefore, only the leading-twist and leading-order contributions $A_{++} = A_{--}$ are considered in Eq. (3.9).

3.3 GDA expression

3.3.1 Relation between GDAs and $\pi\pi$ elastic scattering

The following is the general expression of the GDAs at very large $Q^2 = -q_1^2$ as shown by the asymptotic form of Eq. (1.66):

$$\sum_q \Phi_q^{\pi^0\pi^0}(z,\xi,W^2) = 18 n_f z(1-z)(2z-1)[\tilde{B}_{10}(W) + \tilde{B}_{12}(W)P_2(\cos\theta)],$$
$$\tilde{B}_{nl}(W) = \bar{B}_{nl}(W)\exp(i\delta_l). \tag{3.11}$$

Since the variable ζ is expressed by the angle θ as

$$\zeta = \frac{1+\beta\cos\theta}{2}, \tag{3.12}$$

we have the following relations between $\tilde{B}_{nl}(W)$ and $B_{nl}(W)$:

$$[B_{10}(W) + B_{12}(W)P_2(2\zeta-1)] = [\tilde{B}_{10}(W) + \tilde{B}_{12}(W)P_2(\cos\theta)],$$
$$\tilde{B}_{10}(W) = B_{10}(W) - \frac{1-\beta^2}{2}B_{12}(W),$$
$$\tilde{B}_{12}(W) = \beta^2 B_{12}(W), \quad \beta^2 = 1 - 4m_\pi^2/s. \tag{3.13}$$

In the limit of $W^2 = 0$, there is a relation $B_{12}(0) = -B_{10}(0) = 10/(9n_f)R_\pi$, where R_π is the momentum fraction carried by quarks, as shown in Eq. (1.59), and below the $K\bar{K}$ threshold, the δ_0 and δ_2 are the $\pi\pi$ elastic scattering phase shifts in the isospin=0 channel [7, 89]. In the process $\gamma^*\gamma \to \pi^0\pi^0$, the intermediate states $M\bar{M}$ can be $\pi\pi$, $K\bar{K}$ and $\eta\eta$. The imaginary part of the GDA appears when the intermediate states are on shell.

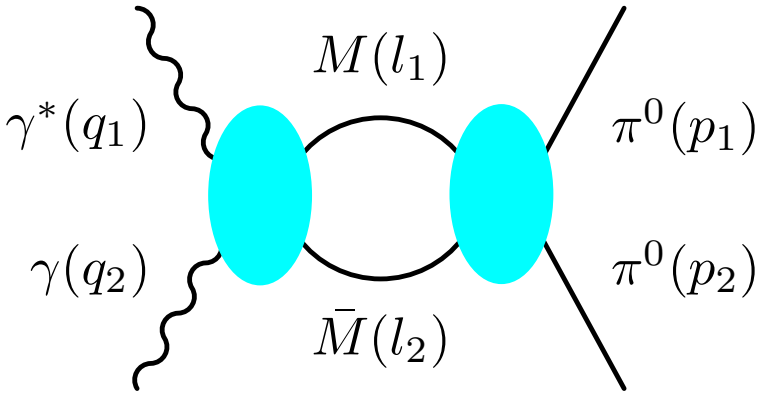

FIGURE 3.6: $\gamma^*\gamma \to \pi^0\pi^0$ through the intermediate states $M\bar{M}$, the amplitude is marked as M_0.

In the Fig. 3.6, the discontinuity part of the amplitude is

$$\begin{aligned}
\mathrm{Disc}M_0 &= \sum_{M\bar{M}} M_2^* M_1, \\
\mathrm{Disc}M_0 &= \frac{-i}{2}\int \frac{d^4 l_1}{(2\pi)^4}(-2\pi i)\delta(l_1^2 - m_\pi^2)(-2\pi i)\delta((k-l_1)^2 - m^2) M_2^*(s,\cos\theta) M_1(s,\cos\theta_l), \\
\mathrm{Disc}M_0 &= \frac{i}{64\pi^2}\beta \int d\Omega M_2^*(s,\cos\theta) M_1(s,\cos\theta_l),
\end{aligned} \tag{3.14}$$

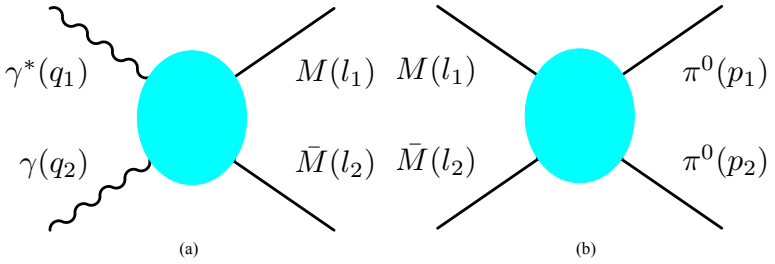

FIGURE 3.7: (a): $\gamma\gamma^* \to M\bar{M}$ process, the amplitude is marked as M_1. (b): $M\bar{M} \to \pi^0\pi^0$ process , the amplitude is marked as M_2 .

where l_1 and l_2 are the momenta of M and $\bar{M}$, respectively, $k = l_1 + l_2$ is the total momentum, $\beta = \sqrt{1 - 4m_\pi^2/s}$, and M_1 is the amplitude of $\gamma^*\gamma \to M\bar{M}$ and M_2 is the amplitude of $M\bar{M} \to \pi^0\pi^0$ shown in the Fig. 3.7 .

Below the $K\bar{K}$ threshold, we only need to consider $\pi\pi$ as the intermediate state, and the amplitude M_2 is just $\pi\pi$ elastic scattering in the isospin=0 channel. Therefore, the amplitude $M_2^*(s,\cos\theta)$ can be expressed as

$$M_2(s, cos\theta) = 32\pi \sum_{l=0}^{\infty}(2l+1)t_l(s)P_l(\cos\theta), \quad t_l(s) = \frac{\sin\delta_l(s)e^{i\delta_l(s)}}{\beta}, \tag{3.15}$$

where s is the center-of-mass energy squared, $P_l(\cos\theta)$ is the Legendre polynomial, and $\delta_l(s)$ is the phase shift in the process of $M\bar{M} \to \pi^0\pi^0$.

Since $\mathrm{Dics}M_0 = 2i\mathrm{Im}M_0$,

$$\mathrm{Im}M_0 = \frac{1}{128\pi^2}\beta \int d\Omega M_2^*(s,\cos\theta) M_1(s,\cos\theta_l), \tag{3.16}$$

and the amplitude M_1 can be determined by the pion GDA (see Eq. (3.10)).

$$M_1(s, cos\theta_l) = 2A_{++} = c[\tilde{B}_{10}(W) + \tilde{B}_{12}(W)P_2(cos\theta_l)], \tag{3.17}$$

where c is a constant. Take the S-wave case as an example, we can prove

$$\begin{aligned}
&\mathrm{Im}M_0 = \frac{1}{128\pi^2}\beta \int d\Omega M_2^*(s,\cos\theta) M_1(s, cos\theta_l),\\
&\mathrm{Im}M_0 = \frac{1}{128\pi^2}\beta(2\pi) \int d\theta \sin\theta (32\pi) \frac{\sin\delta_0(s) e^{-i\delta_0(s)}}{\beta} c(\tilde{B}_{10}(W)),\\
&c * \mathrm{Im}(\tilde{B}_{10}(W)) = c * \tilde{B}_{10}(W) * \sin\delta_0(s) e^{-i\delta_0(s)}.
\end{aligned} \tag{3.18}$$

Therefore, we have $\mathrm{Arg}(\tilde{B}_{10}(W)) = \delta_0(s)$ below the $K\bar{K}$ threshold [7]. Similarly, we can obtain $\mathrm{Arg}(\tilde{B}_{12}(W)) = \delta_2(s)$ [7] for the D wave.

Above the threshold of $K\bar{K}$, the inelastic channels open and we need to introduce additional phase to describe the inelastic effect. We adopt the S-wave and D-wave $\pi\pi$ phase shifts in Refs. [90, 91], and they are shown in Fig. 3.8.

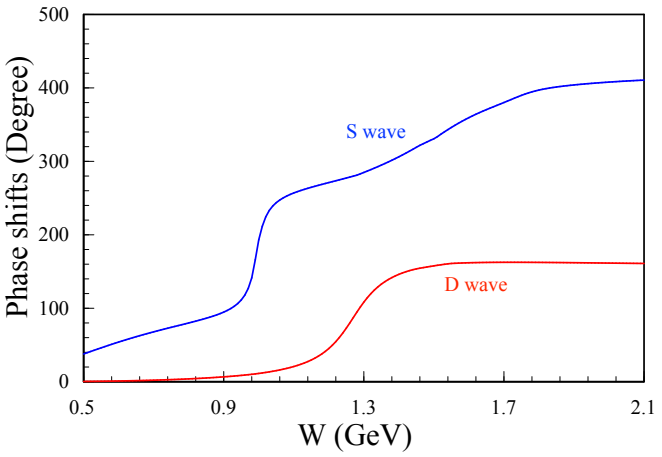

FIGURE 3.8: S-wave and D-wave phase shifts of $\pi\pi$ scattering in the $I = 0$ channel.

3.3.2 Resonance effects in pion GDA

In the process of $\gamma^*\gamma \to \pi^0\pi^0$, the final $\pi^0\pi^0$ can be produced through the resonance states h shown in Fig. 3.9, and they could be scalar mesons (*e.g.* $f_0(500)$) and tensor mesons (*e.g.* $f_2(1270)$). The pion GDAs are related with the resonances especially in the resonance energy regions [92, 93]. The isosinglet scalar mesons contribute to the S-wave production of $\pi^0\pi^0$, and tensor mesons produce the D-wave $\pi^0\pi^0$.

This resonance effect can be significant near the resonance region, namely, the GDA is mainly determined by resonance effect in this region. We can express the resonance

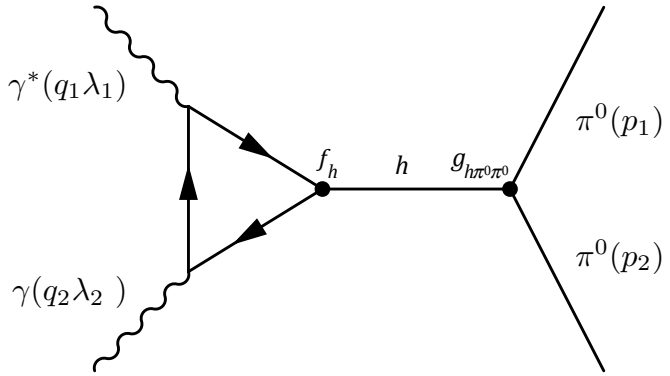

FIGURE 3.9: Resonance effects in GDA.

effect as follows

$$\langle\pi^0(p_1)\pi^0(p_2)|\,\bar{q}(-z/2)\gamma_\mu q(z/2)\,|0\rangle = \langle\pi^0(p_1)\pi^0(p_1)|\,h(P)\rangle\frac{1}{M_h^2 - W^2 - i\Gamma M_h} \times \langle h(P)|\,\bar{q}(-z/2)\gamma_\mu q(z/2)\,|0\rangle + \cdots, \tag{3.19}$$

where $\bar{q}q$ can be $\bar{u}u$ or $\bar{d}d$, and $P^2 = W^2$. The left side of Eq. (3.19) is just the definition of GDA. As for the right side of Eq. (3.19), $\langle h(P)|\,\bar{q}(-z/2)\gamma_\mu q(z/2)\,|0\rangle$ is the DA of hadron h, and $\langle\pi^0(p_1)\pi^0(p_1)|\,h(P)\rangle$ describe the amplitude of $h \to \pi^0\pi^0$. The resonance state h can be S-wave and D-wave. Here, we take S-wave resonance f_0 as an example to illustrate the resonance effect.

We have the following definitions for the f_0 resonance [26–28]

$$\begin{aligned}
&\langle\pi^0(p_1)\pi^0(p_2)|\,f_0(P)\rangle = -ig_{f_0\pi^0\pi^0},\\
&\langle f_0(P)|\,\bar{q}(-z/2)\gamma_\mu q(z/2)\,|0\rangle = \frac{1}{\sqrt{2}}f_{f_0}P_\mu\int\phi(y)e^{i(1-2y)p.z/2}dy,\\
&\langle\pi^0(p_1)\pi^0(p_2)|\,\bar{q}(-z/2)\gamma_\mu q(z/2)\,|0\rangle = P_\mu\int\Phi_q(y,\xi,W^2)e^{i(1-2y)P.z/2}dy,
\end{aligned} \tag{3.20}$$

where f_{f_0} is the decay constant of f_0, it evolves with the energy scale Q^2 as $f_{f_0}(Q^2) = f_{f_0}(Q_0^2)(\alpha_s(Q)/\alpha_s(Q_0))^k$, $k = 32(11-2n_f/3)/9$. As for the coupling constant $g_{f_0\pi^0\pi^0}$, it is determined by the decay with of $\Gamma(f_0 \to \pi^0\pi^0)$. By considering the isospin properties of $\pi^0\pi^0$ and $\pi^+\pi^-$, the two-pion states are expressed as

$$\begin{aligned}
|\pi^0\pi^0\rangle &= \sqrt{\frac{2}{3}}\,|I=2,I_3=0\rangle - \sqrt{\frac{1}{3}}\,|I=0,I_3=0\rangle\,,\\
|\pi^+\pi^-\rangle &= \sqrt{\frac{1}{6}}\,|I=2,I_3=0\rangle + \sqrt{\frac{1}{3}}\,|I=0,I_3=0\rangle + \sqrt{\frac{1}{2}}\,|I=1,I_3=0\rangle\,.
\end{aligned} \tag{3.21}$$

We can obtain $\Gamma(f_0 \to \pi^0\pi^0) = (1/3)\Gamma(f_0 \to \pi\pi)$, since only the $|I = 0, I_3 = 0\rangle$ part of $\pi\pi$ will contribute in the decay $f_0 \to \pi\pi$, and it is given by

$$\frac{1}{3}\Gamma(f_0 \to \pi\pi) = \frac{1}{2}\frac{g^2_{f_0\pi^0\pi^0}}{16\pi M_{f_0}}, \quad g_{f_0\pi\pi} = \sqrt{\frac{2}{3}16\pi\Gamma(f_0 \to \pi\pi)M_{f_0}}, \tag{3.22}$$

where the factor $1/2$ appears on account of identical particles.

In the asymptotic limit, the DA of f_0 is $\phi(y) = 30y(1-y)(2y-1)$, and the S-wave part of GDA in Eq. (3.11) can be expressed as

$$\Phi_q(y, \xi, W^2) = 18y(1-y)(2y-1)\tilde{B}_{10}(W). \tag{3.23}$$

With the help of Eqs. (3.19) and (3.24), one can obtain $\tilde{B}_{10}(W)$ around the resonance region of f_0:

$$\begin{aligned}
\tilde{B}_{10}(W) &= \frac{-5ig_{f_0\pi\pi}f_{f_0}}{3\sqrt{2}[m^2_{f_0} - W^2 - i\Gamma M_{f_0}]}, \\
\bar{B}_{10}(W) &= \frac{5g_{f_0\pi\pi}f_{f_0}}{3\sqrt{2}\sqrt{[(M^2_{f_0} - W^2)^2 + \Gamma^2_{f_0}M^2_{f_0}]}},
\end{aligned} \tag{3.24}$$

where $M_{f_0} = 0.475$ GeV and $\Gamma_{f_0} = 0.55$ GeV [20]. As for the decay constant f_{f_0}, since we do not find any information, it could be considered as a parameter to be determined. If we extend this expression to the whole energy region of W^2, we express $\bar{B}_{10}$ as

$$\bar{B}_{10}(W) = f_{10}(W) + \frac{5g_{f_0\pi\pi}f_{f_0}}{3\sqrt{2}\sqrt{[(M^2_{f_0} - W^2)^2 + \Gamma^2_{f_0}M^2_{f_0}]}}, \tag{3.25}$$

$f_{10}(W)$ describes the S-wave continuum contribution to the GDAs. Because we will take the square of the GDAs for the cross section of $\gamma^*\gamma \to \pi^0\pi^0$ (see Eqs. (3.9) and (3.10)), the second term of Eq. (3.25) will play a role as a Breit-Wigner distribution. Therefore, we only need to parameterize the expression $f_{10}(W)$ in the GDA analysis in comparison with the Belle data.

Similarly, we can also obtain the D-wave resonance effect such as f_2 meson. The coupling constant $g_{f_2\pi^0\pi^0}$ and DA of f_2 [33, 93] are defined as

$$\begin{aligned}
&\langle \pi^0(p_1)\pi^0(p_2)|\, f_2(P,\lambda)\rangle = ig_{f_2\pi^0\pi^0}\epsilon^{(\lambda)}_{\mu\nu}(p_1 - p_2)^\mu(p_1 - p_2)^\nu, \\
&\langle f_2(P,\lambda)|\, \overline{q}(-z/2)\gamma_\mu q(z/2)\,|0\rangle = \frac{f_{f_2}}{\sqrt{2}}M^2_{f_2}\int dy\phi(y)e^{i(1-2y)p.z/2}P_\mu\frac{\epsilon^{(\lambda)*}_{\alpha\beta}z^\alpha z^\beta}{(P\cdot z)^2},
\end{aligned} \tag{3.26}$$

where λ is the helicity of f_2, and $\epsilon^{(\lambda)}_{\mu\nu}$ is the polarization tensor [93]. The decay constant f_{f_2} has the same evolution properties as the decay constant f_{f_0}. In the asymptotic

limit, the DA is $\phi(y) = 30y(1-y)(2y-1)$ for f_2 and the D-wave part of GDA is $\Phi_q(y,\xi,W^2) = 18y(1-y)(2y-1)\tilde{B}_{12}(W)P_2(\cos\theta)$. Finally, $\tilde{B}_{12}(W) = \bar{B}_{12}(W)\exp(i\delta_2)$ mainly depends the D-wave resonance effect in the resonance region as [93]

$$\bar{B}_{12}(W) = \frac{10 g_{f_2\pi^0\pi^0} f_{f_2} M_{f_2}^2}{9\sqrt{2}\sqrt{(M_{f_2}^2 - W^2)^2 + \Gamma_{f_2}^2 M_{f_2}^2}}, \tag{3.27}$$

where $M_{f_2} = 1.275$ GeV, $\Gamma_{f_2} = 0.185$ GeV, and the coupling constant $g_{f_2\pi^0\pi^0}$ is defined by

$$g_{f_2\pi^0\pi^0} = \sqrt{\frac{2}{3}\frac{24\pi\Gamma(f_2\to\pi\pi)}{M_{f_2}^3}}, \quad \Gamma(f_2\to\pi\pi) = 0.85\Gamma_{f_2}. \tag{3.28}$$

Here, the factor 0.85 is the branching ratio of $\Gamma(f_2\to\pi\pi)$ according to the Particle Data Group (PDG) [20]. If $\bar{B}_{12}(W)$ is extended to the whole energy region (0.5 GeV$-$2.1 GeV), we have

$$\bar{B}_{12}(W) = f_{12}(W) + \frac{10 g_{f_2\pi\pi} f_{f_2} M_{f_2}^2}{9\sqrt{2}\sqrt{(M_{f_2}^2 - W^2)^2 + \Gamma_{f_2}^2 M_{f_2}^2}}. \tag{3.29}$$

The first term $f_{12}(W)$ describes the D-wave continuum contribution to the GDAs, and we need to adopt a parameterization for $f_{12}(W)$. If the small W limit is taken, we have the following constraints for $\bar{B}_{10}(W)$ and $\bar{B}_{12}(W)$ [7, 8]:

$$\bar{B}_{10}(0) = \frac{-3+\beta^2}{2}\frac{10R_\pi}{9n_f}, \quad \bar{B}_{12}(0) = \beta^2\frac{10R_\pi}{9n_f}. \tag{3.30}$$

3.4 Belle measurements of process $\gamma^*\gamma \to \pi^0\pi^0$

In Ref. [82], the Belle collaboration measured the $\gamma\gamma^* \to \pi^0\pi^0$ cross section in the energy region of 3.46 GeV$^2 \leqslant Q^2 \leqslant$ 24.25 GeV^2 and 0.5 GeV $< \sqrt{s} = W <$ 2.1 GeV. In principle, we can obtain the pion GDAs by analyzing the Belle data. In older to keep the factorization condition ($Q^2 \gg W^2, \Lambda^2$) satisfied, we only used the Belle data at large Q^2 ($Q^2 \geqslant 8.92$ GeV^2). The energy region of Belle data is 8.92 GeV$^2 \leqslant Q^2 \leqslant$ 24.25 GeV^2 and 0.5 GeV $< \sqrt{s} = W <$ 2.1 GeV in our GDA analysis. In Fig. 3.10, we show the differential cross section of $\gamma\gamma^* \to \pi^0\pi^0$ [82]. The data with $Q^2 = 8.92$ and 13.37 GeV^2 are shown in this figure, and the pion angles are $\cos\theta = 0.1$ and 0.5. We can clearly see the resonance contribution of $f_2(1270)$ around the region $W = 1.2$ GeV, and other resonance effects are not clear due to the large errors of the experimental measurements.

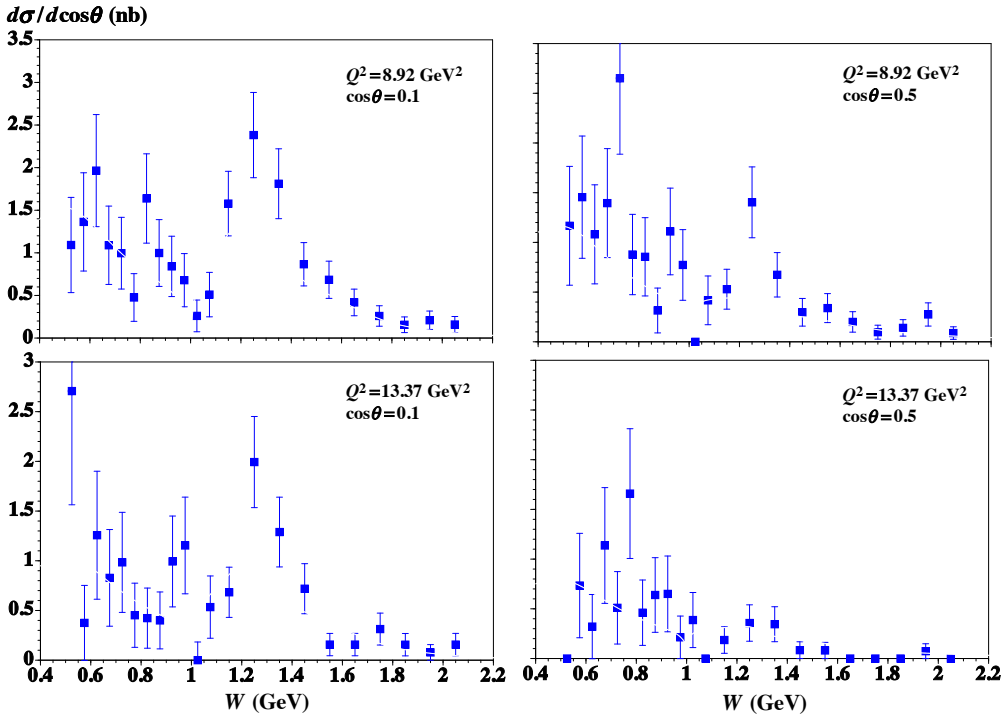

FIGURE 3.10: Differential cross sections of $\gamma^*\gamma \to \pi^0\pi^0$ measured by the Belle collaboration with fixed Q^2 and $\cos\theta$ [82].

In the Sec. 3.3, we discussed the Q^2 independent (asymptotic) form of GDA, and we need to check the Q^2 dependence of the pion GDA based on Belle data before we analyze the experimental measurements. If the differential cross section $d\sigma/d|cos\theta|$ is multiplied by the factor $(Q^2+s)/\beta$, this quantity is proportional to the square of GDA:

$$\frac{(Q^2+s)d\sigma}{\beta\, d|\cos\theta|} \propto \left|\Phi^{\pi^0\pi^0}(z,\cos\theta,W,Q)\right|^2 . \tag{3.31}$$

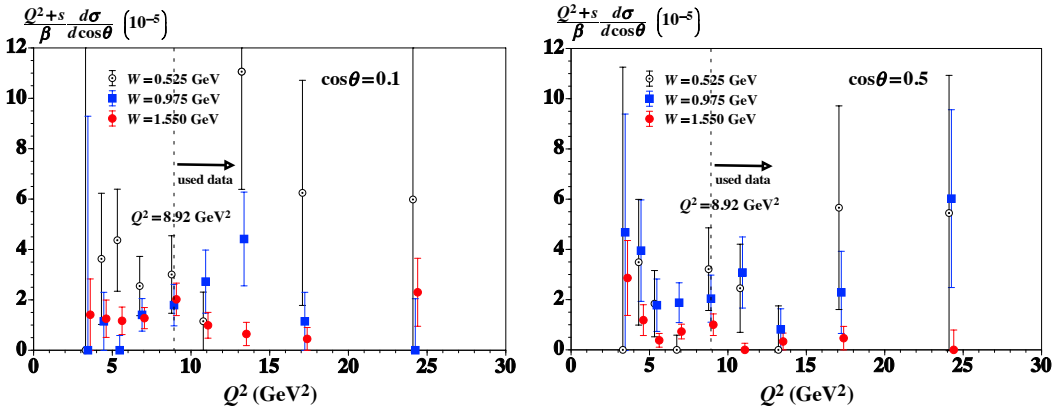

FIGURE 3.11: The scaling violation of the Belle data. The data are denoted by black and white for $W = 0.525$ GeV, blue for $W = 0.975$ GeV, and red for $W = 1.55$ GeV. The left panel is for $\cos\theta = 0.3$ and the right one is for $\cos\theta = 0.5$.

With fixed W and $\cos\theta$, one can test the Q^2 dependence of the GDA from Belle measurements. We present the Belle data of $(Q^2+s)d\sigma/(\beta d|\cos\theta|)$ in Fig. 3.11, where the data of $W = 0.525$ GeV, 0.975 GeV, and 1.55 GeV are plotted as the function of Q^2. The pion GDA should be Q^2 independent when Q^2 is large enough. The typical energy scale for Belle data is $Q^2 = 16.6$ GeV^2. In principle, the pion GDA from the Belle data should be Q^2-dependent at this energy scale. However, the scaling violation of the GDA is not so obvious in Belle measurements on account of the large errors in Fig. 3.11, so that the Q^2-independent GDAs could be used in analyzing the Belle data.

3.5 GDAs analysis of Belle data

Without the resonance effects and phase shifts, a simple expression for the GDAs could be expressed as [94]

$$\begin{aligned}
&\Phi_q^{\pi^0\pi^0}(z,\xi,W^2) = N_h R_q z^\alpha (1-z)^\alpha (2z-1)\zeta(1-\zeta)F_h(W^2),\\
&N_h = \frac{-4(2\alpha+3)}{B(\alpha+1,\alpha+1)},\quad F_h(W^2) = \frac{1}{[1+(W^2-4m_h^2)/\Lambda^2]^{n-1}},
\end{aligned} \tag{3.32}$$

where the momentum carried by quarks is $\sum_q R_q = R_\pi = 0.5$, and α works as a input parameter. The function $F_h(W^2)$ is the form factor of the quark part of the energy-momentum tensor, and it is normalized as $F_h(4m_h^2) = 1$. The parameter Λ is the momentum cutoff in the form factor, and $B(\alpha+1,\alpha+1)$ is the beta function. Here, n is the number of active constituents in a meson, it could be predicted by the constituent counting rule in the high energy limit [95]. In Ref. [94], n is used to distinguish ordinary hadrons $(q\bar{q}, qqq)$ with exotic states $(q\bar{q}q\bar{q}, qqqq\bar{q})$.

In our studies, we include the resonance effects and the phase shifts, which are essential to explain the Belle data. We consider a more general GDA expression [96] to analyze the Belle data. We add the contributions of scalar meson $f_0(500)$ and tensor meson $f_2(1270)$ in Eqs.(3.24) and (3.27) as

$$\begin{aligned}
&\Phi_q^{\pi^0\pi^0}(z,\xi,W^2) = \frac{-3}{20}N_h z^\alpha (1-z)^\alpha (2z-1)[\tilde{B}_{10}(W) + \tilde{B}_{12}(W)P_2(cos\theta)],\\
&\tilde{B}_{10}(W) = \left\{\frac{-3+\beta^2}{2}\frac{10R_\pi}{9n_f}F_h(W^2) + \frac{5g_{f_0\pi^0\pi^0}f_{f_0}}{3\sqrt{2}\sqrt{[(M_{f_0}^2-W^2)^2+\Gamma_{f_0}^2M_{f_0}^2]}}\right\}e^{i\delta_0},\\
&\tilde{B}_{12}(W) = \left\{\beta^2\frac{10R_\pi}{9n_f}F_h(W^2) + \frac{10g_{f_2\pi^0\pi^0}f_{f_2}M_{f_2}^2}{9\sqrt{2}\sqrt{(M_{f_2}^2-W^2)^2+\Gamma_{f_2}^2M_{f_2}^2}}\right\}e^{i\delta_2}.
\end{aligned} \tag{3.33}$$

Below the $K\bar{K}$ threshold, the δ_0 and δ_2 are the $\pi\pi$ elastic scattering phase shifts in the isospin=0 channel, and we introduce the additional phase shift to δ_0 above the $K\bar{K}$

threshold:

$$\delta_0(W) = \delta_0(W)_{\rm BKNS}, W < 2m_k,$$
$$\delta_0(W) = \delta_0(W)_{\rm BKNS} + a_\delta\,(W - 2m_K)^{b_\delta}, W \geqslant 2m_k, \tag{3.34}$$

where the parameters a_δ and b_δ are determined by χ^2 fitting of experimental measurements. In our analysis, we employ the S-wave $\pi\pi$ scattering phase shift $\delta_0(W)_{\rm BKNS}$ and D-wave $\pi\pi$ scattering phase shift $\delta_2(W)_{\rm BKNS}$ (BKNS is short for Bydzovsky, Kaminski, Nazari, and Surovtsev) in Refs. [90, 91], and they are shown shown in Fig. 3.8. The parameter n is fixed as $n = 2$, since it is predicted by the counting rule [95] with $d\sigma/d|cos\theta| \propto 1/W^6$. The parameter $\alpha = 1$ is the asymptotic value for the GDAs, here it is considered as a parameter to be determined. The function N_h is dependent on α, and it is constrained by the following sum rule [8],

$$\int_0^1 dz(2z-1)\,\Phi_q^{\pi^0\pi^0}(z,\,\zeta,\,0) = -2R_\pi\zeta(1-\zeta). \tag{3.35}$$

The resonance contribution of $f_2(1270)$ is significant around $W \simeq 1.27$ GeV in the Fig. 3.10, so that the resonance effect of $f_2(1270)$ is necessary to be introduced to explain the Belle data as given in Eq. (3.33). The mass $M_{f_2} = 1.275$ GeV and decay width $\Gamma_{f_2} = 0.185$ GeV are taken from PDG [20], and the coupling constant $g_{f_2\pi^0\pi^0}$ is obtained by the decay width as explained in Eq. (3.28). For the decay constant, it is $f_{f_2} = 0.101$ GeV at $Q^2 = 1$ GeV^2 in Ref. [34]. Since the average energy scale of Belle data used in the analysis is $Q^2 = 16.6$ GeV^2, the decay constant is estimated as $f_{f_2} = 0.0754$ GeV at this scale by considering the following evolution equation,

$$f_{f_2}(Q^2) = f_{f_2}(Q_0^2)\left\{\frac{\alpha_s(Q)}{\alpha_s(Q_0)}\right\}^{\frac{32(11-2n_f/3)}{9}}. \tag{3.36}$$

In the S-wave resonance effect, the coupling constant $g_{f_0\pi^0\pi^0}$ is determined by the decay width in Eq. (3.22). However, the decay width and mass of $f_0(500)$ are not well measured by experiments, and we use the middle values in the PDG [20] as $\Gamma_{f_0} = 550$ MeV and $M_{f_0} = 475$ MeV. Since we cannot find the theoretical value of $f_{f_0(500)}$, it could be considered as a parameter. In older to distinguish the resonance effect of $f_0(500)$, there are two sets of analysis. In set-1 analysis, only the resonance effect of $f_2(1270)$ is introduced, and there are 4 parameters to be determined. However, both the resonance effects of $f_2(1270)$ and $f_0(500)$ are included in set-2 analysis, and 5 parameters are involved in this analysis.

We need to mention that other resonances could affect the cross section in the relevant energy regions, and the candidates are

$$I^G(0^{PC}) = 0^+(0^{++}) : f_0(980), f_0(1370), f_0(1500), f_0(1710),$$
$$I^G(0^{PC}) = 0^+(2^{++}) : f_2(1525), f_2'(1950), f_2(2010), \tag{3.37}$$

where only neutral scalar or tensor mesons with isospin $I = 0$ could contribute. We do not include these resonances in the analysis, since the resonances such as $f_0(980)$ are not shown in Belle differential cross-setion measurements [82] due to the large experimental errors.

TABLE 3.1: Parameter values of the pion GDA are obtained by χ^2 fitting of experimental measurements for both set 1 and set 2. The decay constant $f_{f_2(1270)}$ is a fixed parameter taken from Ref. [34]

Parameter	Set 1	Set 2
α	0.801 ± 0.042	1.157 ± 0.132
Λ (GeV)	1.602 ± 0.109	1.928 ± 0.213
$f_{f_0(500)}$ (GeV)	0 (fixed)	0.0184 ± 0.0034
$f_{f_2(1270)}$ (GeV)	0.0754 (fixed)	0.0754 (fixed)
a_δ	3.878 ± 0.165	3.800 ± 0.170
b_δ	0.382 ± 0.040	0.407 ± 0.041

The parameters are obtained by fitting the data of the differential cross section $\gamma^*\gamma \to \pi^0\pi^0$ with Eq. (3.9), and they are shown in Table 3.1. Both set-1 analysis and set-2 analysis give a good description of the Belle data with χ^2/d.o.f = 1.22 for set 1 and χ^2/d.o.f = 1.09 for set 2. The parameter value of α is always around 1 for two sets of analysis, which is consistent with the prediction $\alpha = 1$ from the asymptotic form of GDA in Eq. (3.11). The momentum cutoff Λ is close to 2 GeV, which is the typical scale for pion meson.

In Fig. 3.12, we show the comparison between the differential cross section of $\gamma^*\gamma \to \pi^0\pi^0$ from the obtained GDA and the Belle measurements, the energy scale Q^2 is fixed as 8.92 GeV^2 and 13.37 GeV^2 and $\cos\theta$ is set as 0.1 and 0.5. The resonance peak of $f_2(1270)$ is clearly seen around $W = 1.2$ GeV, and other resonances are not shown due to the large errors of experimental measurements.

The differential cross section of $\gamma^*\gamma \to \pi^0\pi^0$ is shown in Fig. 3.13 with the different energy scales $Q^2 = 17.73$ GeV^2 and $Q^2 = 24.25$ GeV^2. Both set 1 and set 2 can describe the experimental cross section well enough, and the big difference between set-1 analysis

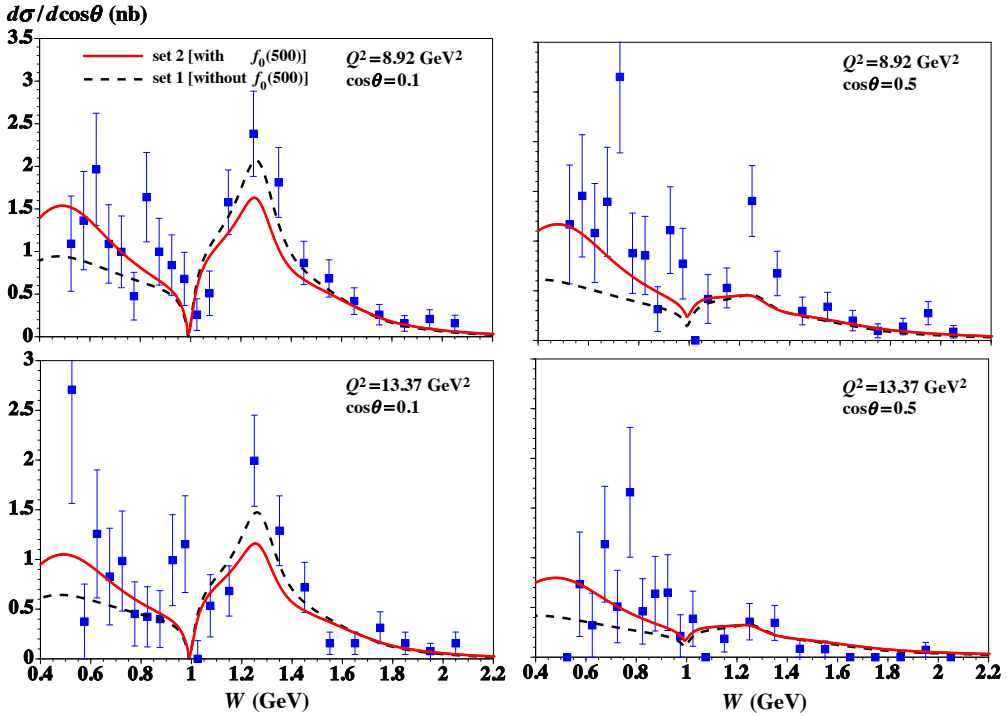

FIGURE 3.12: The differential cross section of $\gamma^*\gamma \to \pi^0\pi^0$ (in units of nb) from the obtained GDA for set-1 analysis and for set-2 analysis. The values of Q^2 are fixed as 8.92 GeV^2 and 13.37 GeV^2, and $\cos\theta$ is 0.1 and 0.5 [96].

and set-2 analysis appears around W=0.5 GeV since the resonance effect of $f_0(500)$ only affect the resonance region.

In this analysis, we add the additional phase shift to δ_0 above the $K\bar{K}$ threshold in Eq. (3.34). In the same way, we can also add the additional phase shift to δ_2 as follows,

$$\begin{aligned}\delta_2(W) &= \delta_2(W)_{\rm BKNS}, W < 2m_k,\\ \delta_2(W) &= \delta_2(W)_{\rm BKNS} + a_\delta\,(W-2m_K)^{b_\delta}, W \geqslant 2m_k,\end{aligned} \tag{3.38}$$

This D-wave analysis gives the similar χ^2/d.o.f as the previous analysis, and the parameter values (α, Λ and $f_{f_0(500)}$) just slightly change.

3.6 Gravitational form factors of pion

As we discussed before, the operator $\bar{q}(-y/2)\gamma^+ q(y/2)$ appears in the definition of GDA,

$$\Phi_q^{h\bar{h}}(z,\zeta,W^2) = \int \frac{dy^-}{2\pi} e^{i(2z-1)P^+y^-/2} \left\langle h(p_1)\bar{h}(p_2)\right| \bar{q}(-y^-/2)\gamma^+ q(y^-/2)\left|0\right\rangle . \tag{3.39}$$

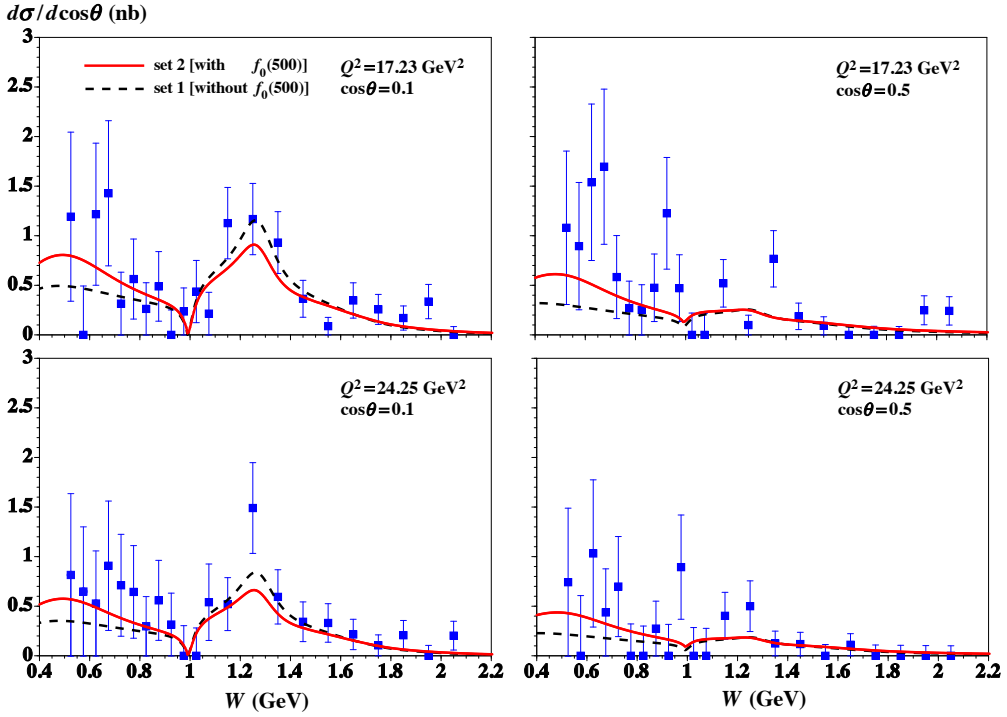

FIGURE 3.13: The differential cross section of $\gamma^*\gamma \to \pi^0\pi^0$ (in units of nb) from the obtained GDA for set-1 analysis and for set-2 analysis. The values of Q^2 are set as 8.92 GeV^2 and 13.37 GeV^2, and $\cos\theta$ is 0.1 and 0.5 [96].

If we take momentum integral of this operator, we obtain [47]

$$\begin{aligned} &2(\frac{P^+}{2})^n \int_0^1 dz\,(2z-1)^{n-1} \int \frac{dy^-}{2\pi} e^{i(2z-1)P^+y^-/2} \overline{q}(-y/2)\gamma^+ q(y/2) \\ =&\overline{q}(0)\gamma^+ \left(i\overleftrightarrow{\partial}^+\right)^{n-1} q(0), \end{aligned} \tag{3.40}$$

where the notation $\overleftrightarrow{\partial}$ is defined as $A\overleftrightarrow{\partial}B = [A(\partial B) - (\partial A)B]/2$. When $n = 1$, the matrix element of the right side of Eq. (3.40), $\left\langle h(p_1)\bar{h}(p_2)\right| \bar{q}(0)\gamma^+ q(0)\left|0\right\rangle$, is the electromagnetic form factor for hadron h in the timelike region, and this is shown in the left panel of Fig. 3.14. This relation is same as those of Eq. (1.43) for GPDs, which probe the form factors in the spacelike region. Furthermore, the matrix elements of the energy-momentum tensor for hadron h can be investigated if $n = 2$, and they are expressed with gravitational form factors which are important quantities for the gravitational interaction shown in the right panel of Fig. 3.14. Similarly, gravitational form factors in the spacelike region can also by obtained by GPDs of hadrons.

$$\int_{-1}^{1} dx x\, H_q(x,\,\xi,\,t) = \frac{1}{2(\bar{P}^+)^2} \langle\, h(p_2)\,|\,T_q^{++}(0)\,|\,h(p_1)\,\rangle, \tag{3.41}$$

here, h is a scalar meson, and the GPD definition can be found in Eq. (1.47). The energy-momentum tensor for the quark q is defined as

$$T_q^{\mu\nu}(x) = \overline{q}(x)\,\gamma^{\{\mu} i\overleftrightarrow{D}^{\nu\}}\,q(x), \tag{3.42}$$

where $A^{\{\mu\nu\}} = 1/2(A^{\mu\nu} + A^{\nu\mu})$ symmetrizes the tensor.

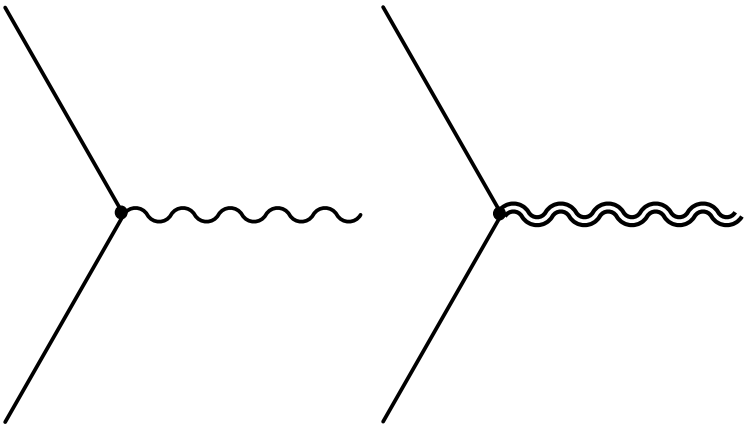

FIGURE 3.14: Left panel: vector current interaction such as electromagnetic interaction. Right panel: tensor current interaction such as gravitational interaction.

With the help of Eq. (3.40), one can connect the GDA to the energy-momentum tensor and gravitational form factors of pion. In general, gravitational form factors can not be directly probed by gravitational interaction since it is too weak; however, the GPDs and GDAs provide us an indirect way to obtain gravitational form factors. In the previous section, we obtained the pion GDA by analyzing Belle data. Futhermore, we can study energy-momentum tensor of pion by using the obtained GDA [8]

$$\int_0^1 dz(2z-1)\,\Phi_q^{\pi^0\pi^0}(z,\,\zeta,\,W^2) = \frac{2}{(P^+)^2}\langle\,\pi^0(p_1)\,\pi^0(p_2)\,|\,T_q^{++}(0)\,|\,0\,\rangle. \tag{3.43}$$

where $T_q^{\mu\nu}$ is the energy-momentum tensor of the quark type q for the pion, and it can be expressed by the gravitational form factors as [9, 10, 97–101]

$$\langle\,\pi^0(p_1)\,\pi^0(p_2)\,|\sum_q T_q^{\mu\nu}(0)\,|\,0\,\rangle = \frac{1}{2}\left[\,(s\,g^{\mu\nu} - P^\mu P^\nu)\;\Theta_1(s) + \Delta^\mu\Delta^\nu\,\Theta_2(s)\,\right], \tag{3.44}$$

where Θ_1 and Θ_2 are the gravitational form factors, and the symmetry of $T_u^{\mu\nu} = T_d^{\mu\nu}$ is used. Θ_1 is related with the mass or energy, and Θ_2 can reveal the pressure distribution and the sheer-force distribution of the hadron shown in Fig. 3.15. The gravitational form factors Θ_1 and Θ_2 for the pion can be estimated from the pion GDA with the help of Eqs. (3.43) and (3.44):

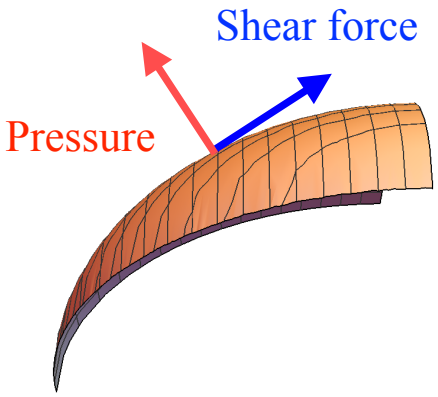

FIGURE 3.15: Pressure and the sheer force of the hadron

$$\Theta_1(s) = \frac{3}{5}(\widetilde{B}_{12}(W^2) - 2\widetilde{B}_{10}(W^2)), \quad \Theta_2(s) = \frac{9}{5\,\beta^2}\widetilde{B}_{12}(W^2). \tag{3.45}$$

$\Theta_1(s)$ is expressed by S-wave term $\widetilde{B}_{10}(W^2)$ and D-wave term $\widetilde{B}_{12}(W^2)$, and $\Theta_2(s)$ is determined only by $\widetilde{B}_{12}(W^2)$. The absolute values of gravitational form factors $\Theta_1(s)$ and $\Theta_2(s)$ are shown in Fig. 3.16. The resonance peak $f_2(1270)$ appears in the $|\Theta_1(s)|$ and $|\Theta_2(s)|$. Since $\Theta_1(s)$ contains both $\widetilde{B}_{10}(W^2)$ and $\widetilde{B}_{12}(W^2)$, and $\widetilde{B}_{10}(W^2)$ interferes with $\widetilde{B}_{12}(W^2)$.

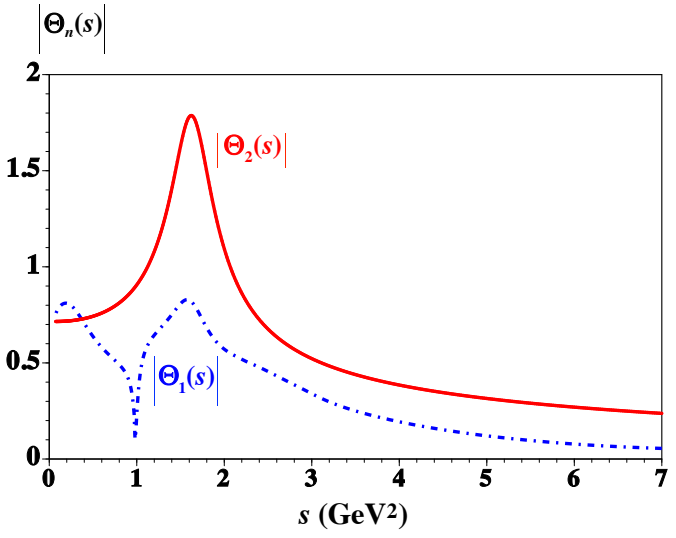

FIGURE 3.16: Absolute values of gravitational form factors $\Theta_1(s)$ and $\Theta_2(s)$ for pion dependent on $s = W^2$ [96].

With the pion GDA, the timelike gravitational form factors are estimated. Moreover, the timelike form factors can be transformed into the spacelike form factors by using the

dispersion relation [102],

$$F^h(t) = \int_{4m_h^2}^{\infty} \frac{ds}{\pi} \frac{\mathrm{Im}\, F^h(s)}{s - t - i\varepsilon}, \tag{3.46}$$

where $F^h(s)$ is the timelike form factor for hadron h, and m_h is the mass of hadron h. By using the dispersion relation, we also calculate the spacelike gravitational form factors $\Theta_1(t)$ and $\Theta_2(t)$. We normalize $\Theta_1(t)$ and $\Theta_2(t)$ as $\Theta_1(0) = 1$ and $\Theta_2(0) = 1$, respectively. The normalized form factors $\Theta_1(t)/\Theta_1(0)$ and $\Theta_2(t)/\Theta_2(0)$ are shown in the left panel of Fig. 3.17. Both $\Theta_1(t)/\Theta_1(0)$ and $\Theta_2(t)/\Theta_2(0)$ decrease as $|t|$ increases, and $\Theta_1(t)/\Theta_1(0)$ drops faster than $\Theta_2(t)/\Theta_2(0)$. In the right panel of Fig. 3.17, they are $\rho_1(r)$ and $\rho_2(r)$ which they are the Fourier transforms of $\Theta_1(t)/\Theta_1(0)$ and $\Theta_2(t)/\Theta_2(0)$, respectively:

$$\rho(r) = \int \frac{d^3q}{(2\pi)^3} e^{-i\vec{q}\cdot\vec{r}} F^h(t) = \int_0^{\infty} \frac{d|\vec{q}|}{2\pi^2} |\vec{q}|^2 j_0(|\vec{q}|r) F^h(t), \tag{3.47}$$

where $t = -|\vec{q}|^2$ and $j_0(|\vec{q}|r)$ is the spherical Bessel function. The function $\rho_1(r)$ is distributed at small the region of $r = 0.1 - 0.3$ fm, and $\rho_2(r)$ is distributed at slightly larger region of $r = 0.1 - 0.5$ fm.

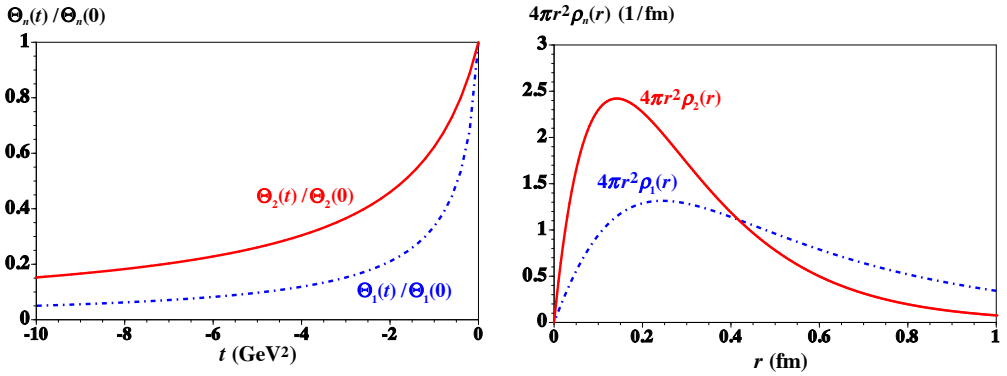

FIGURE 3.17: Left panel: Spacelike gravitational form factors $\Theta_1(t)/\Theta_1(0)$ and $\Theta_2(t)/\Theta_2(0)$. Right panel: $\rho_1(r)$ is the Fourier transforms of $\Theta_1(t)/\Theta_1(0)$, and $\rho_2(r)$ is the Fourier transforms of $\Theta_2(t)/\Theta_2(0)$ [96].

The three-dimensional rms (root mean square) radii are also investigated for gravitational form factors $\Theta_1(t)$ and $\Theta_2(t)$, which are just the slopes at $t = 0$ for $\Theta_1(t)$ and $\Theta_2(t)$.

$$\langle r^2 \rangle_h = \frac{6}{F^h(t=0)} \frac{dF^h(t)}{dt}\bigg|_{|t|\to 0} = \frac{6}{F^h(t=0)} \int_{4m_\pi^2}^{\infty} \frac{ds}{\pi} \frac{\mathrm{Im}\, F^h(s)}{s^2},$$
$$F^h(t=0) = \int_{4m_\pi^2}^{\infty} \frac{ds}{\pi} \frac{\mathrm{Im}\, F^h(s)}{s}, \tag{3.48}$$

where the form factor $F^h(t)$ can be $\Theta_1(t)$ or $\Theta_2(t)$, and the existence of $F^h(t=0)$ is to normalize $F^h(t)$ as $F^h(t)/F^h(t=0)$. The mass radius for Θ_1 is estimated as $\sqrt{\langle r^2\rangle_{\rm mass}} = 0.39$ fm, and the mechanical (pressure and sheer force) radius for Θ_2 is calculated as $\sqrt{\langle r^2\rangle_{\rm mech}} = 0.82$ fm [96]. For the charged pion, the three-dimensional rms charge radius is the slope of electromagnetic form factor which is $\sqrt{\langle r^2\rangle_{\rm charge}} = 0.659 \pm 0.004$ fm [1]. The mass radius is smaller than the charge radius, and this is consistent with the theocratical predictions in Refs. [99, 103]. However, the mechanical radius is slightly larger than the charge radius. At present there are not so many studies of the mechanical radius. In Ref. [104], the form factors $\Theta_1(t)$ and $\Theta_2(t)$ are calculated by lattice QCD, and it indicates that the slope of $\Theta_1(t)$ is larger than the one of $\Theta_2(t)$ at $t = 0$. Namely, the mechanical radius is larger than the mass radius, which agrees with our results. This is a very interesting discovery, and more studies are needed to explain this mechanism in the future.

In this analysis, the additional phase shift was added to S-wave phase shift δ_0 in Eq. (3.34) when $s > 2m_K$, and this additional phase shift reflects the inelastic channel in $\pi\pi$ scattering. Similarly, we can also introduce the additional phase to the D-wave one δ_2 as discussed in Eq. (3.38). The gravitational radii $\sqrt{\langle r^2\rangle_{\rm mass}} = 0.32$ fm and $\sqrt{\langle r^2\rangle_{\rm mech}} = 0.88$ fm are obtained for this D-wave analysis, and they are pretty similar with those of S-wave analysis. By considering both S-wave analysis and D-wave analysis, we can write the three-dimensional rms radii as [96]

$$\begin{aligned}\sqrt{\langle r^2\rangle_{\rm mass}} &= 0.32 \sim 0.39\,\text{fm},\\ \sqrt{\langle r^2\rangle_{\rm mech}} &= 0.82 \sim 0.88\,\text{fm}.\end{aligned} \tag{3.49}$$

3.7 Recent studies on gravitational form factors of the hadron

Recently, there are many studies on the energy-momentum tensor and gravitational form factors of the hadron in both theory and experiment, and much progress is made to help us understand the hadron properties on this topic. Reference [105] is a progress report on recent studies on the energy-momentum tensor of the hadron, and a different definition of the mechanical radius is given from the our Eq. (3.48). In 2018, the pressure distribution come from the quarks in the proton was obtained by analyzing DVCS measurements at JLab [106]. They found that the pressure is repulsive at small range of r (0-0.6 fm), and the binding (attractive) pressure is obtained at large r. The gravitational form factors of the proton and the pion were calculated for the gluon by using Lattice QCD [107]. Furthermore, the pressure distribution and shear force distribution of the nucleon are

studied by considering both the quark contribution and the gluon contribution in Ref. [108]. The recent theoretical studies also showed the relation between the gravitational form factors and the higher-twist effects [109, 110]. The authors of Ref. [111] investigated the gravitational form factors for the light mesons (π, σ and ρ) by using the Nambu-Jona-Lasinio model of QCD, and they find the two-dimensional mass radius of 0.27 fm for the pion . If the multiply the two-dimensional radius with the factor $\sqrt{3/2}$, it is 0.33 fm for the three-dimensional mass radius of the pion, and this is consistent with the mass radius $\sqrt{\langle r^2 \rangle_{\rm mass}} = 0.32 \sim 0.39\,\text{fm}$ which is obtained from our GDA analysis.

3.8 Summary

The three-dimensional structure functions can reveal inner structure of the hadrons, for example, one can obtain the orbital-angular momentum contribution inside the nucleon with the help of GPDs. Moreover, it become more and more popular to investigate the energy-momentum tensor and gravitational form factors of the hadron by using GPDs. Since the gravitational interaction is too weak to probe directly, the GPDs are be considered as an alternative way to study the energy-momentum tensor of the hadron. The GDAs are another kind of three-dimensional structure functions, and they are s-t crossed quantities of the GPDs, so that one could obtain the information on the GPDs from the GDAs. The GDAs can be studied in the two-photon process $\gamma^*\gamma \to h\bar{h}$, and they describes the amplitude of the process $q\bar{q} \to h\bar{h}$. In 2016, the Belle collaboration released the measurements on the differential cross section of $\gamma^*\gamma \to \pi^0\pi^0$. By adopting a simple GDA expression with a few parameters, we analyzed the Belle measurements on $\gamma^*\gamma \to \pi^0\pi^0$ and obtained the pion GDAs. The obtained GDAs give a reasonably good description of the Belle data with $\chi^2/d.o.f = 1.09$. Furthermore, we studied the energy-momentum tensor with the pion GDAs, and the gravitational form factors $\Theta_1(t)$ and $\Theta_2(t)$ were estimated in the timelike region. By using the dispersion relation, the spacelike gravitational form factors $\Theta_1(t)$ and $\Theta_2(t)$ were also obtained. The three-dimensional mass radius was calculated from the $\Theta_2(t)$ as $\sqrt{\langle r^2 \rangle_{\rm mass}} = 0.32 \sim 0.39\,\text{fm}$, and the three-dimensional mechanical radius was computed from the $\Theta_1(t)$ as $\sqrt{\langle r^2 \rangle_{\rm mech}} = 0.82 \sim 0.88\,\text{fm}$. The mass radius is much smaller than the charge radius of pion, while the mechanical radius is slightly larger than the charge radius. This is the first estimate of gravitational radii by analyzing the experimental measurements. At this stage, the Belle measurements are not so precise, and the experimental errors come mainly from the statistical errors. This situation will change soon, since the Belle II collaboration just started taking data with a much higher luminosity Super KEKB in 2019, precise measurements of $\gamma^*\gamma \to \pi^0\pi^0$ are expected. Therefore, a more general GDA analysis which may include Q^2 dependence is needed in the near future, and one

can possibly study gravitational form factors, pressure distribution, and shear force distribution with the accurate GDAs of hadrons.

Chapter 4

Gluon Transversity in Deuteron

4.1 Polarized parton distribution functions in nucleon

4.1.1 Spin vector of nucleon

In the previous sections of this thesis, we discussed the unpolarized PDFs, GPDs, and GDAs of the hadrons. In actual high energy experiments, polarized hadrons are widely used, such as the Relativistic Heavy Ion Collider (RHIC) at Brookhaven National Laboratory, the CEBAF accelerator at JLab and the Electron Ion Collider in future. In order to study the polarized PDFs, we first define the spin vector S^μ of the nucleon [14, 15]:

$$S^\mu = \left(\frac{\vec{p}\cdot\vec{s}}{M_N}, \vec{s} + \frac{(\vec{p}\cdot\vec{s})\,\vec{p}}{M_N(M_N+p^0)} \right), \tag{4.1}$$

where p is the momentum of the nucleon and $\vec{s}$ is the spin vector in the rest frame of the nucleon:

$$S^\mu = (0, \vec{s}), \quad S^2 = -1. \tag{4.2}$$

For example, when the spin of the nucleon is along z axis, it is $S^\mu = (0,0,0,1)$ in the rest frame. Therefore, one can transfer Eq. (4.2) into Eq. (4.1) by taking the Lorentz boost. For the case that $\vec{s}$ is parallel to $\vec{p}$, it is given by $S^\mu = (|\vec{p}|/M_N, \vec{s}+\vec{p}\,|\vec{p}|/[M_N(M_N+p^0)])$, and it is the longitudinal polarization. The nucleon is transversely polarized if $\vec{s}$ is perpendicular to $\vec{p}$. If the energy of the nucleon is high enough, the spin vector of

Eq. (4.1) becomes

$$S^\mu = \lambda \frac{p^\mu}{M_N} + S_T^\mu, \quad S_T^\mu = \left(0,\, \vec{S}_T,\, 0\right) \tag{4.3}$$

where λ is the helicity, and $\vec{S}_T$ is the transverse spin vector.

4.1.2 Polarized quark distribution functions in nucleon

The PDFs are generally expressed in parton correlation functions. The quark correlation function Φ is defined as

$$\Phi_{ij}(x) = \int \frac{d\tau}{2\pi} \left\langle p, S \left| \bar{q}_j(0)\gamma^+ q_i(\tau n) \right| p, S \right\rangle e^{i\tau x}, \tag{4.4}$$

where i is the spinor index, x is momentum fraction carried by the quark, and $n^\mu = 1/\sqrt{2}(1/p^+, 0, 0, -1/p^+)$. Here, the gauge link, for satisfying the color gauge invariance, is abbreviated just for simplicity. The function Φ can be expressed by the PDFs and gamma matrices [13, 112, 113] as

$$\begin{aligned}\Phi(x) =& \frac{1}{2}\left\{ q(x)\not{p} + \lambda \triangle q(x)\not{p} + \triangle_T q(x) \not{p}\gamma^5 \not{S}_T \right\} \\ &+ \frac{M_N}{2}\left\{ e_q(x) + g_T^q(x)\gamma^5 \not{S}_T + \frac{\lambda}{2} h_L^q(x)\gamma^5 \left[\not{p}, \not{n}\right] \right\}. \end{aligned} \tag{4.5}$$

The first term $q(x)$ is the unpolarized PDF in Eq. (1.26), which can be probed by the unpolarized DIS and Drell-Yan process. The second term $\triangle q(x)$ is the helicity distribution which exists in the longitudinally polarized nucleon $S^\mu = \lambda p^\mu / M_N$. The physical picture of $\triangle q(x)$ is shown in Fig. 4.1. In the longitudinally polarized nucleon, the probability of finding a parton with its spin parallel to the hadron spin is $q_+(x)$, and the probability of finding a parton with anti-parallel spin is $q_-(x)$, and the $\triangle q(x)$ is the difference between $q_+(x)$ and $q_-(x)$. In order to probe $\triangle q(x)$, one uses the longitudinally polarized DIS and the longitudinally polarized Drell-Yan process. In the longitudinally polarized proton-proton Drell-Yan process, the differential cross section is expressed as $d\sigma(\lambda_1, \lambda_2)$ with the proton helicities λ_1 and λ_2. If one measures the spin asymmetry A_{LL}^{DY} [114, 115]:

$$\begin{aligned} A_{LL}^{DY} &= \frac{d\sigma(+,+) - d\sigma(+,-)}{d\sigma(+,+) + d\sigma(+,-)} \\ &= \frac{\sum_q e_q^2 \left[\triangle q(x_1)\triangle\bar{q}(x_2) + \triangle\bar{q}(x_1)\triangle q(x_2)\right]}{\sum_q e_q^2 \left[q(x_1)\bar{q}(x_2) + \bar{q}(x_1)q(x_2)\right]}, \end{aligned} \tag{4.6}$$

the helicity distributions $\triangle q(x)$ are obtained with the knowledge of the unpolarized PDFs $q(x)$. At present, the quark helicity distributions are well determined by many experimental measurements.

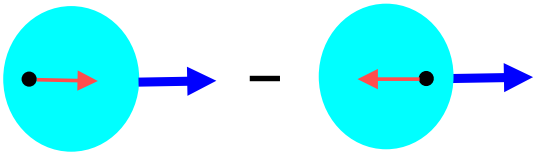

FIGURE 4.1: Helicity distribution of the nucleon, the blue arrow is the spin vector of the nucleon, and the red arrow is the spin vector of the quark.

The function $\triangle_T q(x)$ in Eq. (4.5) is called the transversity distribution, which appears in the transversely polarized nucleon. It indicates the probability to find a quark with spin along the transverse nucleon spin minus the one to find it oppositely. In the Fig. 4.2, it is the hadron tensor for DIS, the lower part is the transversity distribution $\triangle_T q(x)$ which flips the helicity of the hadron (from $\lambda = +$ to from $\lambda = -$). However, the higher (hard) part of Fig. 4.2 is zero, because the operator $\not{p}\gamma^5 \not{S}_T$ in Eq. (4.5) is chirally odd. Therefore, we cannot use the DIS process to investigate the quark transversity distribution. In the transversely polarized Drell-Yan process, proton$(\vec{S}_{1T})$ + proton$(\vec{S}_{2T}) \to \mu^+\mu^- + X$, the tansverse spin asymmetry A_{TT}^{DY} [13, 116, 117] is given by

$$\begin{aligned} A_{TT}^{DY} =& \frac{d\sigma(\vec{S}_{1T}, \vec{S}_{2T}) - d\sigma(\vec{S}_{1T}, -\vec{S}_{2T})}{d\sigma(\vec{S}_{1T}, \vec{S}_{1T}) + d\sigma(\vec{S}_{1T}, -\vec{S}_{2T})} \\ =& |\vec{S}_{1T}||\vec{S}_{2T}| \frac{\sin^2\theta \cos(2\phi - \phi_{s_1} - \phi_{s_2})}{1 + \cos^2\theta} \\ & \times \frac{\sum_q e_q^2 \left[\triangle_T q(x_1) \triangle_T \bar{q}(x_2) + \triangle_T \bar{q}(x_1) \triangle_T q(x_2)\right]}{\sum_q e_q^2 \left[q(x_1)\bar{q}(x_2) + \bar{q}(x_1) q(x_2)\right]}, \end{aligned} \tag{4.7}$$

where θ is the polar angle of $\mu^+\mu^-$ and ϕ_{s_i} denotes the azimuthal angle of the spin vector $\vec{S}_{iT}$. By using Eq. (4.7), the transversity distributions $\triangle_T q(x)$ can be measured in the Drell-Yan process. However, there is not enough experimental data to determine the transversity distributions, and it is poorly known.

In the nonrelativistic limit (low Q^2), the transversity distributions $\triangle_T q(x)$ are approximately equal to the helicity distributions $\triangle q(x)$,

$$\triangle_T q(x, Q^2) \approx \triangle q(x, Q^2). \tag{4.8}$$

This relation is often used in the theoretical studies since the transversity distributions are not well determined at this stage. The scale dependence of the transversity was investigated in Ref. [118]. There are also some bounds for the PDFs, and they are often

used in numerical calculations:

$$
\begin{aligned}
&|\triangle q(x)| \leqslant q(x), \\
&|\triangle_T q(x)| \leqslant q(x), \\
&2|\triangle_T q(x)| \leqslant \triangle q(x) + q(x).
\end{aligned} \tag{4.9}
$$

The last relation is called the Soffer inequality [119].

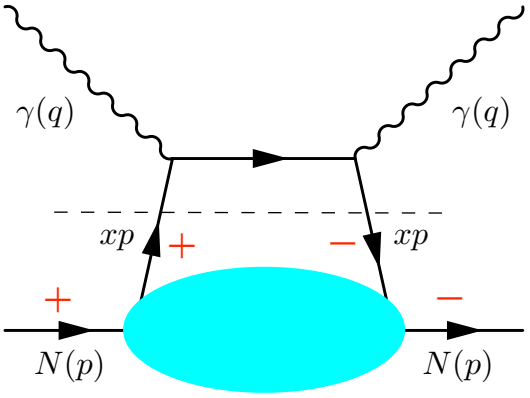

FIGURE 4.2: Transversity distribution in DIS. The lower (soft) part is the transversity distribution, and it flips the helicity of the nucleon.

The other terms of Eq. (4.5) are the higher twist (twist-3) PDFs, and there is a factor $M_N/2$ before higher twist PDFs. In comparison with the leading-twist terms with $\not{p}$, the contributions of the twist-3 PDFs are suppressed by M_N/Q in the cross section, and they can be neglected at large Q^2. The function $e(x)$ is the unpolarized twist-3 PDF, and $h_L^q(x)$ exists in the longitudinally polarized nucleon. As for the twist-3 PDF $g_T^q(x)$, it appears in the transversely polarized nucleon, and it can be measured in the transversely polarized DIS unlike the transversity distribution $\triangle_T q(x)$.

4.1.3 Polarized gluon distribution functions in nucleon

In the previous section, we discussed the quark distribution functions. How about the gluon distribution functions? They are very important especially in the small x region. In future, the Electron Ion Collider (EIC) could be built in US with high energy and high luminosity, and it is perfect to probe the gluon PDFs. For example, one of the main purposes of EIC is to measure the gluon helicity distribution, namely gluon helicity contribution for proton spin, in the proton, and this will help us solve the proton spin puzzle.

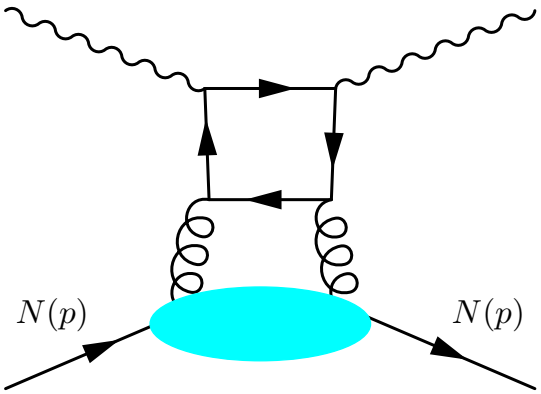

FIGURE 4.3: Gluon distribution functions in the electron-proton DIS. The lower (soft) part is the gluon distribution, and the higher part is a NLO correction of QCD in the cross section.

The gluon distributions often appear as the next-to-leading-order(NLO) correction in the cross section. In Fig. 4.3, it is a NLO correction of the DIS, where the additional α_s suppresses contributions of the gluon distributions in the high energy region.

In order to study the gluon distributions, one can define the gluon density matrix [120],

$$\rho_{\mu\nu}(x) = \int \frac{d\tau}{2\pi} \langle p, S | A^{\mu}(0) A^{\nu}(\tau n) | p, S \rangle \, e^{i\tau x}, \tag{4.10}$$

where A^{μ} is the gluon field. By considering hermiticity, parity invariance and time-reversal invariance, the gluon density matrix $\rho_{\mu\nu}(x)$ [120] can be expresssed as

$$\begin{aligned} \rho_{\mu\nu}(x) = &-\frac{1}{2x} g(x) g_{T\mu\nu} - \frac{1}{2x} \triangle g(x) i M_N \epsilon^{\mu\nu\alpha\beta} p_\alpha n_\beta (S \cdot n) \\ &- \frac{1}{x} g_3(x) i M_N \epsilon^{\mu\nu\alpha\beta} S_{T\alpha} n_\beta + \frac{1}{x} g_4(x) M_N^2 n^\mu n^\nu. \end{aligned} \tag{4.11}$$

Here, $g(x)$ is the unpolarized gluon distribution function (twist-2) and the definition of $g_{T\mu\nu}$ is given in Eq. (1.39). The function $\triangle g(x)$ is the gluon helicity distribution which exists in the longitudinally polarized nucleon, and the physical interpretation is shown in Fig. (4.1). The factor $\epsilon^{\mu\nu\alpha\beta}$ is Levi-Civita tensor with $\epsilon^{0123} = 1$ and the vector n is same as the one in Eq. (4.5). The third function $g_3(x)$ is the twist-3 gluon distribution function, and it requires a transversely polarized nucleon. The last one $g_4(x)$ is the unpolarized twist-4 gluon distribution function which is suppressed by M_N^2/Q^2 at high Q^2.

If Eq. (4.5) is compared with Eq. (4.11), we find there is no gluon transversity distribution, whereas the quark transversity distribution $\triangle_T q(x)$ exist in the nucleon. This is because there is no way to satisfy the helicity (angular momentum) conservation. In Fig. 4.10, the gluon transversity distribution [16, 68, 121–123] flips the helicity by the

unit of 2 for the gluon; however, the nucleon helicity is changed from $\lambda_1 = +$ to $\lambda_2 = -$. The angular momentum conservation $\lambda_1/2 + h_2 = \lambda_2/2 + h_1$ is not satisfied due to spin 1/2 nature of the nucleon. For a spin-1 hadron such as ρ or deuteron, the gluon transversity distribution exists and the angular momentum conservation is satisfied.

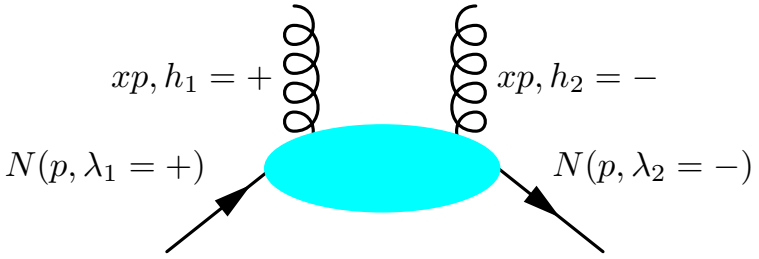

FIGURE 4.4: Gluon transversity in the nucleon. h_1 and h_2 are the helicities of the outgoing gluon and the incoming gluon, respectively. λ_1 and λ_2 are the helicities of the initial and final nucleons.

4.2 Next-to-leading order corrections in hadron reactions

4.2.1 Leading-order Drell-Yan process

Since experimental measurements become more and more precise recently in high-energy hadron reactions, it is necessary to study next-to-leading order (NLO) corrections. Here, we take the unpolarized Drell-Yan as an example to illustrate the NLO corrections in hadron reactions.

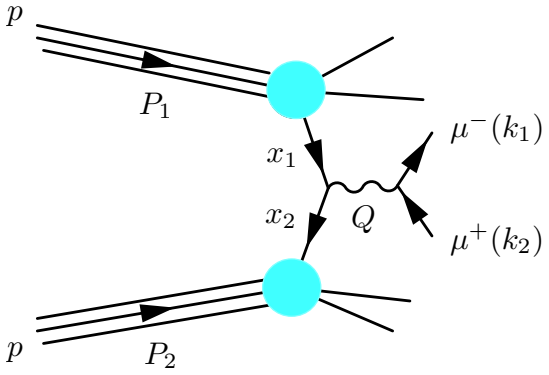

FIGURE 4.5: Leading-order contribution of proton-proton Drell-Yan process.

At the leading-order (LO) level, the cross section of Drell-Yan process can be expressed by the quark and antiquark distribution functions as [124] ,

$$d\sigma = q(x_1)\bar{q}(x_2)dx_1dx_2\hat{\sigma}(q + \bar{q} \to \mu^+\mu^-), \tag{4.12}$$

where $\hat{\sigma}(q + \bar{q} \to \mu^+\mu^-)$ is the cross section for the subprocess $q + \bar{q} \to \mu^+\mu^-$ shown in Fig. 4.5. The variable s is the proton-proton center-of-mass energy squared, and the center-of-mass energy squared of the subprocess is $\hat{s} = x_1 x_2 s$. In the high energy limit, one can neglect the muon mass, so that the cross section for the subprocess $q(p_1) + \bar{q}(p_2) \to \mu^+(k_1) + \mu^-(k_2)$ is expressed as

$$\sigma^0 = \hat{\sigma}(q + \bar{q} \to \mu^+\mu^-) = \frac{4\pi\alpha^2 e_q^2}{9m^2}, \tag{4.13}$$

where $m^2 = (k_1 + k_2)^2$ is the center-of-mass energy squared of muon pair, α is the fine structure constant, and e_q is the quark charge. If we define $x_1 = \sqrt{\tau}e^y$ and $x_2 = \sqrt{\tau}e^{-y}$, y is rapidity and $\tau = m^2/s$. With $dx_1 dx_2 = d\tau dy$, the cross section can be reexpressed,

$$\begin{aligned} \frac{d\sigma}{d\tau dy} &= \frac{4\pi\alpha^2}{9m^2} P_{q\bar{q}}(x_1, x_2), \\ P_{q\bar{q}}(x_1, x_2) &= \sum_q e_q^2 \left[q(x_1)\bar{q}(x_2) + \bar{q}(x_1)q(x_2)\right]. \end{aligned} \tag{4.14}$$

If one integrate Eq. (4.14) over y, it becomes

$$\frac{d\sigma}{d\tau} = \frac{4\pi\alpha^2}{9m^2} \int_\tau^1 \frac{dx_1}{x_1} P_{q\bar{q}}(x_1, \frac{\tau}{x_1}). \tag{4.15}$$

With the experimental measurements of Drell-Yan process, the PDFs can be determined.

4.2.2 Next-to-leading-order corrections of Drell-Yan process and their relation to prompt-photon production process

At the NLO level, one needs to consider the contributions of other Feynman diagrams such as $q(p_1) + g(p_2) \to \mu^+(k_1) + \mu^-(k_2) + q(q_2)$ shown in Fig. 4.6. In this subprocess, three are three particles in the final state, and the cross section is expressed as [124]

$$d\hat{\sigma}(q + g \to \mu^+ + \mu^- + q) = \frac{1}{2\hat{s}} \frac{M_\mu M_\nu^\dagger}{m^4} L^{\mu\nu} dR_3, \tag{4.16}$$

where M^μ is the amplitude of $q + g \to \gamma^* + q$, and m^4 comes from the propagator of the virtual photon. dR_3 is the three-body phase space, and $L^{\mu\nu}$ is the lepton tensor for muon pair. We decompose the three-body phase space into the two-body phase space as

$$\begin{aligned} d\hat{\sigma}(q + g \to \mu^+ + \mu^- + q) &= \frac{1}{2\hat{s}} M_\mu M_\nu^\dagger \frac{L^{\mu\nu}}{m^4} dR_{12} dm^2 \frac{d\hat{t}}{16\pi^2\hat{s}}, \\ dR_3 &= dR_{12} dm^2 \frac{d\hat{t}}{16\pi^2\hat{s}}, \end{aligned} \tag{4.17}$$

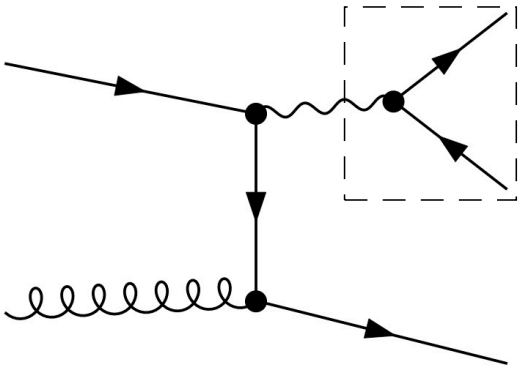

FIGURE 4.6: The subprocess $q(p_1) + g(p_2) \to \mu^+(k_1) + \mu^-(k_2) + q(q_2)$.

where dR_{12} is the two-body phase space for muon pair, and $\hat{t} = (p_1 - q_1)^2$ is defined for the process $q + g \to \gamma^* + q$. The variable q_1 is the momentum of the virtual photon, and $\hat{s}$ is the center-of-mass energy squared for this subprocess. Integrating $L^{\mu\nu}$ with the two-body phase space, we obtain

$$\begin{aligned} T^{\mu\nu} =& \frac{L^{\mu\nu}}{m^4} dR_{12}, \\ =& (q_1^\mu q_1^\nu - m^2 g^{\mu\nu}) \frac{2\alpha e_q^2}{3m^4}. \end{aligned} \tag{4.18}$$

The term $q_1^\mu q_1^\nu$ does not contribute due to $M_\mu q_1^\mu = 0$, so that the cross section becomes

$$\begin{aligned} d\hat{\sigma}(q + g \to \mu^+ + \mu^- + q) &= \frac{1}{2\hat{s}} M_\mu M_\nu^\dagger (-g^{\mu\nu}) \frac{2\alpha e_q^2}{3m^2} dm^2 \frac{d\hat{t}}{16\pi^2 \hat{s}}, \\ \frac{d\hat{\sigma}(q + g \to \gamma^* + q)}{d\hat{t}} &= \frac{1}{16\pi \hat{s}^2} M_\mu M_\nu^\dagger (-g^{\mu\nu}). \end{aligned} \tag{4.19}$$

The term $M_\mu M_\nu^\dagger(-g^{\mu\nu})$ is actually the amplitude squared of $q + g \to \gamma^* + q$, and the polarization sum of the vitual photon is $-g^{\mu\nu}$. Integrating the cross section over $\hat{t}$, we have

$$\frac{d\hat{\sigma}(q + g \to \mu^+ + \mu^- + q)}{\sigma^0 d\hat{\tau}} = \frac{3}{4\pi^2 \alpha e_q^2} \hat{s}\hat{\sigma}(q + g \to \gamma^* + q). \tag{4.20}$$

where σ^0 is shown in Eq. (4.13) and $\hat{\tau} = m^2/\hat{s}$. Then, the $2 \to 3$ process is described by the $2 \to 2$ process by considering the virtual photon as a massive boson, and this will simplify our calculation. Therefore, the Drell-Yan formalism can be used for describing the cross section of the prompt-photon-production process.

There are both ultraviolet divergences and infrared divergences in the NLO calculation. The ultraviolet divergences appear in the photon-quark vertex correction and external quark-leg corrections. The infrared divergences exist since we consider quarks as massless particles, and we will encounter them in the photon-quark vertex correction, the external quark-leg correction, and the quark propagator $1/\hat{t}$ (see Fig. 4.6). In order to handle the divergences, one needs to regularize them.

A popular regularization scheme is the dimensional regularization, where one calculates the amplitude and phase space in the $D = 4 + \epsilon$ dimensions, and the divergences show up as $1/\epsilon$. Both the infrared divergences and the ultraviolet divergences are regularized at the same time in the dimensional regularization, therefore, it is a convenient method. Moreover, the dimensional regularization is widely used in the higher-older calculations such as next-to-next-to-leading order corrections. In this thesis, we will use the dimensional regularization for discussing the NLO corrections of Drell-Yan process. In the $D = 4 + \epsilon$ dimensions, Eq. (4.20) is slightly changed,

$$\frac{d\hat{\sigma}(q + g \to \mu^+ + \mu^- + q)}{\sigma^0 d\hat{\tau}} = \frac{3}{4\pi^2 \alpha e_q^2 (1 + \frac{\epsilon}{2})} \hat{s}\hat{\sigma}(q + g \to \gamma^* + q), \tag{4.21}$$

where σ^0 is the Born cross section in the $D = 4 + \epsilon$ dimensions.

There are two subprocesses for the NLO corrections of the Drell-Yan process: $q + \bar{q} \to \gamma^* + g$ and $q + g \to \gamma^* + q$. We will first consider the contribution of $q + \bar{q} \to \gamma^* + g$, and quark PDFs and antiquark PDFs are involved in this process. Integrating the amplitude squared of $q + \bar{q} \to \gamma^* + g$ with the two-body phase space in the $D = 4 + \epsilon$ dimensions, we have

$$\begin{aligned} d\hat{\sigma}(q + \bar{q} \to \gamma^* + g) =& \int \frac{1}{2\hat{s}} |\overline{M}|^2 dR_2, \\ =& \frac{1 - \hat{\tau}}{32\pi \hat{s} 2^\epsilon \Gamma(1 + \epsilon/2)} \left[\frac{m^2(1 - \hat{\tau})^2}{4\pi\hat{\tau}} \right]^{\epsilon/2} \int_{-1}^{1} |\overline{M}|^2 (1 - y^2)^{\epsilon/2} dy, \end{aligned} \tag{4.22}$$

where the two-body phase space dR_2 is given in Appendix A.1, $y = \cos\theta$, $\hat{\tau} = m^2/\hat{s}$, and the angle between p_1 and q_1 is θ. In Fig. 4.7, there are two Feynman diagrams which contribute to the amplitude.

The amplitude squared of M_1 can be expressed as

$$\begin{aligned} |\overline{M}_1|^2 =& c_f \mathrm{Tr}\left[\not{p}_2 \gamma^\mu \not{k} \gamma^\beta \not{p}_1 \gamma_\beta \not{k} \gamma_\mu \right] \frac{1}{(k^2)^2}, \\ =& 2c_f (2 + \epsilon)^2 \frac{\hat{u}}{\hat{t}}, \end{aligned} \tag{4.23}$$

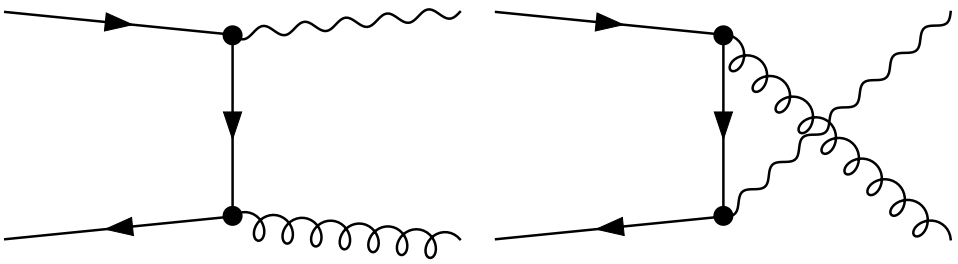

FIGURE 4.7: Feynman diagrams of $q(p_1) + \bar{q}(p_2) \to \gamma^*(q_1) + g(q_2)$ at the order of α_s. M_1 is the t channel amplitude and M_2 is the u channel one.

where $c_f = \frac{16\pi^2\alpha\alpha_D^s e_q^2}{9}$, $\hat{t} = k^2 = (p_1 - q_1)^2 = (p_2 - q_2)^2$, and $\hat{u} = k_1^2 = (p_1 - q_2)^2 = (p_2 - q_1)^2$. In the D dimensions, the strong coupling constant α_D^s should have the mass dimension of ϵ, and $\alpha_D^s = \alpha_s(m_s)^\epsilon$ is introduced to make sure α_s is dimensionless. Here, m_s is called regularization mass.

Similarly, the amplitude squared for M_2 can be calculated as

$$\begin{aligned}|\overline{M}_2|^2=&c_f \mathrm{Tr}\left[\not{p}_2\gamma^\beta \not{k}_1\gamma^\mu \not{p}_1\gamma_\mu \not{k}_1\gamma_\beta\right]\frac{1}{(k_1^2)^2}\\ =&2c_f(2+\epsilon)^2\frac{\hat{t}}{\hat{u}}.\end{aligned} \tag{4.24}$$

There are also contributions for the interference terms of M_1 and M_2:

$$\begin{aligned}M_1M_2^\dagger + M_2M_1^\dagger =&2\mathrm{Re}(M_1M_2^\dagger)\\ =&2c_f \mathrm{Tr}\left[\not{p}_2\gamma^\mu \not{k}\gamma^\beta \not{p}_1\gamma_\mu \not{k}_1\gamma_\beta\right]\frac{1}{k^2}\frac{1}{k_1^2}\\ =&16c_f(1+\frac{\epsilon}{2})(\frac{\hat{s}m^2}{\hat{u}\hat{t}}+\frac{\epsilon}{2}).\end{aligned} \tag{4.25}$$

Summing over all the contributions, we have

$$\begin{aligned}|\overline{M}|^2=&|\overline{M}_1|^2+|\overline{M}_2|^2+2\mathrm{Re}(M_1M_2^\dagger)\\ =&8c_f(1+\frac{\epsilon}{2})\left[\frac{\hat{u}^2+\hat{t}^2+2m^2\hat{s}}{\hat{u}\hat{t}}+\frac{\epsilon}{2}\frac{(\hat{u}+\hat{t})^2}{\hat{u}\hat{t}}\right].\end{aligned} \tag{4.26}$$

Expressing $\hat{u}$ and $\hat{t}$ with $y = \cos\theta$ and $\hat{\tau}$, we obtain

$$|\overline{M}|^2 = 8c_f(1+\frac{\epsilon}{2})\left[\frac{2(1+\hat{\tau})^2+2(1-\hat{\tau})^2y^2}{(1-\hat{\tau})^2(1-y^2)}+\epsilon\frac{2}{1-y^2}\right],$$
$$\hat{t} = -\frac{\hat{s}}{2}(1-\hat{\tau})(1-y), \hat{u} = -\frac{\hat{s}}{2}(1-\hat{\tau})(1+y). \tag{4.27}$$

We substitute Eq. (4.27) into Eq. (4.22) and integrate over y. Then, the cross section is obtained for $q+\bar{q}\to\gamma^*+g$ as

$$\hat{\sigma}(q+\bar{q}\to\gamma^*+g) = \frac{4\pi\alpha\alpha_s e_q^2}{9\hat{s}}\left[\frac{m^2(1-\hat{\tau})^2}{\pi\hat{\tau}m_s^2}\right]^{\epsilon/2}(1+\frac{\epsilon}{2})\frac{(1-\hat{\tau})}{2^\epsilon\Gamma(1+\frac{\epsilon}{2})}$$
$$\times\left\{\frac{\sqrt{\pi}\Gamma(\frac{\epsilon}{2})}{\Gamma(\frac{\epsilon}{2}+\frac{3}{2})}+2\left[\frac{(1+\hat{\tau})^2}{(1-\hat{\tau})^2}+\epsilon\right]\frac{\sqrt{\pi}\Gamma(\frac{\epsilon}{2})}{\Gamma(\frac{\epsilon}{2}+\frac{1}{2})}\right\} \tag{4.28}$$

where the integrals over y are found in Appendix A.2. By using Eq. (4.21), one obtains the cross section $\hat{\sigma}_{q\bar{q}} = \hat{\sigma}(q+\bar{q}\to\mu^+ + \mu^- + g)$ as

$$\frac{d\hat{\sigma}_{q\bar{q}}}{d\hat{\tau}} = \frac{4\alpha_s}{3\pi}\sigma^0\left[\frac{m^2(1-\hat{\tau})^2}{\pi\hat{\tau}m_s^2}\right]^{\epsilon/2}\frac{\Gamma(1+\frac{\epsilon}{2})}{\Gamma(1+\epsilon)}\left[\frac{(1+\hat{\tau}^2)}{1-\hat{\tau}}\frac{2}{\epsilon}+\epsilon\frac{1-\hat{\tau}}{1+\epsilon}\right], \tag{4.29}$$

where the following relation is used,

$$\frac{\Gamma(1+\frac{\epsilon}{2})}{\Gamma(1+\epsilon)}\left[\frac{(1+\hat{\tau}^2)}{1-\hat{\tau}}\frac{2}{\epsilon}+\epsilon\frac{1-\hat{\tau}}{1+\epsilon}\right]$$
$$= \frac{(1-\hat{\tau})}{2^\epsilon 4\Gamma(1+\frac{\epsilon}{2})}\left\{\frac{\sqrt{\pi}\Gamma(\frac{\epsilon}{2})}{\Gamma(\frac{\epsilon}{2}+\frac{3}{2})}+2\left[\frac{(1+\hat{\tau})^2}{(1-\hat{\tau})^2}+\epsilon\right]\frac{\sqrt{\pi}\Gamma(\frac{\epsilon}{2})}{\Gamma(\frac{\epsilon}{2}+\frac{1}{2})}\right\}. \tag{4.30}$$

In Eq. (4.29), it seems that the most divergent term is $\sim 1/\epsilon$. However, one can find the term of $\sim 1/\epsilon^2$ by expanding ϵ [125]:

$$(1-\hat{\tau})^{(\epsilon-1)} = \frac{1}{\epsilon}\delta(1-\hat{\tau})+\frac{1}{(1-\hat{\tau})_+}+\epsilon\left[\frac{\ln(1-\hat{\tau})}{1-\hat{\tau}}\right]_+. \tag{4.31}$$

Then, the most divergent term in Eq. (4.29) actually behaves like $\sim 1/\epsilon^2$,

$$\frac{d\hat{\sigma}_{q\bar{q}}}{d\hat{\tau}} \sim \frac{16\alpha_s}{3\pi}\sigma^0\left[\frac{m^2}{4\pi m_s^2}\right]^{\epsilon/2}\Gamma(1-\frac{\epsilon}{2})\frac{1}{\epsilon^2}\delta(1-\hat{\tau}). \tag{4.32}$$

The definition of the plus function $[f(x)]_+$ is given in Appendix A.3.

There are also virtual corrections for the quark-antiquark annihilation process $q+\bar{q}\to\gamma^*$, and Feynman diagrams are shown in Fig. 4.8. The first diagram is the quark vertex correction, and the other two are external quark-leg corrections. There are both infrared divergences and the ultraviolet divergences in those diagrams, and they can be also

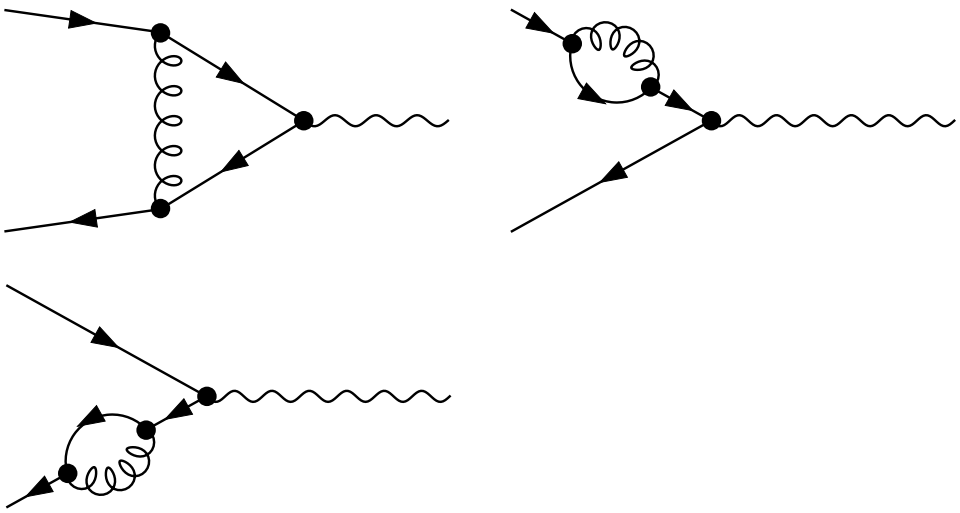

FIGURE 4.8: Quark vertex correction and the quark-leg corrections at next-to-leading order.

regularized by dimensional regularization. The cross section of these virtual corrections is expressed as

$$\frac{d\hat{\sigma}_r}{d\hat{\tau}} = \frac{2\alpha_s\sigma^0}{3\pi}\left[\frac{m^2}{4\pi m_s^2}\right]^{\epsilon/2}\Gamma(1-\frac{\epsilon}{2})\left[-\frac{8}{\epsilon^2}-\frac{6}{\epsilon}-8+\pi^2\right]\delta(1-\hat{\tau}). \tag{4.33}$$

When one combines the contribution in Eq. (4.29) with the virtual corrections in Eq. (4.33), the divergent term of $1/\epsilon^2$ is exactly cancelled (see Eq. (4.32)):

$$\begin{aligned}
\frac{d\hat{\sigma}_{q\bar{q}}}{\sigma^0 d\hat{\tau}} =& \frac{\alpha_s}{\pi}P_{qq}(\hat{\tau})\ln(\frac{m^2}{m_s^2}) + \frac{2\alpha_s}{3\pi}(\frac{4\pi^2}{3}-\frac{7}{2})\delta(1-\hat{\tau}) + 2\alpha_s f_q(\hat{\tau}),\\
\alpha_s f_q(\hat{\tau}) =& \frac{2\alpha_s}{3\pi}\Big\{2(1+\hat{\tau}^2)\left[\frac{\ln(1-\hat{\tau})}{1-\hat{\tau}}\right]_+ - \frac{(1+\hat{\tau}^2)}{1-\hat{\tau}}\ln(\hat{\tau}) - (\frac{\pi^2}{3}+\frac{9}{4})\delta(1-\hat{\tau})\Big\},\\
&+\frac{\alpha_s}{2\pi}P_{qq}(\hat{\tau})\left[\frac{2}{\epsilon}+\gamma_e-\ln(4\pi)\right],
\end{aligned} \tag{4.34}$$

where $P_{qq}(\hat{\tau})$ is the splitting function for $q \to q$ in Eq.(1.28). Therefore, the divergent term of $1/\epsilon$ still appears in the total cross section, and this term is purely the infrared divergence [124].

Now let us discuss the contributions of the subprocess $q(p_1)+g(p_2) \to \mu^+(k_1)+\mu^-(k_2)+q(q_2)$. There are two Feynman diagrams for this subprocess shown in Fig. 4.9, the first

one is s-channel and the second one is t-channel.

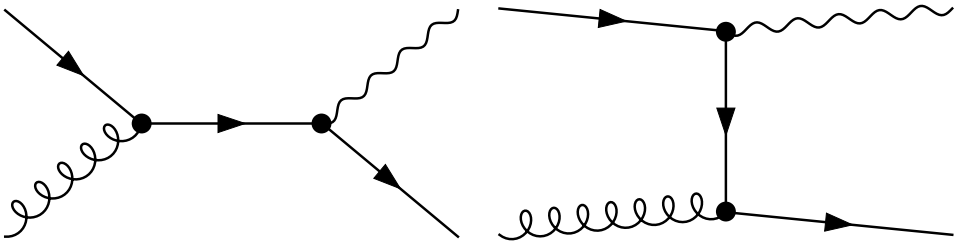

FIGURE 4.9: Feynman diagrams of $q(p_1) + g(p_2) \to \gamma^* + q(q_2)$ at the order of α_s.

The amplitude squared of the s-channel Feynman diagram is expressed as

$$\begin{aligned} |\overline{L}_1|^2 =& c_f \mathrm{Tr}\left[\not{p}_2\gamma^\mu \not{p}\gamma^\beta \not{p}_1\gamma_\beta \not{p}\gamma_\mu\right] \frac{1}{(p^2)^2} \\ =& 2c_f(2+\epsilon)^2 \frac{-\hat{t}}{\hat{s}}, \end{aligned} \tag{4.35}$$

where $\hat{s} = p^2 = (p_1 + p_2)^2 = (q_1 + q_2)^2$ and $\hat{t} = (p_1 - q_1)^2 = (p_2 - q_2)^2$. The amplitude squared $|\overline{L}_1|^2$ is free of divergence. Similarly, we calculate the contribution of the t-channel amplitude as

$$\begin{aligned} |\overline{L}_2|^2 =& c_f \mathrm{Tr}\left[\not{q}_2\gamma^\beta \not{k}\gamma^\mu \not{q}_1\gamma_\mu \not{k}\gamma_\beta\right] \frac{1}{(k^2)^2} \\ =& 2c_f(2+\epsilon)^2 \frac{-\hat{s}}{\hat{t}}. \end{aligned} \tag{4.36}$$

The divergence appears in $|\overline{L}_1|^2$ due to the term $1/\hat{t} \sim 1/(1-y)$, and it is the infrared divergence. Finally, we will consider the contribution from the interference terms:

$$\begin{aligned} L_1 L_2^\dagger + L_2 L_1^\dagger =& 2\mathrm{Re}(L_1 L_2^\dagger), \\ =& 2c_f \mathrm{Tr}\left[\not{q}_2\gamma^\beta \not{k}\gamma^\mu \not{p}_1\gamma_\beta \not{p}\gamma_\mu\right] \frac{1}{k^2}\frac{1}{p^2}, \\ =& 16c_f(1+\frac{\epsilon}{2})(-\frac{\hat{u}m^2}{\hat{s}\hat{t}} - \frac{\epsilon}{2}), \end{aligned} \tag{4.37}$$

where the infrared divergence appears in the collinear limit. The amplitude squared for $q+g\to\gamma^*+q$ is obtained as

$$\begin{aligned}|\overline{L}|^2=&|\overline{L}_1|^2+|\overline{L}_2|^2+2\mathrm{Re}(L_1L_2^\dagger),\\ =&8c_f(1+\frac{\epsilon}{2})\left[-\frac{\hat{s}^2+\hat{t}^2+2m^2\hat{u}}{\hat{s}\hat{t}}-\frac{\epsilon}{2}\frac{(\hat{s}+\hat{t})^2}{\hat{s}\hat{t}}\right].\end{aligned}\tag{4.38}$$

Substituting $\hat{t}=-\frac{\hat{s}}{2}(1-\hat{\tau})(1-y)$ and $\hat{u}=-\frac{\hat{s}}{2}(1-\hat{\tau})(1+y)$ into Eq. (4.38), we have

$$\begin{aligned}|\overline{L}|^2=&\,3c_f(1+\frac{\epsilon}{2})\left[\frac{4+(1-\hat{\tau})^2(1-y)^2-4\hat{\tau}(1-\hat{\tau})(1+y)}{2(1-\hat{\tau})(1-y)},\right.\\ &\left.+\,\epsilon\frac{[4+(1-\hat{\tau})(1+y)]^2}{4(1-\hat{\tau})(1-y)}\right].\end{aligned}\tag{4.39}$$

Next, integrating $|\overline{L}|^2$ with the phase space by using Eq. (4.22), we obtain

$$\begin{aligned}d\hat{\sigma}(q+g\to\gamma^*+q)=&\frac{\pi\alpha\alpha_s e_q^2\Gamma(1+\epsilon/2)}{6\hat{s}\Gamma(1+\epsilon)}\left[\frac{m^2(1-\hat{\tau})^2}{4\pi\hat{\tau}}\right]^{\epsilon/2}(1+\epsilon/2)\\ &\times\left[2(\tau^2+(1-\hat{\tau})^2)\frac{2}{\epsilon}+(3+\tau-3\tau^2)\right],\end{aligned}\tag{4.40}$$

where the integrals over y is found in Appendix A.2. The divergence behaves like $1/\epsilon$, and it is the infrared divergence which appears in the collinear limit ($y=0$). The cross section of $q+g\to\gamma^*+q$ is changed for the one of $q+g\to\mu^++\mu^-+q$ [124] as

$$\frac{d\hat{\sigma}_{qg}}{\sigma^0 d\hat{\tau}}=\frac{\alpha_s}{2\pi}\left[\frac{m^2(1-\hat{\tau})^2}{\pi\hat{\tau}m_s^2}\right]^{\epsilon/2}\frac{\Gamma(1+\frac{\epsilon}{2})}{\Gamma(1+\epsilon)}\left[\frac{1}{2}(\tau^2+(1-\hat{\tau})^2)\frac{2}{\epsilon}+\frac{1}{4}(3+2\tau-3\tau^2)\right].\tag{4.41}$$

Expanding $\left[\frac{m^2(1-\hat{\tau})^2}{\pi\hat{\tau}m_s^2}\right]^{\epsilon/2}$ over ϵ, we obtain

$$\begin{aligned}\frac{d\hat{\sigma}_{qg}}{\sigma^0 d\hat{\tau}}=&\frac{\alpha_s}{2\pi}P_{qg}(\hat{\tau})\ln(\frac{m^2}{m_s^2})+\alpha_s f_g(\hat{\tau}),\\ \alpha_s f_g(\hat{\tau})=&\frac{\alpha_s}{4\pi}\Big\{\left(\tau^2+(1-\hat{\tau})^2\right)\ln\frac{(1-\hat{\tau})^2}{\hat{\tau}}+\frac{1}{2}(3+2\tau-3\tau^2)\Big\}\\ &+\frac{\alpha_s}{2\pi}P_{qg}(\hat{\tau})\left[\frac{2}{\epsilon}+\gamma_e-\ln(4\pi)\right],\end{aligned}\tag{4.42}$$

where $P_{qg}(\hat{\tau})$ is the gluon splitting function for $g\to q$ in Eq. (1.30). Substituting Eq. (4.42) and Eq. (4.34) into the cross section of Drell-Yan process, we have

$$\frac{d\sigma_{DY}}{d\tau}=\int_\tau^1\frac{dx_1}{x_1}\int_{\tau/x_1}^1\frac{dx_2}{x_2}q(x_1)q(x_2)\frac{d\hat{\sigma}}{d\hat{\tau}}.\tag{4.43}$$

With the NLO corrections, the cross section can be expressed as [124]

$$
\begin{aligned}
s\frac{d\sigma_{DY}}{dm^2} =& \sum_q \frac{4\pi\alpha e_q^2}{9m^2}\int_\tau^1 \frac{dx_1}{x_1}\int_{\tau/x_1}^1 \frac{dx_2}{x_2}\left[q(x_1)\bar{q}(x_2)+\bar{q}(x_1)q(x_2)\right] \\
&\times\left[(1+\alpha_s(\frac{8\pi}{9\pi}-\frac{7}{3\pi}))\delta(1-\hat{\tau})+\frac{\alpha_s}{\pi}P_{qq}(\hat{\tau})\ln(\frac{m^2}{m_s^2})+2\alpha_s f_q(\hat{\tau})\right] \\
&+\left[q(x_1)g(x_2)+g(x_1)q(x_2)\right]\left[\frac{\alpha_s}{2\pi}P_{qg}(\hat{\tau})\ln(\frac{m^2}{m_s^2})+\alpha_s f_g(\hat{\tau})\right] \\
&+\left[\bar{q}(x_1)g(x_2)+g(x_1)\bar{q}(x_2)\right]\left[\frac{\alpha_s}{2\pi}P_{qg}(\hat{\tau})\ln(\frac{m^2}{m_s^2})+\alpha_s f_g(\hat{\tau})\right]. \qquad (4.44)
\end{aligned}
$$

In this cross section, we still find infrared divergence $1/\epsilon$ in $f_q(\hat{\tau})$ and $f_g(\hat{\tau})$, and it belongs to the nonpertubative part of QCD. In order to handle the divergence, one needs to renormalize the PDFs, namely, the divergence terms are absorbed into the nonpertubative PDFs. Therefore, one considers the PDFs in Eq.(4.44) as the bare PDFs $q^0(x)$, and the physical PDFs are defined as

$$
\begin{aligned}
q(x,m^2) =& q^0\otimes\left[1+\frac{\alpha_s}{2\pi}P_{qq}\ln(\frac{m^2}{m_s^2})+\frac{\alpha_s}{2\pi}P_{qq}\left(\frac{2}{\epsilon}+\gamma_e-\ln(4\pi)\right)\right] \\
&+g^0\otimes\left[1+\frac{\alpha_s}{2\pi}P_{qg}\ln(\frac{m^2}{m_s^2})+\frac{\alpha_s}{2\pi}P_{qg}\left(\frac{2}{\epsilon}+\gamma_e-\ln(4\pi)\right)\right], \\
g(x,m^2) =& g^0\otimes\left[1+\frac{\alpha_s}{2\pi}P_{qq}\ln(\frac{m^2}{m_s^2})+\frac{\alpha_s}{2\pi}P_{gg}\left(\frac{2}{\epsilon}+\gamma_e-\ln(4\pi)\right)\right] \\
&+\sum_q q^0\otimes\left[\frac{\alpha_s}{2\pi}P_{gq}\ln(\frac{m^2}{m_s^2})+\frac{\alpha_s}{2\pi}P_{gq}\left(\frac{2}{\epsilon}+\gamma_e-\ln(4\pi)\right)\right]. \qquad (4.45)
\end{aligned}
$$

Here, we define the convolution integral notation:

$$
f(z)=g\otimes c=\int_z^1\frac{dy}{y}g(z/y)c(y)=\int_z^1\frac{dy}{y}g(y)c(z/y). \qquad (4.46)
$$

If we differentiate the physical PDFs with respect to m^2 for the quark and gluon distributions, one obtains the DGLAP evolution equation in Eq. (1.27) and Eq. (1.29). Reexpress Eq. (4.44) with the physical PDFs [124],

$$
\begin{aligned}
s\frac{d\sigma_{DY}}{dm^2} =& \sum_q \frac{4\pi\alpha e_q^2}{9m^2}\int_\tau^1 \frac{dx_1}{x_1}\int_{\tau/x_1}^1 \frac{dx_2}{x_2}\left[q(x_1,m^2)\bar{q}(x_2,m^2)+\bar{q}(x_1,m^2)q(x_2,m^2)\right] \\
&\times\left[1+\alpha_s(\frac{8\pi}{9\pi}-\frac{7}{3\pi})\delta(1-\hat{\tau})+2\alpha_s c_q(\hat{\tau})\right] \\
&+\left[q(x_1,m^2)g(x_2,m^2)+g(x_1,m^2)q(x_2,m^2)\right]\left[\alpha_s c_g(\hat{\tau})\right] \\
&+\left[\bar{q}(x_1,m^2)g(x_2,m^2)+g(x_1,m^2)\bar{q}(x_2,m^2)\right]\left[\alpha_s c_g(\hat{\tau})\right]. \qquad (4.47)
\end{aligned}
$$

This final cross section is free of divergence, and we can use this theoretical cross section

to investigate experimental measurements. The functions $c_q(\hat{\tau})$ and $c_g(\hat{\tau})$ are defined as follows

$$\begin{aligned}\alpha_s c_q(\hat{\tau}) =& \frac{2\alpha_s}{3\pi}\Big\{2(1+\hat{\tau}^2)\left[\frac{\ln(1-\hat{\tau})}{1-\hat{\tau}}\right]_+ - \frac{(1+\hat{\tau}^2)}{1-\hat{\tau}}\ln(\hat{\tau}) - (\frac{\pi^2}{3}+\frac{9}{4})\delta(1-\hat{\tau})\Big\},\\ \alpha_s c_g(\hat{\tau}) =& \frac{\alpha_s}{4\pi}\Big\{\left(\tau^2+(1-\hat{\tau})^2\right)\ln\frac{(1-\hat{\tau})^2}{\hat{\tau}} + \frac{1}{2}(3+2\tau-3\tau^2)\Big\}. \end{aligned} \tag{4.48}$$

4.3 Gluon transveristy of deuteron in DIS

4.3.1 Introduction to gluon transveristy in deuteron

In Section 4.1.3, we discussed the polarized gluon distributions in the nucleon. We noticed that there is no gluon transversity in the nucleon because of the angular-momentum conservation. However, there exists gluon transversity in ρ meson and deuteron since their spin is $S = 1$ [16, 68, 121–123]. The deuteron is a stable hadron which is widely used as targets in high energy hadron experiments, so it is possible to investigate the gluon transversity in the deuteron.

The deuteron is considered as a loosely bound system of proton and neutron, and it is often used to investigate structure functions of the neutron since the neutron cannot be used as a stable target. If the deuteron is loosely bounded, the gluon transversity is small because the spin-1/2 nucleons do not contribute [123]. Therefore, a finite gluon transversity could reflect an interesting dynamical aspect in the deuteron. In this case, it is very interesting to measure the gluon transversity experimentally for the deuteron. In Chapter 2, we studied the tensor-polarized structure of the deuteron, and the experimental measurements by HERMES collaboration do not quite agree with the conventional picture that the deuteron as a bound state of proton and neutron. Together with the tensor-polarized structure, the gluon transversity will probe interesting dynamical structure of the deuteron.

In Ref. [123], the gluon transversity was first theoretically estimated by a model that the deuteron state is $|\, d\,\rangle = |\, NN\,\rangle + \epsilon|\, \Delta\Delta\,\rangle$. The spin of Δ baryon is bigger than 1, and the deuteron gluon transversity comes from the component $|\, \Delta\Delta\,\rangle$. The gluon transversity is the leading-twist PDF in the deuteron, so that the contribution could be significant to be measured. It will be measured in the electron-deuteron DIS process at JLab [126].

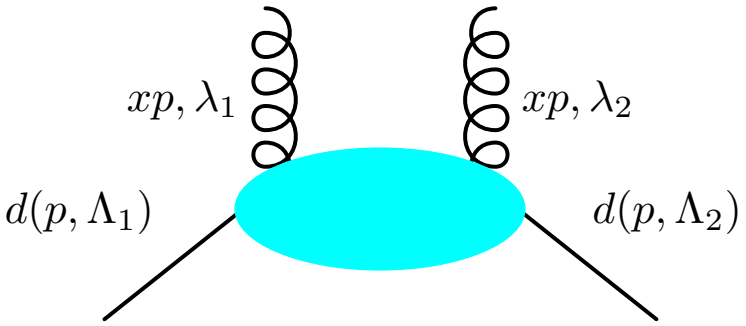

FIGURE 4.10: Gluon transversity in the deuteron. Λ_1 and Λ_2 are helicities of deuteron, and λ_1 and λ_2 are helicities of gluon.

4.3.2 Deuteron polarizations

Gluon distribution in the deuteron is schematically shown in Fig. 4.10, and it appears if the helicities of the deuteron and gluon are flipped. In order to keep the angular-momentum conservation $\Lambda_1 + \lambda_2 = \Lambda_2 + \lambda_1$ so as to have the gluon transversity, the helicities should be $\Lambda_1 = \lambda_1 = \pm$ and $\Lambda_2 = \lambda_2 = \mp$. Polarization vectors $\epsilon^\mu(\Lambda)$ are used to describe the spin states of the deuteron. For the deuteron with its momentum $P = (P^0, 0, 0, P^3)$, the helicity states $\Lambda = \pm$ are expressed by $\epsilon(\Lambda = \pm) = \frac{1}{\sqrt{2}}(0, \mp 1, -i, 0)$ in the same way with the photon case. In addition to the helicity state of $\Lambda = \pm$, there is also the helicity $\Lambda = 0$ state:

$$\epsilon^\mu(\Lambda = 0) = \left(\frac{P^3}{M_d}, 0, 0, \frac{P^0}{M_d}\right), \tag{4.49}$$

where M_d is the deuteron mass. In order to describe the polarization states of deuteron, the spin vector S^μ is also used:

$$S_\mu = -\epsilon_{\mu\nu\alpha\beta} \frac{P^\nu}{M_d} \mathrm{Im}(\epsilon^{*\alpha}\epsilon^\beta). \tag{4.50}$$

For polarization vector $\epsilon^\mu(\Lambda = \pm)$, we have $S^\mu = \left(\pm\frac{P^3}{M_d}, 0, 0, \pm\frac{P^0}{M_d}\right)$. If the deuteron is linearly polarized,

$$\epsilon_x = (0, 1, 0, 0), \epsilon_y = (0, 0, 1, 0), \tag{4.51}$$

the spin vector is $S^\mu = 0$.

4.3.3 Gluon transveristy in DIS

The gluon transversity is probed in the electron-deuteron DIS process shown in Fig. 4.11, where the virtual photon comes from the electron. The deuteron helicity is flipped from $\pm$ to $\mp$ by the polarized-gluon emission and absorption, and the helicity of the photon is also flipped to compensate the helicity change of the gluon. The hard part is just the helicity amplitude of $\gamma^*(q_1,\lambda_1)g(q_2,\Lambda_1) \to \gamma^*(q_2,\lambda_1)g(q_2,\Lambda_2)$ where the intermediate state is on shell.

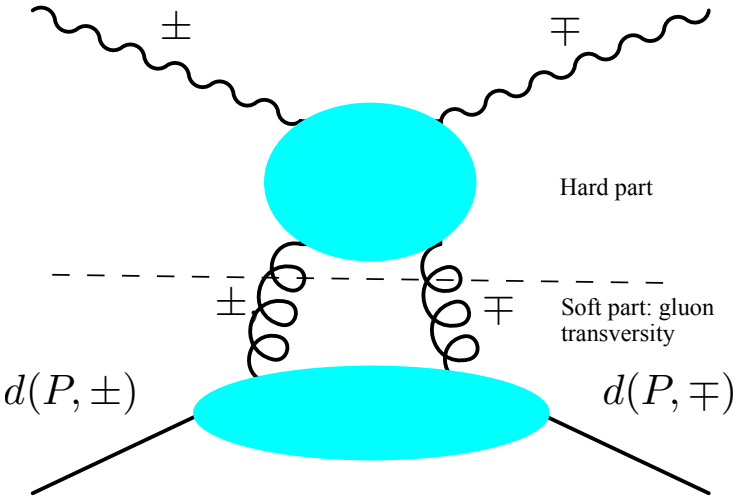

FIGURE 4.11: Helicity amplitude $\gamma^*(q_1,\lambda_1)g(q_2,\Lambda_1) \to \gamma^*(q_2,\lambda_1)g(q_2,\Lambda_2)$.

In the following, we show how to calculate the helicity amplitude of $\gamma^*(q_1,\lambda_1)g(q_2,\Lambda_1) \to \gamma^*(q_2,\lambda_1)g(q_2,\Lambda_2)$ [16, 68, 121, 123, 126, 127], and we define the helicity amplitude as

$$A_{\lambda_1\Lambda_1,\lambda_2\Lambda_2} = \epsilon_p(\lambda_1)^\alpha \epsilon_p^*(\lambda_2)^\beta T_{\alpha\beta,\mu\nu} \epsilon_g(\Lambda_1)^\mu \epsilon_g^*(\Lambda_2)^\nu, \tag{4.52}$$

where ϵ_p is the photon polarization vector and ϵ_g is the gluon polarization vector. By considering the parity invariance, $A_{--,++} = A_{++,--}$ and $A_{+-,-+} = A_{-+,+-}$, the helicity amplitude vanishes for $A_{+-,-+} = A_{-+,+-}$ since the auglular momentum is not conserved. Then, we have the relations:

$$\begin{aligned} A_{++,--} &= A_{++,--} + A_{+-,-+} \\ &= \epsilon_p(+)^\alpha \epsilon_p^*(-)^\beta T_{\alpha\beta,\mu\nu} \left[\epsilon_g(+)^\mu \epsilon_g^*(-)^\nu + \epsilon_g(-)^\mu \epsilon_g^*(+)^\nu \right], \\ A_{--,++} &= A_{--,++} + A_{-+,+-} \\ &= \epsilon_p(-)^\alpha \epsilon_p^*(+)^\beta T_{\alpha\beta,\mu\nu} \left[\epsilon_g(-)^\mu \epsilon_g^*(+)^\nu + \epsilon_g(+)^\mu \epsilon_g^*(-)^\nu \right], \end{aligned} \tag{4.53}$$

Adding these two equations, we obtain

$$2A_{++,--} = \left[\epsilon_p(-)^\alpha \epsilon_p^*(+)^\beta + \epsilon_p(+)^\alpha \epsilon_p^*(-)^\beta\right] T_{\alpha\beta,\mu\nu} \left[\epsilon_g(-)^\mu \epsilon_g^*(+)^\nu + \epsilon_g(+)^\mu \epsilon_g^*(-)^\nu\right], \tag{4.54}$$

Therefore, we define a photon tensor as $E_{Tp}^{\alpha\beta} = \epsilon_p(-)^\alpha \epsilon_p^*(+)^\beta + \epsilon_p(+)^\alpha \epsilon_p^*(-)^\beta$ and a gluon tensor as $E_{Tg}^{\mu\nu} = \epsilon_g(-)^\mu \epsilon_g^*(+)^\nu + \epsilon_g(+)^\mu \epsilon_g^*(-)^\nu$. If the virtual-photon momentum is chosen as the z axis and the gluon momentum is $-z$ axis, we can use Eq. (1.34) as the photon polarization vectors and Eq. (3.2) as the gluon polarization vectors:

$$E_{Tp} = E_{Tg} = E_T = \begin{pmatrix} 0 & 0 & 0 & 0 \\ 0 & -1 & 0 & 0 \\ 0 & 0 & 1 & 0 \\ 0 & 0 & 0 & 0 \end{pmatrix}. \tag{4.55}$$

It is actually $E_T^{\mu\nu} = -(\epsilon_x^\mu \epsilon_x^\nu - \epsilon_y^\mu \epsilon_y^\nu)$ in Eq.(4.51), namely, the gluon transversity can be considered as the difference between linearly x polarization and linearly y polarization.

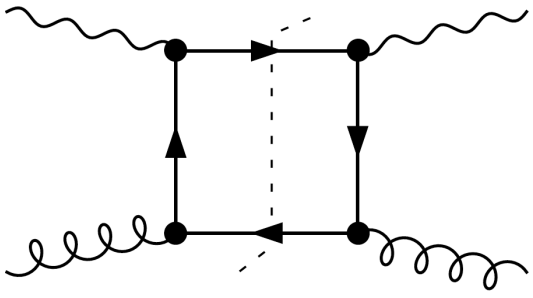

FIGURE 4.12: Leading-order contribution to the amplitude $\gamma^*(q_1)g(q_2) \to \gamma^*(q_1)g(q_2)$, where quark and antiquark are on shell.

The leading-order contribution for the amplitude $\gamma^*(q_1)g(q_2) \to \gamma^*(q_2,)g(q_2)$ is shown in Fig. 4.12, which is just the amplitude squared of $\gamma^*(q_1)g(q_2) \to q(k_1)\bar{q}(k_2)$. In the

center-of-mass frame of q_1 and q_2, the kinematical variables are defined as follows:

$$
\begin{aligned}
&q_1 = (q_v, 0, 0, q), \quad q_2 = (q, 0, 0, -q), \quad q_1^2 = -Q^2, \quad q = \frac{s+Q^2}{2\sqrt{s}}, \\
&k_1 = \frac{\sqrt{s}}{2}\,(1, \sin\theta\cos\phi, \sin\theta\cos\phi, \cos\theta), \\
&k_2 = \frac{\sqrt{s}}{2}\,(1, -\sin\theta\cos\phi, -\sin\theta\cos\phi, -\cos\theta), \\
&t = -\frac{s+Q^2}{2}\,(1-\cos\theta), \quad u = -\frac{s+Q^2}{2}\,(1+\cos\theta), \\
&k_T^2 = \frac{s\,\sin^2\theta}{4}, \quad k_x^2 - k_y^2 = \frac{s\,\sin^2\theta\,(\cos^2\phi - \sin^2\phi)}{4},
\end{aligned}
\tag{4.56}
$$

where $k_T^2 = k_x^2 + k_y^2$, $k_{1x} = -k_{2x} = k_x$ and $k_{1y} = -k_{2y} = k_y$. Here, the initial photon and gluon momenta are q_1 and q_2, and the quark and antiquark momenta are k_1 and k_2. The polar and azimuthal angles of the quark are denoted as θ and ϕ, and k_T is its transverse momentum.

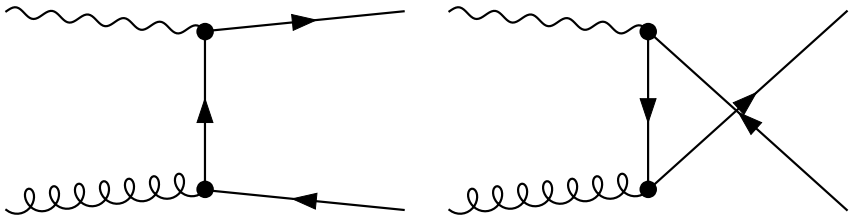

FIGURE 4.13: Feynman diagrams of $\gamma^*(q_1)g(q_2) \to q(k_1)\bar{q}(k_2)$.

In Fig. 4.13, there are two Feynman diagrams for the process $\gamma^*(q_1)g(q_2) \to q(k_1)\bar{q}(k_2)$. The amplitude L_1 is called the t-channel one, and its squared is expressed as

$$
\begin{aligned}
|L_1|^2 &= (e^2 e_q^2 g_s^2)\mathrm{Tr}\left[\not{k}_1\gamma_\alpha(\not{q}_2 - \not{k}_2)\gamma_\mu \not{k}_2\gamma_\nu(\not{q}_2 - \not{k}_2)\gamma_\beta\right]\frac{1}{t^2}E_T^{\alpha\beta}E_T^{\mu\nu} \\
&= 16(e^2 e_q^2 g_s^2)\frac{-k_T^2 t - 2(k_x^2 - k_y^2)^2}{t^2}
\end{aligned}
\tag{4.57}
$$

Similarly, the u channel amplitude squared is

$$
\begin{aligned}
|L_2|^2 &= (e^2 e_q^2 g_s^2)\mathrm{Tr}\left[\not{k}_1\gamma_\mu(\not{k}_1 - \not{q}_2)\gamma_\alpha \not{k}_2\gamma_\nu(\not{k}_1 - \not{q}_2)\gamma_\beta\right]\frac{1}{u^2}E_T^{\alpha\beta}E_T^{\mu\nu} \\
&= 16(e^2 e_q^2 g_s^2)\frac{-k_T^2 u - 2(k_x^2 - k_y^2)^2}{u^2}.
\end{aligned}
\tag{4.58}
$$

Finally, the interference terms between L_1 and L_2 are

$$\begin{aligned} 2L_2^\dagger L_1 &= 2(e^2 e_q^2 g_s^2)\mathrm{Tr}\left[\not{k}_1'\gamma_\alpha(\not{q}_2 - \not{k}_2')\gamma_\mu \not{k}_2'\gamma_\beta(\not{k}_1' - \not{q}_2)\gamma_\nu\right]\frac{1}{ut}E_T^{\alpha\beta}E_T^{\mu\nu} \\ &= 16(e^2 e_q^2 g_s^2)\frac{-k_T^2(u+t) - 4(k_x^2 - k_y^2)^2 - ut}{ut}. \end{aligned} \tag{4.59}$$

In total, the absolute-value squared of the amplitude becomes

$$\begin{aligned} |L|^2 &= -\,16\,e^2\,e_q^2\,g_s^2\,\frac{ut\left\{2k_T^2(u+t)+ut\right\} + 2(k_x^2-k_y^2)^2(u+t)^2}{u^2t^2} \\ &= -16\,e^2\,e_q^2\,g_s^2\left[\frac{s^2\,\cos 4\phi}{Q^2+s} + (\frac{Q^2}{Q^2+s})^2\right]. \end{aligned} \tag{4.60}$$

There is no collinear divergence in the amplitude at $k_T = 0$. Therefore, it does not need the dimensional regularization as we had in the longitudinal polarized DIS process. If $|L|^2$ is integrated over the two-body phase space $dR_2 = 1/(4\pi)^2 \sin\theta d\phi$, we obtain

$$|L|^2 dR_2 = -2\,e^2\,e_q^2\,g_s^2\,\frac{z^2}{\pi}, \quad z = \frac{Q^2}{Q^2+s}. \tag{4.61}$$

The amplitude vanishes at $Q^2 = 0$, namely, the massless quark and antiquark pair cannot be produced from the real-photon and real-gluon collision with the same helicity. This happens because of the vector current nature of QCD and QED. However, if Q^2 is finite (Q^2 should be bigger than a few GeV^2) in the DIS, the gluon transversity can be measured in a transversely polarized or linearly-polarized deuteron in the DIS. For example, the DIS process is possible at JLab with the unpolarized electron beam and the transversely polarized deuteron target, and the differential cross section of $e(l)+d(P) \to e+\gamma^*(q)+d(P) \to e(l_1)+X$ [16, 68, 121, 123, 126, 127] is expressed as

$$\begin{aligned} &\frac{d\sigma}{dxdyd\phi_1} = \frac{e^4 ME}{4\pi^2 Q^4}\left[xy^2F_1(x,Q^2) + (1-y)F_2(x,Q^2) - \frac{x(1-y)}{2}\Delta(x,Q^2)\cos\phi_1\right], \\ &x = \frac{Q^2}{2P\cdot q}, \quad y = \frac{q\cdot P}{P\cdot l}, \end{aligned} \tag{4.62}$$

where ϕ_1 is the azimuthal angle for l_1, and the structure functions $F_1(x,Q^2)$ and $F_2(x,Q^2)$ of the deuteron are found in Eq. (1.24). As for the structure function $\Delta(x,Q^2)$, it contains the information of the deuteron gluon transversity $g_x(x,Q^2) - g_y(x,Q^2)$:

$$\Delta(x,Q^2) = \frac{\alpha_s}{2\pi}\sum_q e_q^2 x^2 \int_x^1 \frac{dy}{y^3}\left[g_x(x,Q^2) - g_y(x,Q^2)\right]. \tag{4.63}$$

4.4 Gluon transveristy in proton-deuteron collision

4.4.1 Introduction to prompt photon production

The deuteron gluon transversity has been studied in the DIS process; however, it has never been investigated in the proton-deuteron collision, both theoretically and experimentally. Here, we theretically propose a possible process on prompt-photon production in the proton-deuteron collision with linearly-polarized deuteron.

In the proton-deuteron collision, there are some processes that we can use them to explore the gluon transversity of the deuteron. For example, we consider the hadron production $p + d \to \Lambda + X$ and the prompt photon production $p + d \to \gamma + X$. In the first processes, the cross section vanishes as far as we studied, so they cannot be used to study the gluon transversity. However, the gluon transversity is involved in the prompt-photon production with the higher-twist (twist-3) term of the proton. In the following, we explain the prompt-photon production and show how we obtain the gluon transversity.

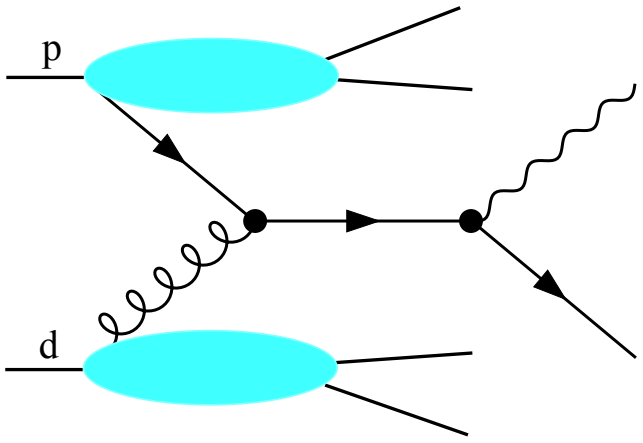

FIGURE 4.14: Prompt-photon production in the proton-deuteron collision, $p(p_a) + d(p_b) \to \gamma(q_1) + q(q_2) + X$.

In Fig. 4.14, the prompt-photon production [128–132] in the proton-deuteron collision is shown. In the center mass frame of proton and deuteron, we define the kinematical

variables of Fig. 4.14 as follows:

$$\begin{aligned}
&\hat{s} = x_a x_b s = (p_1 + p_2)^2, \\
&\hat{t} = (p_1 - q_1)^2 = (p_2 - q_2)^2 = -x_a p_T \sqrt{s} e^{-y}, \\
&\hat{u} = (p_1 - q_2)^2 = (p_2 - q_1)^2 = -x_b p_T \sqrt{s} e^{y}, \\
&p_1 = x_a p_a = \frac{x_a \sqrt{s}}{2}(1,0,0,1), \quad p_2 = x_b p_b = \frac{x_b \sqrt{s}}{2}(1,0,0,-1), \\
&q_1 = p_T(\cosh y, \cos\phi, \sin\phi, \sinh y).
\end{aligned} \tag{4.64}$$

Here, p_1 is the momentum of the quark which comes from proton, p_2 is the momentum of the gluon, y is rapidity for photon, q_1 and q_2 are momenta of the photon and the quark in the final state, respectively. The cross section of the prompt-photon production is written as [128]

$$\begin{aligned}
d\sigma =& \frac{1}{2\hat{s}}\, q(x_a)\, g(x_b)\, dx_a\, dx_b\, |M(q + g \to \gamma + q)|^2 \\
&\times (2\pi)^4\, \delta^4(p_1 + p_2 - q_1 - q_2)\, \frac{d^3 q_1}{(2\pi)^3 2q_1^0}\, \frac{d^3 q_2}{(2\pi)^3 2q_2^0}.
\end{aligned} \tag{4.65}$$

Integrating the cross section over q_2, we have

$$q_1^0 \frac{d\sigma}{d^3 q_1} = \int \frac{\hat{s}}{\pi} q(x_a) g(x_b) dx_a dx_b \frac{d\hat{\sigma}(q + g \to \gamma + q)}{d\hat{t}} \delta(\hat{s} + \hat{t} + \hat{u}). \tag{4.66}$$

By substituting $\hat{s} = -x_a p_T \sqrt{s} e^{-y}$ and $\hat{u} = -x_b p_T \sqrt{s} e^{y}$ and integrating over x_b to remove the δ function, the cross section becomes [128]

$$\frac{d\sigma}{p_T\, dp_T\, d\phi\, dy} = \frac{2}{\pi} \int_{x_{amin}}^{1} q(x_a) g(x_b) dx_a \frac{x_a x_b}{2x_a - x_T e^{y}} \frac{d\hat{\sigma}(q + g \to \gamma + q)}{d\hat{t}}, \tag{4.67}$$

where the following relations are used: $d^3 q_1 / q_1^0 = p_T dp_T d\phi dy$, $x_T = 2p_T/\sqrt{s}$, $x_b = (x_a x_T e^{-y})/(2x_a - x_T e^{y})$, and the minimum value is $x_{amin} = (x_T e^{y})/(2 - x_T e^{-y})$.

4.4.2 Gluon transveristy in prompt-photon production

The following differential cross section combination is investigated for the prompt-photon production in the proton-deuteron collision:

$$d\sigma_\tau = [d\sigma(s_1, \epsilon_x; +) - d\sigma(s_1, \epsilon_x; -)] - [d\sigma(s_1, \epsilon_y; +) - d\sigma(s_1, \epsilon_y; -)], \tag{4.68}$$

where $\epsilon_x = (0,1,0,0)$ and $\epsilon_y = (0,0,1,0)$ are linear-polarization vectors of the deuteron, and the helicity of final photon is marked as $+/-$. s_1 is the transverse-polarization

vector of the proton:

$$s_1 = (0, \cos\phi_s, \sin\phi_s, 0). \tag{4.69}$$

In the transversely-polarized proton, only three types of the PDFs exist up to the twist-3 level. They are unpolarized PDFs $q(x)$, transversity distributions $\triangle_T q(x)$, and the twist-3 PDFs $g_T^q(x)$ (see Eq. (4.5)). The contribution of unpolarized PDFs vanishes in Eq. (4.68). As for the transversity distribution $\triangle_T q(x)$, it is chirally odd and it brings two γ matrices into the amplitude squared of $q(p_1) + g(p_2) \to \gamma(q_1) + q(q_2)$, so the amplitude squared will vanish. Then the only choice left is the twist-3 PDFs $g_T^q(x)$, and the contribution in the final cross section is suppressed by M_p/Q.

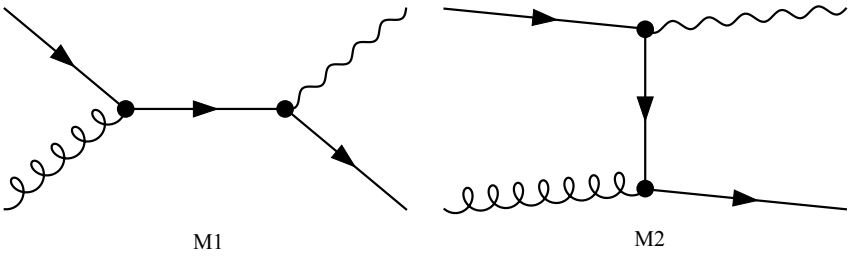

FIGURE 4.15: Feynman diagrams of $q(p_1) + g(p_2) \to \gamma(q_1) + q(q_2)$. The amplitude of s channel is marked as M_1 and the amplitude of t channel is marked as M_2.

In the prompt-photon production, there are two leading Feynman diagrams on $q(p_1) + g(p_2) \to \gamma(q_1) + q(q_2)$ as shown in Fig. 4.15. Since the deuteron spin asymmetry is taken between ϵ_x and ϵ_y, the gluon polarization tensor [127, 133–135] in this subprocess is

$$E_T^{\alpha\beta} = \epsilon_x^\alpha \epsilon_x^{*\beta} - \epsilon_y^\alpha \epsilon_y^{*\beta} = -\left[\epsilon(+)^\alpha \epsilon^{*\beta}(-) + \epsilon(-)^\alpha \epsilon^{*\beta}(+)\right], \tag{4.70}$$

and the gluon helicity is flipped by ± 2 for $q(p_1) + g(p_2) \to \gamma(q_1) + q(q_2)$. The amplitude of Fig. 4.15 is expressed as

$$M = (M_1^\omega + M_2^\omega)\, \epsilon_\omega^*(\lambda), \tag{4.71}$$

where $\epsilon_\mu^*(\lambda)$ is the polarization vector of the outgoing photon. Furthermore, one obtains the amplitude squared of Eq. (4.71) as

$$M M^\dagger = (M_1^\omega M_1^{\dagger\sigma} + M_2^\omega M_2^{\dagger\sigma} + M_1^\omega M_2^{\dagger\sigma} + M_2^\omega M_1^{\dagger\sigma})[\epsilon_\omega^*(+)\epsilon_\sigma(+) - \epsilon_\omega^*(-)\epsilon_\sigma(-)]. \tag{4.72}$$

There are two choices to define the antisymmetric photon polarization tensor $P_{\omega\sigma} = \epsilon_\omega^*(+)\epsilon_\sigma(+) - \epsilon_\omega^*(-)\epsilon_\sigma(-)$:

(1) $\epsilon^*_\omega(+)\epsilon_\sigma(+) - \epsilon^*_\omega(-)\epsilon_\sigma(-) = \epsilon^*_\omega(+)\epsilon_\sigma(+) - \epsilon_\omega(+)\epsilon^*_\sigma(+)$ is antisymmetric, Lorentz invariant, and vertical to photon momentum q_1, so that this combination should be expressed as $\propto \epsilon_{\omega\sigma\mu\nu}q_1^\mu r^\nu$. Since $\epsilon_\omega(\lambda)$ can be defined as the convenient one which does not have zero component ($\epsilon_0(\lambda) = 0$), we take $r^\nu = q_2^\nu$ to cancel the zero component in the tensor [136–138]:

$$P_{\omega\sigma} = \epsilon^*_\omega(+)\epsilon_\sigma(+) - \epsilon^*_\omega(-)\epsilon_\sigma(-) = i\frac{\epsilon_{\omega\sigma\mu\nu}q_1^\mu q_2^\nu}{q_1\cdot q_2}. \tag{4.73}$$

(2) It is convenient to express $\epsilon_\omega(\lambda)$ by the Lorentz invariants in the process $q(p_1) + g(p_2) \to \gamma(q_1) + q(q_2)$. If the direction of the photon momentum is chosen as the z axis, the x axis can be defined as $e_x^\omega = -(q_1\cdot q_2 p_1^\omega - q_1\cdot p_1 q_2^\omega - p_1\cdot q_2 q_1^\omega)$, and the y axis can be defined as $e_y^\omega = -\epsilon_{\omega\rho\mu\nu}q_2^\rho p_1^\mu q_1^\nu$. Therefore, one writes the photon polarization vectors $\epsilon(\pm)$ by e_x and e_y as [139, 140]

$$\epsilon(+) = -\sqrt{\frac{2}{\hat{s}\hat{t}\hat{u}}}(e_x + ie_y),\ \epsilon(-) = \sqrt{\frac{2}{\hat{s}\hat{t}\hat{u}}}(e_x - ie_y).$$

Then, the antisymmetric photon polarization tensor $P_{\omega\sigma}$ is expressed by the Lorentz invariants.

In order to confirm our results, the two different choices of antisymmetric photon polarization tensor $P_{\omega\sigma}$ are used in calculating the amplitude squared of $q + g \to \gamma + q$.

There are four terms in the amplitude squared:

$$\begin{aligned}
M_1^\omega M_1^{\dagger\sigma} &= c_f\frac{1}{\hat{s}^2}\mathrm{Tr}\left[\gamma^5 \not{s}_1\gamma_\beta(\not{p}_1 + \not{p}_2)\gamma_\sigma \not{q}_2\gamma_\omega(\not{p}_1 + \not{p}_2)\gamma_\alpha\right]E_T^{\alpha\beta},\\
M_2^\omega M_2^{\dagger\sigma} &= c_f\frac{1}{\hat{t}^2}\mathrm{Tr}\left[\gamma^5 \not{s}_1\gamma_\sigma(\not{p}_1 - \not{q}_1)\gamma_\beta \not{q}_2\gamma_\alpha(\not{p}_1 - \not{q}_1)\gamma_\omega\right]E_T^{\alpha\beta},\\
M_1^\omega M_2^{\dagger\sigma} &= c_f\frac{1}{\hat{s}\hat{t}}\mathrm{Tr}\left[\gamma^5 \not{s}_1\gamma_\beta(\not{p}_1 + \not{p}_2)\gamma_\sigma \not{q}_2\gamma_\alpha(\not{p}_1 - \not{q}_1)\gamma_\omega\right]E_T^{\alpha\beta},\\
M_2^\omega M_1^{\dagger\sigma} &= c_f\frac{1}{\hat{s}\hat{t}}\mathrm{Tr}\left[\gamma^5 \not{s}_1\gamma_\sigma(\not{p}_1 - \not{q}_1)\gamma_\beta \not{q}_2\gamma_\omega(\not{p}_1 + \not{p}_2)\gamma_\alpha\right]E_T^{\alpha\beta},
\end{aligned} \tag{4.74}$$

where the factor c_f is given by $c_f = \frac{M_p}{2}\frac{1}{6}e_a^2 g^2 g_s^2 x_a$, M_p is the proton mass which exists due to the twist-3 PDFs $g_T^q(x)$ in Eq. (4.5), and 1/6 is the color factor. The summation of these terms are

$$\begin{aligned}
|M|^2 =& (M_1^\omega M_1^{\dagger\sigma} + M_2^\omega M_2^{\dagger\sigma} + M_1^\omega M_2^{\dagger\sigma} + M_2^\omega M_1^{\dagger\sigma})P_{\omega\sigma}\\
=& -\frac{16 q\cdot E_T\cdot s_1}{\hat{t}}(\frac{M_p}{2}\frac{1}{6}e_a^2 g^2 g_s^2 x_a)\\
=& \frac{16\cos(\phi+\phi_s)}{x_a\sqrt{s}e^{-y}}(\frac{M_p}{2}\frac{1}{6}e_a^2 g^2 g_s^2 x_a).
\end{aligned} \tag{4.75}$$

where $A \cdot E_T \cdot B = A_\alpha E_T^{\alpha\beta} B_\beta$ and $q \cdot E_T \cdot s_1 = -k_3 \cdot E_T \cdot s_1 = p_T \cos(\phi + \phi_s)$ are used. In Eq. (4.75), the factor $1/\hat{t}$ appears which is divergent at the collinear limit ($p_T = 0$). However, we do not need to handle this divergence as we did in Sec. 4.2 because the relatively large-p_T region ($p_T > 1$ GeV) is investigated for the prompt photon production.

The differential cross section of $q + g \to \gamma + q$ is expressed as

$$\frac{d\hat{\sigma}_\tau}{d\hat{t}} = \frac{1}{16\pi \hat{s}^2} |M|^2. \tag{4.76}$$

Substituting Eq. (4.76) into Eq. (4.67), one finally obtains the differential cross section for the prompt photon production:

$$\frac{d\sigma_\tau}{p_T\, dp_T\, d\phi\, dy} = \frac{2}{\pi} \int_{x_{amin}}^{1} dx_a\, g_T^q(x_a, Q^2)\, \Delta_T g(x_b, Q^2)\, \frac{x_a x_b}{2x_a - x_T e^y} \frac{d\hat{\sigma}_\tau}{d\hat{t}}, \tag{4.77}$$

where $g_T^q(x)$ is the twist-3 quark PDF in Eq. (4.5), and $\Delta_T g(x, Q^2) = g_x(x, Q^2) - g_y(x, Q^2)$ is the deuteron gluon transversity. The energy scale $Q^2 = p_T^2$ is often used in the prompt-photon production.

4.4.3 Summary

The deuteron gluon transversity is a very important quantity, since it reflects new dynamical structure inside the deuteron. The knowledge of the deuteron gluon transversity will help us to understand an interesting exotic aspect of the deuteron structure beyond the simple two-nucleon bound state. However, we know nothing about the deuteron gluon transversity until now. Therefore, it will be very interesting investigate it in the proton-deuteron collision. In this work, we proposed that the prompt photon production process can be used to study the deuteron gluon transversity. In experiment, the measurement of this process is still difficult at this stage because of higher-twist (twist-3) effect and because it may be not easy to detect the helicity of final photon.

Chapter 5

Summary

The tensor-structure of the deuteron can be investigated at high energies by both the structure function b_1 in the DIS process and the spin asymmetry A_Q in the proton-deuteron Drell-Yan process. It is much easier to probe the tensor-polarized antiquark distributions by the asymmetry A_Q. In this work, we gave the theoretical estimate of the spin asymmetry A_Q of the Drell-Yan process by using possible tensor-polarized PDFs to explain the HERMES data, and we found that the asymmetry A_Q is of the order of a few percent. We also found the existence of tensor-polarized gluon PDFs as the Q^2 evolves. In the near future, the structure function b_1 and the asymmetry A_Q will be measured by JLab and Fermilab, respectively. Since the standard deuteron model predication is much different from the HERMES measurement, there is a possibility that a new field of spin physics could be developed by these experimental measurements. The deuteron tensor structure is expected to be understood much better by these measurements.

In order to understand the origin of proton spin, it is necessary to understand contributions from partonic orbital angular momenta. As the observables to probe such contributions, three-dimensional (3D) structure functions are proposed. They contain information on form factors and PDFs. In particular, the generalized parton distributions (GPDs) have been investigated as one of such 3D structure functions. Other important three-dimensional structure functions are the generalized distribution amplitudes (GDAs), and the GPDs can be obtained by the s-t crossing from the GDAs. One way to study the GDAs is the two-photon process $\gamma^*\gamma \to h\bar{h}$, which is possible at KEKB. In this work, we analyzed the Belle cross-section measurements of $\gamma^*\gamma \to \pi^0\pi^0$

in the e^+e^- collision. The pion GDAs used in this analysis are expressed by a few parameters, and resonance contributions of $f_0(500)$ and $f_2(1270)$ are included. The obtained GDAs explain the Belle data well enough with $\chi^2/d.o.f. = 1.09$. The matrix elements of the energy-momentum tensor and the gravitational form factors were investigated from the pion GDA. It is difficult to probe the gravitational form factors directly in experiments since gravitational interactions are too weak. The GPDs and GDAs provide us an alternative way to study these form factors. We also estimated the three-dimensional gravitational radii, and they are $\sqrt{\langle r^2\rangle_{\rm mass}} = 0.32 \sim 0.39\,\text{fm}$ for mass radius and $\sqrt{\langle r^2\rangle_{\rm mech}} = 0.82 \sim 0.88\,\text{fm}$ for the mechanical radius. The mass radius is smaller than the pion charge radius (0.659 ± 0.004 fm [1]), and the mechanical radius is bigger than the charge radius. This is the first estimate of the gravitational radii by analyzing actual experimental measurements. In our analysis, the Belle measurements still have large errors which mainly come from the statistical errors. However, the Belle II collaboration just started taking data with a much higher luminosity in 2019, and the errors are expected to be reduced significantly. Therefore, more precise GDAs can be obtained for the pion and other hadrons in the near future. Accurate GDAs will help us to study gravitational form factors, pressure distributions, and shear-force distributions for hadrons.

The gluon transversity is a twist-2 distribution function for the deuteron, so that it is important for the structure studies of deuteron. The deuteron is a bound state of the proton and neutron. However, the nucleons do not contribute to the gluon transversity directly because they are spin-1/2 particles, so that the gluon transversity is expected to be small. However, a finite gluon transversity could reflect non-nucleonic components in the deuteron, and it probes a new dynamical aspect in hadrons. The deuteron gluon transversity will be measured in the electron-deuteron DIS. In this work, we proposed a possible process to probe the deuteron gluon transversity by using the prompt-photon production process in the proton-deuteron collision. We showed that the cross section is proportional to the gluon transversity of the deuteron and the twist-3 structure function $g_T(x)$ of the proton by using the linearly-polarized deuteron and the trasversely-polarized proton. The studies of the gluon transversity could lead to a finding of a new exotic component in the deuteron.

Acknowledgements

I would first like to thank my thesis advisor Prof. Shunzo Kumano. After I came to Japan, my supervisor helped me a lot both on research and life. No matter how busy he is, he spends time for discussions with me. He also encourages me to discuss with other leading physicists. It was very helpful for me to discuss with Prof. Oleg Teryaev, Prof. Sadaharu Uehara, Prof. Kazuhiro Tanaka, Prof. Dustin Keller, Prof. Wen-Chen Chang and Dr. Daisuke Nomura on my research works, and I want to thank them.

I would also like to thank the people at the KEK theory center. In my first year of graduate studies, I took many lectures on particle physics, nuclear physics, and astrophysics. The lecturers always try their best to educate me. The students of the KEK theory center are very kind, and they always helped me when I was in trouble. I also want to thank the Sokendai office staff for their helpful suggestions.

Finally, I want to thank my family since they always supported me.

Appendix A

Formulae in dimensional regularization

A.1 Two-body phase space in D dimension

In the process $q(p_1) + g(p_2) \to \gamma^*(q_1) + q(q_2)$, the virtual photon is considered as a massive boson. We can define the kinematical variables in the center-mass frame of p_1 and p_2 as follows

$$\begin{aligned}
&\hat{s} = p^2 = (p_1 + p_2)^2, \hat{t} = (p_1 - q_1)^2 = (p_2 - q_2)^2, \\
&\hat{u} = (p_1 - q_2)^2 = (p_2 - q_1)^2, q_1^2 = m^2, \hat{\tau} = \frac{m^2}{\hat{s}}, \\
&E_2 = |\vec{q}_1| = |\vec{q}_2| = \frac{\hat{s} - m^2}{2\sqrt{\hat{s}}}.
\end{aligned} \tag{A.1}$$

The phase space in the D dimension is expressed as

$$\begin{aligned}
dR_2 &= \int \frac{d^{D-1}q_1}{(2\pi)^{D-1}2E_1} \frac{d^{D-1}q_2}{(2\pi)^{D-1}2E_2} (2\pi)^D \delta^D(p - p_1 - p_2), \\
&= \int \frac{1}{(2\pi)^{D-2}} \frac{d^{D-1}q_1}{(2E_1)(2E_2)} \delta(\sqrt{s} - E_1 - E_2).
\end{aligned} \tag{A.2}$$

If we define the momentum p_1 as the z-axis, the angle between p_1 and q_1 is θ. Then, the D-dimensional integral is calculated by

$$\int d^{D-1}q_1 = \frac{2\pi^{\frac{D-2}{2}}}{\Gamma(D/2-1)} E_2^{D-2} dE_2 (1-y^2)^{D/2-2} dy, \tag{A.3}$$

where $y = \cos\theta$. We use Eq. (A.3) for Eq. (A.2) and integrate it over $E_2 = |\vec{q}_1|$ to obtain

$$dR_2 = \int \frac{\pi^{1-D/2}}{2^{D-3}\Gamma(D/2-1)} \frac{E_2^{D-3}}{4\sqrt{\hat{s}}} (1-y^2)^{D/2-2} dy. \tag{A.4}$$

A.2 Integrals used in dimensional regularization

The following integrals are used in the dimensional regularization:

$$\begin{aligned}
&\int dy \frac{y^2}{1-y^2}(1-y^2)^{\frac{\epsilon}{2}} = \frac{\sqrt{\pi}\Gamma(\frac{\epsilon}{2})}{2\Gamma(\frac{\epsilon}{2}+\frac{3}{2})},\\
&\int dy \frac{1}{1-y^2}(1-y^2)^{\frac{\epsilon}{2}} = \frac{\sqrt{\pi}\Gamma(\frac{\epsilon}{2})}{\Gamma(\frac{\epsilon}{2}+\frac{1}{2})},\\
&\int dy \frac{1}{1-y}(1-y^2)^{\frac{\epsilon}{2}} = \frac{\sqrt{\pi}\Gamma(\frac{\epsilon}{2})}{\Gamma(\frac{\epsilon}{2}+\frac{1}{2})},\\
&\int dy \frac{(1-y)^2}{1-y}(1-y^2)^{\frac{\epsilon}{2}} = \frac{\sqrt{\pi}\Gamma(\frac{\epsilon}{2}+1)}{\Gamma(\frac{\epsilon}{2}+\frac{3}{2})},\\
&\int dy \frac{(1+y)}{1-y}(1-y^2)^{\frac{\epsilon}{2}} = \frac{\sqrt{\pi}(\epsilon+2)\Gamma(\frac{\epsilon}{2})}{2\Gamma(\frac{\epsilon}{2}+\frac{3}{2})},\\
&\int dy \frac{(1+y)^2}{1-y}(1-y^2)^{\frac{\epsilon}{2}} = \frac{\sqrt{\pi}(\epsilon+4)\Gamma(\frac{\epsilon}{2})}{2\Gamma(\frac{\epsilon}{2}+\frac{3}{2})},
\end{aligned} \tag{A.5}$$

where there is no divergence in the forth integral; however, the divergence appears as $\Gamma(\frac{\epsilon}{2}) \sim 2/\epsilon$ in the other ones.

A.3 Plus function

The plus function $[f(x)]_+$ is defined as follows [124, 141]

$$\begin{aligned}
&\int_0^1 [f(x)]_+ \, dx = 0,\\
&[f(x)]_+ = \lim_{\beta\to 0}\left[f(x)\theta(1-x-\beta) - \delta(1-x-\beta)\int_0^{1-\beta} f(y)dy \right],
\end{aligned} \tag{A.6}$$

where $\theta(x)$ is the step function. The plus function often appears in the integral, so it is more convenient to reexpress

$$\begin{aligned}&\int_x^1 g(z)\left[f(z)\right]_+ dz\\ =&\int_x^1 \left[g(z)g(1)\right] f(z)dz - f(1)\int_0^x g(z)dz.\end{aligned} \tag{A.7}$$

If $f(x) = 1/(1-x)$, we have

$$\begin{aligned}&\int_x^1 g(\frac{x}{y})\left[\frac{1}{1-y}\right]_+ \frac{dy}{y}\\ =&\int_x^1 \frac{g(\frac{x}{y}) - yg(x)}{1-y}\frac{dy}{y} + g(x)\log(1-x).\end{aligned} \tag{A.8}$$

For $f(x) = \ln(1-x)/(1-x)$, it is given by

$$\begin{aligned}&\int_x^1 g(\frac{x}{y})\left[\frac{\ln(1-y)}{1-y}\right]_+ \frac{dy}{y}\\ =&\int_x^1 \frac{\ln(1-y)\left[g(\frac{x}{y}) - yg(x)\right]}{1-y}\frac{dy}{y} + \frac{g(x)}{2}\log^2(1-x).\end{aligned} \tag{A.9}$$

Bibliography

[1] M. Tanabashi *et al.* [Particle Data Group], Phys. Rev. D **98** (2018) no.3, 030001.

[2] J. Ashman *et al.* [European Muon Collaboration], Phys. Lett. B **206** (1988) 364.

[3] J. Ashman *et al.* [European Muon Collaboration], Nucl. Phys. B **328** (1989) 1.

[4] X. D. Ji, Phys. Rev. Lett. **78** (1997) 610.

[5] X. D. Ji, J. Phys. G **24** (1998) 1181.

[6] M. Diehl, T. Gousset, B. Pire and O. Teryaev, Phys. Rev. Lett. **81** (1998) 1782.

[7] M. Diehl, T. Gousset and B. Pire, Phys. Rev. D **62** (2000) 073014.

[8] M. V. Polyakov, Nucl. Phys. B **555** (1999) 231.

[9] H. Pagels, Phys. Rev. **144** (1966) 1250.

[10] M. V. Polyakov and C. Weiss, Phys. Rev. D **60** (1999) 114017.

[11] S. E. Kuhn, J.-P. Chen and E. Leader, Prog. Part. Nucl. Phys. **63** (2009) 1.

[12] A. Deur, S. J. Brodsky and G. F. De Teramond, arXiv:1807.05250 [hep-ph].

[13] R. L. Jaffe and X. D. Ji, Nucl. Phys. B **375** (1992) 527.

[14] V. Barone, A. Drago and P. G. Ratcliffe, Phys. Rept. **359** (2002) 1.

[15] Vincenzo Barone and Philip G Ratcliffe, *Transverse Spin Physics* (World Scientific, 2003).

[16] P. Hoodbhoy, R. L. Jaffe and A. Manohar, Nucl. Phys. B **312** (1989) 571.

[17] A. Airapetian *et al.* [HERMES Collaboration], Phys. Rev. Lett. **95** (2005) 242001.

[18] F. Halzen and A. D. Martin, "Quarks and Leptons: An Introductory Course in Modern Particle Physics," Wiley Press Inc., (1984) .

[19] G. P. Lepage and S. J. Brodsky, Phys. Rev. D **22** (1980) 2157.

[20] C. Patrignani *et al.* [Particle Data Group], Chin. Phys. C **40** (2016) no.10, 100001.

[21] G. P. Lepage and S. J. Brodsky, Phys. Lett. **87B** (1979) 359.

[22] A. V. Efremov and A. V. Radyushkin, Phys. Lett. **94B** (1980) 245.

[23] P. Ball, JHEP **9901** (1999) 010.

[24] I. C. Cloet, L. Chang, C. D. Roberts, S. M. Schmidt and P. C. Tandy, Phys. Rev. Lett. **111** (2013) 092001.

[25] J. H. Zhang, J. W. Chen, X. Ji, L. Jin and H. W. Lin, Phys. Rev. D **95** (2017) no.9, 094514.

[26] H. Y. Cheng and K. C. Yang, Phys. Rev. D **71** (2005) 054020.

[27] H. Y. Cheng, C. K. Chua and K. C. Yang, Phys. Rev. D **73** (2006) 014017.

[28] H. Y. Cheng, C. K. Chua and K. C. Yang, Phys. Rev. D **77** (2008) 014034.

[29] P. Ball and V. M. Braun, Phys. Rev. D **54** (1996) 2182.

[30] P. Ball, V. M. Braun, Y. Koike and K. Tanaka, Nucl. Phys. B **529** (1998) 323.

[31] P. Ball and V. M. Braun, Nucl. Phys. B **543** (1999) 201.

[32] V. M. Braun and N. Kivel, Phys. Lett. B **501** (2001) 48.

[33] H. Y. Cheng, Y. Koike and K. C. Yang, Phys. Rev. D **82** (2010) 054019.

[34] V. M. Braun, N. Kivel, M. Strohmaier and A. A. Vladimirov, JHEP **1606** (2016) 039.

[35] A. V. Radyushkin, Phys. Rev. D **56** (1997) 5524.

[36] J. C. Collins and A. Freund, Phys. Rev. D **59** (1999) 074009.

[37] K. Goeke, M. V. Polyakov and M. Vanderhaeghen, Prog. Part. Nucl. Phys. **47** (2001) 401.

[38] J. C. Collins, L. Frankfurt and M. Strikman, Phys. Rev. D **56** (1997) 2982.

[39] S. V. Goloskokov and P. Kroll, Eur. Phys. J. C **50** (2007) 829.

[40] S. V. Goloskokov and P. Kroll, Eur. Phys. J. C **53** (2008) 367.

[41] S. V. Goloskokov and P. Kroll, Eur. Phys. J. C **65** (2010) 137.

[42] L. Favart, M. Guidal, T. Horn and P. Kroll, Eur. Phys. J. A **52** (2016) no.6, 158.

[43] E. R. Berger, M. Diehl and B. Pire, Eur. Phys. J. C **23** (2002) 675.

[44] S. Kumano, M. Strikman and K. Sudoh, Phys. Rev. D **80** (2009) 074003.

[45] T. Sawada, W. C. Chang, S. Kumano, J. C. Peng, S. Sawada and K. Tanaka, Phys. Rev. D **93** (2016) no.11, 114034.

[46] X. Ji, Ann. Rev. Nucl. Part. Sci. **54** (2004) 413.

[47] M. Diehl, Phys. Rept. **388** (2003) 41.

[48] A. V. Belitsky and A. V. Radyushkin, Phys. Rept. **418** (2005) 1.

[49] S. Boffi and B. Pasquini, Riv. Nuovo Cim. **30** (2007) 387.

[50] S. Wallon, "Hard Exclusive Processes in Perturbative QCD: from Medium to Aymptotical Energies," Doctoral Schools ED 107 and ED 517.

[51] S. J. Brodsky, D. S. Hwang, B. Q. Ma and I. Schmidt, Nucl. Phys. B **593** (2001) 311.

[52] X. d. Ji, J. P. Ma and F. Yuan, Nucl. Phys. B **652** (2003) 383.

[53] M. Diehl, Eur. Phys. J. C **19** (2001) 485.

[54] I. V. Anikin, B. Pire and O. V. Teryaev, Phys. Rev. D **62** (2000) 071501.

[55] A. Courtoy, "Generalized Parton Distributions of Pions," PhD thesis.

[56] E. R. Berger, F. Cano, M. Diehl and B. Pire, Phys. Rev. Lett. **87** (2001) 142302.

[57] D. Amrath "Exclusive scattering off the deuteron," PhD thesis.

[58] W. Cosyn and B. Pire, Phys. Rev. D **98** (2018) no.7, 074020.

[59] M. Penttinen, M. V. Polyakov, A. G. Shuvaev and M. Strikman, Phys. Lett. B **491** (2000) 96.

[60] N. Kivel, M. V. Polyakov and M. Vanderhaeghen, Phys. Rev. D **63** (2001) 114014.

[61] A. V. Belitsky, D. Mueller and A. Kirchner, Nucl. Phys. B **629** (2002) 323.

[62] B. Lehmann-Dronke, P. V. Pobylitsa, M. V. Polyakov, A. Schafer and K. Goeke, Phys. Lett. B **475** (2000) 147.

[63] M. Diehl, T. Feldmann, P. Kroll and C. Vogt, Phys. Rev. D **61** (2000) 074029.

[64] N. Kivel and L. Mankiewicz, Phys. Rev. D **63** (2001) 054017.

[65] M. Diehl, P. Kroll and C. Vogt, Eur. Phys. J. C **26** (2003) 567.

[66] I. V. Anikin, B. Pire and O. V. Teryaev, Phys. Rev. D **69** (2004) 014018.

[67] B. Pire and O. V. Teryaev, Phys. Lett. B **496** (2000) 76.

[68] R. L. Jaffe and A. Manohar, Nucl. Phys. B **321** (1989) 343.

[69] H. Khan and P. Hoodbhoy, Phys. Rev. C **44** (1991) 1219.

[70] G. A. Miller, Phys. Rev. C **89** (2014) no.4, 045203.

[71] N. N. Nikolaev and W. Schafer, Phys. Lett. B **398** (1997) 245 Erratum: [Phys. Lett. B **407** (1997) 453].

[72] J. Edelmann, G. Piller and W. Weise, Z. Phys. A **357** (1997) 129.

[73] K. Bora and R. L. Jaffe, Phys. Rev. D **57** (1998) 6906.

[74] W. Cosyn, Y. B. Dong, S. Kumano and M. Sargsian, Phys. Rev. D **95** (2017) no.7, 074036.

[75] S. Kumano and Q. T. Song, Phys. Rev. D **94** (2016) no.5, 054022.

[76] S. Kumano, J. Phys. Conf. Ser. **543** (2014) no.1, 012001.

[77] F. E. Close and S. Kumano, Phys. Rev. D **42** (1990) 2377.

[78] S. Hino and S. Kumano, Phys. Rev. D **59** (1999) 094026.

[79] S. Hino and S. Kumano, Phys. Rev. D **60** (1999) 054018.

[80] A. D. Martin, W. J. Stirling, R. S. Thorne and G. Watt, Eur. Phys. J. C **63** (2009) 189.

[81] S. Kumano, Phys. Rev. D **82** (2010) 017501.

[82] M. Masuda *et al.* [Belle Collaboration], Phys. Rev. D **93** (2016) no.3, 032003.

[83] I. F. Ginzburg, A. Schiller and V. G. Serbo, Eur. Phys. J. C **18** (2001) 731.

[84] A. V. Radyushkin, Phys. Rev. D **80** (2009) 094009.

[85] S. S. Agaev, V. M. Braun, N. Offen and F. A. Porkert, Phys. Rev. D **83** (2011) 054020.

[86] Y. M. Wang and Y. L. Shen, JHEP **1712** (2017) 037.

[87] C. Berger and W. Wagner, Phys. Rept. **146** (1987) 1.

[88] N. Kivel, L. Mankiewicz and M. V. Polyakov, Phys. Lett. B **467** (1999) 263.

[89] N. Warkentin, M. Diehl, D. Y. Ivanov and A. Schafer, Eur. Phys. J. A **32** (2007) 273.

[90] P. Bydzovsky, R. Kamiski and V. Nazari, Phys. Rev. D **90** (2014) no.11, 116005.

[91] P. Bydzovsky, R. Kamiski and V. Nazari, Phys. Rev. D **94** (2016) no.11, 116013.

[92] I. V. Anikin, B. Pire, L. Szymanowski, O. V. Teryaev and S. Wallon, Phys. Rev. D **71** (2005) 034021.

[93] I. V. Anikin, I. O. Cherednikov, N. G. Stefanis and O. V. Teryaev, Eur. Phys. J. C **61** (2009) 357.

[94] H. Kawamura and S. Kumano, Phys. Rev. D **89** (2014) no.5, 054007.

[95] S. J. Brodsky and G. R. Farrar, Phys. Rev. Lett. **31** (1973) 1153.

[96] S. Kumano, Q. T. Song and O. V. Teryaev, Phys. Rev. D **97** (2018) 014020.

[97] M. V. Polyakov, Phys. Lett. B **555** (2003) 57.

[98] K. Goeke, J. Grabis, J. Ossmann, M. V. Polyakov, P. Schweitzer, A. Silva and D. Urbano, Phys. Rev. D **75** (2007) 094021.

[99] W. Broniowski and E. Ruiz Arriola, Phys. Rev. D **78** (2008) 094011.

[100] H. D. Son and H. C. Kim, Phys. Rev. D **90** (2014) no.11, 111901.

[101] J. Hudson and P. Schweitzer, Phys. Rev. D **96** (2017) no.11, 114013.

[102] See Sec. 18.8. in J. D. Bjorken and S. D. Drell, *Relativistic Quantum Fields* (McGraw-Hill, New York, 1965).

[103] O. V. Selyugin and O. V. Teryaev, Phys. Rev. D **79** (2009) 033003.

[104] D. Brommel, *Pion structure from the Lattice*, PhD thesis.

[105] M. V. Polyakov and P. Schweitzer, Int. J. Mod. Phys. A **33** (2018) no.26, 1830025.

[106] V. D. Burkert, L. Elouadrhiri and F. X. Girod, Nature **557** (2018) no.7705, 396.

[107] P. E. Shanahan and W. Detmold, Phys. Rev. D **99** (2019) no.1, 014511.

[108] P. E. Shanahan and W. Detmold, Phys. Rev. Lett. **122** (2019) no.7, 072003.

[109] K. Tanaka, Phys. Rev. D **98** (2018) no.3, 034009.

[110] Y. Hatta, A. Rajan and K. Tanaka, JHEP **1812** (2018) 008.

[111] A. Freese and I. C. Cloët, Phys. Rev. C **100** (2019) no.1, 015201.

[112] M. Anselmino, A. Efremov and E. Leader, Phys. Rept. **261**, 1 (1995) Erratum: [Phys. Rept. **281**, 399 (1997)].

[113] R. D. Tangerman, PhD thesis, RX-1583 (AMSTERDAM).

[114] J. C. Collins and D. E. Soper, Phys. Rev. D **16** (1977) 2219.

[115] F. E. Close and D. W. Sivers, Phys. Rev. Lett. **39** (1977) 1116.

[116] J. P. Ralston and D. E. Soper, Nucl. Phys. B **152** (1979) 109.

[117] J. L. Cortes, B. Pire and J. P. Ralston, Z. Phys. C **55** (1992) 409.

[118] F. Baldcchini, N. S. Cragie, V. Roberto, and M. Socolovsky, Forschr. Phys. **30** (1981) 505; X. Artru and M. Mekhfi, Z. Phys. C **45** (1990) 669; S. Kumano and M. Miyama, Phys. Rev. D **56** (1997) R2504; A. Hayashigaki, Y. Kanazawa, and Y. Koike, Phys. Rev. D **56** (1997) 7350; W. Vogelsang, Phys. Rev. D **57**, 1886 (1998); W. Vogelsang, Acta Phys. Polon. B29 (1998) 1189. M. Hirai, S. Kumano, and M. Miyama, Comput. Phys. Commun. **111**, 150 (1998).

[119] J. Soffer, Phys. Rev. Lett. **74** (1995) 1292.

[120] X. D. Ji, Phys. Lett. B **289** (1992) 137.

[121] R. L. Jaffe and A. Manohar, Phys. Lett. B **223** (1989) 218.

[122] E. Sather and C. Schmidt, Phys. Rev. D **42** (1990) 1424.

[123] M. Nzar and P. Hoodbhoy, Phys. Rev. D **45** (1992) 2264.

[124] Richard D. Field, *Applications of perturbative QCD* (Addidon-Weseley Publishing Company, 1989).

[125] T. Gehrmann, Nucl. Phys. B **498** (1997) 245.

[126] J. Maxwell *et al.*, arXiv:1803.11206 [nucl-ex].

[127] J. P. Ma, C. Wang and G. P. Zhang, arXiv:1306.6693 [hep-ph].

[128] J. F. Owens, Rev. Mod. Phys. **59** (1987) 465.

[129] L. Cormell and J. F. Owens, Phys. Rev. D **22** (1980) 1609.

[130] N. S. Craigie, K. Hidaka, M. Jacob, A. Penzo and J. Soffer, Nucl. Phys. B **204** (1982) 365.

[131] E. L. Berger, E. Braaten and R. D. Field, Nucl. Phys. B **239** (1984) 52.

[132] P. Aurenche, R. Baier, M. Fontannaz and D. Schiff, Nucl. Phys. B **297** (1988) 661.

[133] A. Bacchetta and P. J. Mulders, Phys. Rev. D **62** (2000) 114004.

[134] A. Bacchetta, *Probing the transverse spin of quarks in deep inelastic scattering*, PhD thesis.

[135] D. Boer, S. Cotogno, T. van Daal, P. J. Mulders, A. Signori and Y. J. Zhou, JHEP **1610** (2016) 013.

[136] P. Ratcliffe, Nucl. Phys. B **223** (1983) 45.

[137] W. Vogelsang and A. Weber, Nucl. Phys. B **362** (1991) 3.

[138] L. E. Gordon and W. Vogelsang, Phys. Rev. D **48** (1993) 3136.

[139] P. De Causmaecker, R. Gastmans, W. Troost and T. T. Wu, Phys. Lett. **105B** (1981) 215.

[140] P. De Causmaecker, R. Gastmans, W. Troost and T. T. Wu, Nucl. Phys. B **206** (1982) 53.

[141] B. Lampe and E. Reya, Phys. Rept. **332** (2000) 1.

1. Publication list in the doctoral course

(a) Journal papers

(1) S. Kumano, **Qin-Tao Song** and O. V. Teryaev, "Hadron tomography by generalized distribution amplitudes in pion-pair production process $\gamma^*\gamma \to \pi^0\pi^0$ and gravitational form factors for pion," Phys. Rev. D **97** (2018) 014020, arXiv:1711.08088 [hep-ph].

(2) S. Kumano and **Qin-Tao Song**, "Theoretical estimate on tensor-polarization asymmetry in proton-deuteron Drell-Yan process," Phys. Rev. D **94** (2016) 054022, arXiv:1606.03149 [hep-ph].

(b) Conference procedings

(1) **Qin-Tao Song**, "Hadron tomography for pion and its gravitational form factors," accepted by JPS Conference Proceedings, arXiv:1903.02298 [hep-ph].

(2) **Qin-Tao Song**, "Structure of deuteron by polarized proton-deuteron Drell-Yan process," accepted by JPS Conference Proceedings.

(3) **Qin-Tao Song**, "Generalized distribution amplitudes and gravitational form factors for pion," PoS DIS **2018** (2018) 142, arXiv:1808.03422 [hep-ph].

(4) S. Kumano, **Qin-Tao Song** and O. V. Teryaev, "Hadron tomography and its application to gravitational radii of hadrons," Few Body Syst. **59** (2018) no.5, 102, arXiv:1801.06264 [hep-ph].

(5) S. Kumano, **Qin-Tao Song** and O. V. Teryaev, "Tomography and gravitational radii for hadrons by three-dimensional structure functions," EPJ Web Conf. **181** (2018) 01025, arXiv:1801.00526 [hep-ph].

(6) S. Kumano, **Qin-Tao Song** and O. Teryaev, "3D structure of hadrons by generalized distribution amplitudes and gravitational form factors," PoS DIS **2017** (2018) 244, arXiv:1711.10086 [hep-ph].

(7) S. Kumano and **Qin-Tao Song**, "Estimate on Spin Asymmetry for Drell-Yan Process at Fermilab with Tensor-Polarized Deuteron," JPS Conf. Proc. **13** (2017) 020048, arXiv:1611.00474 [hep-ph].

2. Oral presentations at conferences

(1) **Qin-Tao Song**, "Structure functions of spin-1 deuteron," 25 minutes. Progress on QCD and nucleon structure in 2019 , February 28 - March 1, 2019, Tsukuba, Japan.

(2) **Qin-Tao Song**, "Hadron tomography for pion and its gravitational form factors," 20 minutes. 8th International Conference on Quarks and Nuclear Physics , November

13-17, 2018, Tsukuba, Japan.

(3) **Qin-Tao Song**, "Structure functions of spin-1 deuteron in Drell-Yan process," 30 minutes. Workshop on Progress on Hadron structure functions in 2018 , November 18-19, 2018, Tsukuba, Japan.

(4) **Qin-Tao Song**, "Hadron tomography in meson-pair production and gravitational form factors," 35 minutes. 23nd International Spin Symposium, September 9-14, 2018, Ferrara, Italy.

(5) **Qin-Tao Song**, "Tensor-polarized structure functions of spin-one deuteron," 20 minutes. 23nd International Spin Symposium, September 9-14, 2018, Ferrara, Italy.

(6) **Qin-Tao Song**, "Generalized distribution amplitudes in meson pair production and gravitational form factors," 20 minutes. YKIS2018b Symposium, June 11-15, 2018, Kyoto University, Kyoto, Japan.

(7) **Qin-Tao Song**, "Generalized distribution amplitudes and gravitational form factors for pion," 20 minutes. XXVI International Workshop on Deep-Inelastic Scattering and Related Subjects, April 16-20, 2018, Kobe University, Japan.

(8) **Qin-Tao Song**, " Generalized distribution amplitudes of pion and its gravitational form factors," 20 minutes. 73th JPS annual meeting, March 22-25, 2018, Tokyo Science Univesity, Noda, Japan.

(9) **Qin-Tao Song**, "Determination of generalized distribution amplitudes from experimental measurements," 20 minutes. 5th International Workshop on Transverse polarization Phenomena in Hard process, December 11-15, 2017, Frascati, Italy.

(10) **Qin-Tao Song**, "Gravitational radii for pion by analysis of KEKB measurements," 25 minutes. Workshop on Gravitational physics with particle accelerators 2017, November 30, 2017, KEK Tokai Campus, Japan.

(11) **Qin-Tao Song**, "Tensor-polarized parton distribution functions for spin-1 deuteron," 1 hour. INT Workshop INT-17-68W, The Flavor Structure of Nucleon Sea, October 2 - 13, 2017, Seattle, USA.

(12) **Qin-Tao Song**, "Analysis of generalized distribution amplitudes," 20 minutes. INT Program INT-17-3, Spatial and Momentum Tomography of Hadrons and Nuclei, August 28 - September 29, 2017, Seattle, USA.

(13) **Qin-Tao Song**, "Generalized distribution amplitudes for pion in two-photon process," 20 minutes. The 2017 JPS Autumn Meeting, September 12-15, 2017, Utsunomiya University, Utsunomiya, Japan.

(14) **Qin-Tao Song**, "Mass radii of hadrons from hadron tomography ," 30 minutes. Mini-workshop on Origin of nucleon mass and its decomposition, September 1, 2017, KEK Tsukuba Campus, Japan.

(15) **Qin-Tao Song**, "Generalized distribution amplitudes in meson-pair production,"

30 minutes. Workshop on hadron tomography at J-PARC and KEKB, January 6, 2017, KEK, Tsukuba, Japan.

(16) **Qin-Tao Song**, "Spin asymmetry for proton-deuteron Drell-Yan process with tensor-polarized deuteron," 25 minutes. 22nd International Spin Symposium, September 25-29, 2016, University of Illinois, Champaign, Illinois, USA.

(17) **Qin-Tao Song**, "Estimate on spin asymmetry for Drell-Yan process at Fermilab with tensor-polarized deuteron," 20 minutes. 14th International Conference on Meson-Nucleon Physics and the Structure of the Nucleon, July 25-30, 2016, Kyoto University, Kyoto, Japan.